Technical Report Documentation Page

1. Report No. FHWA-SA-91-043	2. PB92-177120	3. Recipient's Catalog No.
4. Title and Subtitle THE CONE PENETROMETER TEST		5. Report Date February 1992
		6. Performing Organization Code
7. Author(s) Jean-Louis Riaund and Jerome Miran		8. Performing Organization Report No.
9. Performing Organization Name and Address PSC Associates, Inc. 200 Blossom Lane Mountain View, CA 94041		10. Work Unit No. (TRAIS)
		11. Contract or Grant No.
12. Sponsoring Agency Name and Address Federal Highway Administration Office of Technology Applications 400 Seventh Street, SW Washington, D.C. 20590		13. Type of Report and Period Covered Final Report
		14. Sponsoring Agency Code

15. Supplementary Notes

FHWA Project Manager: Chien-Tan Chang, HTA-22 Contractor project manager: Peter Chan

FHWA Technical Consultants: Richard Cheney, Jerry DiMaggio, and Chris Dumas (HNG-31)

16. Abstract

The cone penetrometer test consists of pushing a series of cylindrical rods with a cone at the base into the soil at a constant rate of 2 cm/sec. Continuous measurements of penetration resistance on the cone tip and friction on a friction sleeve are recorded during the penetration. The Piezo-cone records pore pressures in addition to point and friction resistance.

The continuous profiles obtained with the cone penetrometer test allow the user to visualize the stratigraphy, to evaluate the soil type, to estimate a large number of fundamental soil parameters, and to directly design shallow and deep foundations subjected to vertical loads.

17. Key Words Cone penetrometer, soil parameters, foundation design, in situ testing	18. Distribution Statement No restrictions. This document is available to the public from the National Technical Information Service, Springfield, Virginia 22161

19. Security Classif. (of this report) Unclassified	20. Security Classif. (of this page) Unclassified	21. No. of Pages 172	22. Price

Form DOT F 1700.7 (8-72) Reproduction of completed page authorized

UNIT CONVERSIONS

Acceleration	$9.81\ m/s^2 = 386.22\ in./s^2 = 32.185\ ft/s^2$, Paris: $g = 9.80665\ m/s^2$ London: $g = 3.2174 \times 10^1\ ft/s^2$
Area	$1\ m^2 = 1.5500 \times 10^3\ in.^2 = 1.0764 \times 10^1\ ft^2 = 1.196\ yd^2 = 10^6\ mm^2 = 10^4\ cm^2 = 2.471 \times 10^{-4}\ acres^2 = 3.861 \times 10^{-7}\ mi^2$
Coefficient of Consolidation	$1\ m^2/s = 10^4\ cm^2/s = 6 \times 10^5\ cm^2/min = 3.6 \times 10^7\ cm^2/h$ $= 8.64 \times 10^8\ cm^2/day = 2.628 \times 10^{10}\ cm^2/month$ $= 3.1536 \times 10^{11}\ cm^2/year$ $= 1.550 \times 10^3\ in.^2/s = 4.0734 \times 10^9\ in.^2/month$ $= 1.3392 \times 10^8\ in.^2/day = 4.8881 \times 10^{10}\ in.^2/year$ $= 9.4783 \times 10^5\ ft^2/day = 2.8830 \times 10^7\ ft^2/month$ $= 3.3945 \times 10^8\ ft^2/year$
Flow	$1\ m^3/s = 10^6\ cm^3/s = 8.64 \times 10^4\ m^3/day = 8.64 \times 10^{10}\ cm^3/day$ $= 3.5314 \times 10^1\ ft^3/s = 3.0511 \times 10^6\ ft^3/day$
Force	$10\ kN = 2.2482 \times 10^3\ lb = 2.2482\ kip = 1.1241\ t$ (short ton = 2000 lb) $= 1.0194 \times 10^3\ kg = 1.0194 \times 10^6\ g = 1.0194\ T$ (metric ton = 1000 kg) $= 10^9$ dynes $= 3.5971 \times 10^4$ ounces $= 1.022$ t1 (long ton = 2200 lb)
Force per Unit Length	$1\ kN/m = 6.8526 \times 10^1\ lb/ft = 6.8526 \times 10^{-2}\ kip/ft$ $= 3.4263 \times 10^{-2}\ t/ft$ $= 1.0194 \times 10^2\ kg/m = 1.0194 \times 10^{-1}\ T/m$
Length	$1\ m = 3.9370 \times 10^1$ in. $= 3.2808$ ft $= 1.0936$ yd $= 10^{10}$ Amgstrom $= 10^6$ microns $= 10^3$ mm $= 10^2$ cm $= 10^{-3}$ km $= 6.2137 \times 10^{-4}$ mile $= 5.3996 \times 10^{-4}$ nautical mile
Moment or Energy	$1\ kN.m = 7.3759 \times 10^2\ lb.ft = 7.3759 \times 10^{-1}\ kip.ft = 3.6879 \times 10^{-1}\ t.ft$ $= 1.0194 \times 10^3\ g.cm = 1.0194 \times 10^2\ kg.m = 1.0194 \times 10^{-1}\ T.m$ $= 10^3\ N.m = 10^3$ Joule
Moment of Inertia	$1\ m^4 = 2.4025 \times 10^6\ in.^4 = 1.1586 \times 10^2\ ft^4 = 6.9911 \times 10^{-1}\ yd^4$ $= 10^8\ cm^4 = 10^{12}\ mm^4$
Moment per Unit Length	$1\ kN.m/m = 2.2482 \times 10^2\ lb.ft/ft = 2.2482 \times 10^{-1}\ kip.ft/ft$ $= 1.1241 \times 10^{-1}\ t.ft/ft$ $= 1.0194 \times 10^2\ kg.m/m = 1.0194 \times 10^{-1}\ T.m/m$
Pressure	$100\ kPa = 10^2\ kN/m^2 = 1.4503 \times 10^1\ lb/in.^2 = 2.0885 \times 10^3\ lb/ft^2$ $= 1.4503 \times 10^{-2}\ kip/in.^2 = 2.0885\ kip/ft^2$ $= 1.0442\ t/ft^2 = 7.5003 \times 10^1$ cm of Hg (0 °C) $= 1.0197\ kg/cm^2 = 1.0197 \times 10^1\ T/m^2$ $= 9.8689 \times 10^{-1}$ Atm $= 3.3455 \times 10^1$ ft of H_2O (4 °C) $= 1.0000$ bar $= 10^6\ dynes/cm^2$
Temperature	°C = 5/9 (°F - 32), °K = °C + 273.15
Time	1 yr. = 12 mo. = 365 day = 8760 hr = 5.256×10^5 min = 3.1536×10^7 s
Unit Weight, Coefficient of Subgrade Reaction	$10\ kN/m^3 = 6.3654 \times 10^1\ lb/ft^3 = 3.6837 \times 10^{-2}\ lb/in.^3$ $= 1.0196\ g/cm^3 = 1.0196\ T/m^3 = 1.0196 \times 10^3\ kg/m^3$
Velocity or Permeability	$1\ m/s = 3.6\ km/h = 2.2369\ mile/h = 6 \times 10^1\ m/min = 10^2\ cm/s$ $= 1.9685 \times 10^2\ ft/min = 3.2808\ ft/s$ $= 1.0346 \times 10^8\ ft/year = 2.8346 \times 10^5\ ft/day$
Volume	$1\ m^3 = 6.1024 \times 10^4\ in.^3 = 3.5315 \times 10^1\ ft^3 = 7.6455\ 10^{-1}\ yd^3$ $= 10^9\ mm^3 = 10^6\ cm^3 = 10^3\ dm^3$ $= 10^3$ liter $= 2.1998 \times 10^2$ gallon (U.K.) $= 2.6417 \times 10^2$ gallon (U.S.)
Volume Loss in a Tubing	$1\ cm^3/m/kPa = 8.91 \times 10^{-4}\ in.^3/ft/psf$

PB92177120

Publication No. FHWA-SA-91-043

February 1992

U.S. Department
of Transportation

**Federal Highway
Administration**

The Cone Penetrometer Test

Office of Technology Applications
400 Seventh Street, SW.
Washington, D.C. 20590

Innovation Through Partnerships

REPRODUCED BY
U.S. DEPARTMENT OF COMMERCE
NATIONAL TECHNICAL
INFORMATION SERVICE
SPRINGFIELD, VA 22161

NOTICE

This publication is disseminated under the sponsorship of the Department of Transportation in the interest of information exchange. The report does not consitute a standard, specification, or regulation.

The United States Government does not endorse products or manufacturers. Trade or manufactures' names appear in the publication only because they are considered essential to the object of this document.

-A-

TABLE OF CONTENTS

	Page
1. INTRODUCTION	1
1.1 Introduction	1
1.2 History of the CPT	3
1.3 Definitions	7
1.4 Soils suited for a CPT	7
2. COMPONENTS OF THE DEVICE	10
2.1 Penetrometer	10
2.2 Pushing Equipment	15
2.3 Data Acquisition System	17
2.4 Selecting the Right Equipment	17
3. CALIBRATION, MAINTENANCE. SATURATION	19
3.1 Calibration	19
3.2 Maintenance	23
3.3 Saturation of the Filter Element (CPTU)	24
4. RUNNING THE TEST	26
4.1 Procedure	26
4.2 Problems that May Occur During the Test	26
4.3 CPTU Dissipation Test Procedure	27
5. REDUCING THE DATA	31
5.1 Data Reduction	31
5.1.1 Pore Pressure	31
5.1.2 Cone Resistance	31
5.1.3 Friction Resistance	33
5.1.4 Friction Ratio	34
5.2 Data Presentation and Report	34
5.2.1 Data Presentation	34
5.2.2 Report	36
5.3 Precision and Accuracy of the Measurements	36
6. INTERPRETATION OF THE DATA	37
6.1 Stratigraphy	37
6.2 In-Situ Horizontal Stress	42
6.3 Soil Classification	42
6.4 In-Situ Density D_r	48
6.5 Friction Angle ϕ'	48
6.6 Constrained Modulus, M	55
6.7 Young's Modulus, E	57
6.8 Maximum Shear Modulus, G_{max}	62
6.9 Stress History	67
6.10 Sensitivity	71
6.11 Undrained Shear Strength	71
6.12 Coefficient of Consolidation, Permeability	73

6.13 Liquefaction 75
6.14 Comparison with SPT 79

7. DESIGN EXAMPLES AND APPLICATIONS 81

7.1 Design of Shallow Foundations 81

7.1.1 Sand 81

7.1.1.1 Bearing capacity: Procedure 81
7.1.1.2 Bearing capacity: Precision of procedures 1 to 3. 82
7.1.1.3 Bearing capacity: Eccentric load, inclined load, footing shape, depth of embedment, base and ground inclination. 82
7.1.1.4 Settlement: Schmertmann's (1970) step-by-step procedure. 88
7.1.1.5 Settlement, precision of Schmertmann's method. 90
7.1.1.6 Robertson and Campanella revision of Schmertmann's method. 90
7.1.1.7 Settlement: Meyerhof's (1974) method. 92
7.1.1.8 Settlement: Precision of Meyerhof's method. 92

7.1.2 Clay 92

7.1.2.1 Bearing capacity: Procedure 1. 92
7.1.2.2 Bearing capacity: Precision of procedure 1. 94
7.1.2.3 Bearing capacity: Procedure 2. 94
7.1.2.4 Bearing capacity: Precision of procedure 2. 98
7.1.2.5 Bearing capacity: Eccentric load, inclined load, base and ground inclination, footing shape. 98
7.1.2.6 Settlement: Sanglerat's (1972) step-by-step procedure. 99
7.1.2.7 Settlement: Precision of Sanglerat's (1972) method. 103

7.1.3 Design Examples 106

7.1.3.1 Example problem 1: Rectangular footing on sand. 106
7.1.3.2 Example problem 2: Rectangular footing on clay. 109
7.1.3.3 Example problem 3: Rectangular footing on layered soil. 113

7.2 Design of Vertically Loaded Piles 117

7.2.1 Ultimate bearing capacity: Introduction 117
7.2.2 Ultimate bearing capacity: Step-by-step procedure 118
7.2.3 Ultimate bearing capacity: De Ruiter and Beringen method 118
7.2.4 Ultimate bearing capacity: Schmertmann's method 119
7.2.5 Ultimate bearing capacity: L.P.C. method 123
7.2.6 Ultimate bearing capacity: Precision of the methods 132
7.2.7 Settlement: Introduction 136
7.2.8 Settlement: Verbrugge (1981) step-by-step procedure 136
7.2.9 Settlement: Precision of Verbrugge method 143
7.2.10 Design examples 143

8. ADVANTAGES, DISADVANTAGES AND COSTS 152
8.1 Advantages 152
8.2 Disadvantages 152
8.3 Cost and Time Required 153
9. REFERENCES 154

LIST OF FIGURES

Figure		Page
1.1	Dutch Mantle Cone	4
1.2	Electric Penetrometer Tip (q_c)	4
1.3	Electric Penetrometer Tip ($q_c + f_s$)	4
1.4	Mantle Mechanical Cone Fitted with a Side Friction Sleeve of the Begemann Type	4
1.5	C.E.B.T.P Electric Penetrometer Tip	6
1.6	L.P.C. Electric Penetrometer Tip	6
2.1	Electric Penetrometer Tip	11
2.2	Mechanical Penetrometer Tip	11
2.3	Standard Dimensions of the Electric Penetrometer Tip	11
2.4	Simple Cone	12
2.5	Piezo-Cone	12
2.6	Locations of the Porous Filter	12
2.7	Subtracting Penetrometer	13
2.8	Tension Penetrometer	13
2.9	Comparison Between q_c Obtained with Delft Mechanical and Fugro Electric Static Cone Tips	16
3.1	Calibration Curve	20
4.1	Effect of Cone Inclination on CPT Profile	28
4.2	Correlation Between Fines Content and 50% Dissipation Time for 10 cm^2 CPT	30
5.1	Correction of Measured Cone Resistance for Pore Pressure effects	32
5.2	Data Presentation for a CPT	35
6.1	Simplified Examples of q_c - Log Profiles Showing Likely and Possible Interpretations for Soil Types and Conditions	38
6.2	Example Showing the Use of CPT q_c Profiles to Discover the Variation in Thickness and Quality of Potential Pile Bearing Layers Across a Site	39
6.3	Example of the Use of Static Cone Soundings to Quickly Check Rock Surface Profile and Confirm Pothole and Probably Underconsolidated Clay Nature of Cavity Fill	40
6.4	Penetration of Fugro Type Tip Through Loose to Dense Sand Boundary	41
6.5	K_0 as a Function of CPT Sleeve Friction and Overconsolidation Ratio	43
6.6	CPT Behavior Chart	45
6.7	Simplified Soil Behavior Type Classification Chart	46

6.8	Soil Behavior Type Classification Charts for CPT	47
6.9	Relative Density Relationship for N.C., Moderately Compressible, Uncemented, Unaged Quartz Sands	49
6.10	Influence of Compressibility on N.C. Uncemented, Unaged, Predominantly Quartz Sands	50
6.11	Expanded Soil Behavior Type Classification Chart with Equivalent Overburden Normalized Friction Angle and Relative Density Trends	51
6.12	Proposed Correlation Between Cone Bearing and Peak Friction Angle for Uncemented Quartz Sands	53
6.13	Relationship Between Bearing Capacity Number and Friction Angle from Large Calibration Chamber Tests	54
6.14	Relationship of Bearing Capacity Parameters, Symbols Used and Assumed Failure Planes	56
6.15	Relationship Between Cone Bearing and Constrained Modulus for Normally Consolidated, Uncemented Quartz Sands	58
6.16	Constrained Modulus of Sand from Cone Penetration Resistance	59
6.17	Evaluation of Drained Young's Modulus fro CPT for Silica Sands	61
6.18	Selection of Soil Stiffness Ratio for Clays	63
6.19	Evaluation of Small Strain Shear Modulus from CPT for Uncemented Silica Sand	64
6.20	Correlation of G_{max} vs. q_c from Seismic Cone in Po River Sand	65
6.21	Correlation Between Small Strain Modulus, q_c and Soil Type	66
6.22	Normalized S_u/σ'_{vo} Ratio vs. OCR for Use in Estimating OCR	68
6.23	Statistical Relationship Between S_u/σ'_{vo} Ratio and Plasticity Index, for Normally Consolidated Clays	68
6.24	Stress History (OCR) from CPT	69
6.25	Correlation of OCR to Piezo-cone Parameters	70
6.26	Proposed Chart to Obtain S_u from Excess Pore Pressure, Δu Measured During a CPTU	72
6.27	Theoretical Curves for Cylindrical Pore Pressure Dissipation for Various Stiffness Ratios	74
6.28	Correction Factor for Cone Resistance to Predict Liquefaction Potential of Sand	76
6.29	Approximate Grain Size from Cone Resistance and Sleeve Friction	77
6.30	Liquefaction Potential from Cone Resistance	78
6.31	Variation of q_c/N with Mean Grain Size	80
7.1	Chart for Estimating the Ultimate Bearing Capacity of Shallow Footing on Sand average q_c Over Depth 1.5B Below Footing	83

7.2	Comparison of Estimated and Observed Bearing Capacity of Shallow Foundation on Sand	84
7.3	Definition for Load Eccentricity, Inclined Base and Ground Surface	86
7.4	Load Projection	87
7.5	Influence Factor for Footings on Sand	87
7.6a	Comparison of Estimated and Observed Settlement of Shallow Foundation on Sand Using Schmertmann's 1970 Method	91
7.6b	Ratio of Predicted Settlement to Measured Settlement Versus Measured Settlement for Schmertmann's 1970 Method of Estimating Settlement in Sands	91
7.7	Comparison of Estimated and Observed Settlement of Shallow Foundation in Sand Using Meyerhof's Method	93
7.8	Skempton's Bearing Factor N_c for Undrained Clay Conditions	95
7.9	Bearing Ratio R_k vs. Embedment Ratio	97
7.10	Vertical Stress Under Corner of Uniformly Loaded Rectangular Area	102
7.11	Comparison of Predicted Versus Measured Average Settlement for Sanglerat's Method	104
7.12	Example Problem 1	106
7.13	Example Problem 2	109
7.14	Example Problem 3	113
7.15	Point Bearing of Pile in Sand	120
7.16	Limit Values for Point Bearing of Piles in Sand	120
7.17	Penetrometer Design Curves for Pile Side Friction in Sand	121
7.18	Design Curves for Pile Side Friction in Clay	124
7.19	Description of Pile Categories for the Proposed L.P.C. method	125
7.20	Pile Type and Insertion Procedures for the Proposed L.P.C. Method	127
7.21	Maximum Friction Curves for L.P.C. Method	129
7.22	Cone Bearing Capacity Factors for Proposed L.P.C. method	132
7.23	de Ruiter and Beringen Method. Predicted vs. Measured Loads at D/10 + PL/AE	133
7.24	Schmertmann's Method. Predicted vs. Measured Loads at D/10 + PL/AE	133
7.25	L.P.C. Cone Method. Predicted vs. Measured Loads at D/10 + PL/AE	133
7.26	Modified Verbrugge Load Transfer Curves	137
7.27	L.P.C. Cone Method. Predicted vs. Measured Settlement at Qult/2	138
7.28	Cone Penetration Test	139
7.29	Interpreted q_c and f_s Profiles	140
7.30	Example Pile for Load-Settlement Calculation	141

LIST OF TABLES

Table		Page
1.1	Types of cone equipment	2
1.2	Truck with 20 ton push capability	8
1.3	Drill rig with 5 ton push capability	8
2.1	Piezo-cone filter locations	18
5.1	Empirical values of K for adjustment of pore pressures	32
6.1	Estimation of constrained modulus, M, for clays	60
6.2	A_f Values for clays	72
6.3	Anisotropic permeability of clays	75
7.1	Sanglerat's correlation for M	101
7.2	C values	122
7.3	Statistical analysis for ultimate loads	134
7.4	Statistical analysis for ultimate loads	134
7.5	De Ruiter and Beringen method	148
7.6	Schmertmann method	148
7.7	L.P.C. method	148

1. INTRODUCTION

1.1 Introduction

The purpose of this report is to provide guidelines for the proper use of the electric cone penetrometer; much of the manual also applies to the mechanical cone penetrometer. This includes the proper way to perform a cone penetration test (CPT), to reduce and interpret the data, and to use the data in design. This manual is essentially an update of the manual written by John Schmertmann for FHWA in 1978 (Schmertmann, 1978).

Various types of sensors have been adapted to cone equipment which may or may not measure the standard CPT parameters (Table 1.1). However, the scope of this report is limited to the standard CPT and the piezo-cone CPTU. The standard CPT consists of pushing into the soil at a constant rate, a series of cylindrical rods with a cone at the base, and measuring continuously or at selected depth intervals the penetration resistance of the cone and the friction resistance on a friction sleeve. In addition, the pore water pressure generated in the soil near the penetrometer tip can be measured during penetration for the piezo-cone CPTU by means of a pore pressure sensor in the penetrometer tip. The scope is limited to soils; the ideal use of the CPT is in areas of known geology with soils being gravelly sands or finer.

The design applications of the standard CPT and piezometric CPTU include: shallow foundation under vertical or inclined loads, deep foundations under vertical loads, and any other geotechnical problems which can make use of the soil properties from the CPT and CPTU (chapter 6).

The CPT has gained widespread popularity in the United States over the last 15 years. A large factor of the cone's popularity is that it allows a rapid, continuous, in situ profiling of a site, which no other routine investigation does. The CPT is much less operator dependent than other in situ tests, such as the Standard Penetration test, and is quite simple to perform.

The greatest usefulness of any test comes when analyses are performed using that test data, rather than when using correlations of that data to other parameters. However, there are not many equations developed specifically for CPT data, thus correlations are usually required. The practitioner must be aware of the limitation of any correlation, or any equation, before simply using the resultant data.

The CPT must be seen within the framework of the overall geotechnical investigation. For example, on a large bridge project the CPT speed and simplicity make it ideal for

Table 1.1 - Types of cone equipment
1. **Standard CPT** (cone end bearing and friction sleeve) Measures soil resistance to mechanical penetrations, in bearing and sliding shear failure modes. An inclinometer is frequently included to ensure verticality.
2. **Piezo-cone CPT** (addition of pore pressure sensor) Measures soil pore pressure response to mechanical penetration; can be used to obtain ambient pore pressures and an indication of permeability.
3. **Resistivity CPT** (addition of electrical field measurement) Measures electrical resistance of soil around CPT instrument; responds to degree of saturation and electrolyte type; for contaminated plume detection because waste in water changes resistivity (Lunne et al., 1989).
4. **Thermal CPT** (addition of thermistors) Measures soil thermal response to mechanical penetration; can be used to determine ambient temperatures (Schaap and Hoogedoorn, 1984; Mitchell, 1988).
5. **Seismic CPT** (addition of geophones) Measures soil response to surface seismic excitation, with superior sensor-soil coupling. Down hole and crosshole tests may be performed; useful for machine foundation and liquefaction analyses (Campanella and Robertson, 1984; Baldi et al., 1988).
6. **Nuclear CPT** (addition of nuclear moisture-density-source) Measures soil response to low level radiation, indicating in situ densities and moisture content (Tjelta et al., 1985).
7. **Pressuremeter CPT** (addition of a pressuremeter cell) Measures radial response of soil to radial expansion and contraction of cell (Briaud, 1991; ISSMFE, 1991).
8. **Fluid Sampler CPT** (addition of lysimeter) Allows acquisition of select or continuous samples of in situ gases or liquids (Torstensson, 1984).
9. **Heat Conductivity CPT** Measures thermal properties of soil (Mitchell, 1988).
10. **Lateral Stress CPT** (addition of horizontal pressure cell) Measures lateral stress on cone shaft (Baligh et al., 1985).
11. **Acoustic CPT** (Mitchell, 1988)
12. **Ion Detector CPT** (Robertson, 1990)
13. **Vibratory Cone** (Sasaki et al., 1984; Bruzzi, 1987).

development of initial profiles of the site and to develop rough measurements of engineering properties. Next, specific tests for specific foundation behavior, such as lateral motion of piles through use of the pressuremeter, should be performed. Then analyses of cone penetrometer and pressuremeter data can be performed to indicate general foundation constraints and general range of importance of each type of foundation behavior. For example, if the strength of clay seemed important and the calculation of undrained strength from a CPT reveals a factor of safety of 4 or 5 against a failure, then it is probably not necessary to perform any additional work. However, if a low factor of safety is calculated then the uncertainty in correlation of the cone penetrometer must be considered and careful sampling and laboratory testing should probably be performed.

The operator independence, simplicity, and repeatability of the Cone Penetrometer Test gives it great value to a geotechnical exploration program, but engineering judgement must still be recognized in any geotechnical problem. The CPT must be used appropriately and in conjunction with other tests.

1.2 History of the CPT

The first true static cone penetrometer tests whereby contact between soil and push rods above the cone was avoided were made in 1931 in the Netherlands by P. Barentsen (Zuidberg, 1991). His simple cone was provided with a jacket by Vermeiden in 1947 (mantle cone as shown in Fig. 1.1). This apparatus was designed to measure the penetration resistance q_c of the mechanical cone only. In 1946, the Soil Mechanics Laboratory in Delft (the Netherlands), in conjunction with Goudsche Machinefabriek of Gouda, manufactured a hand-operated mechanical penetrometer with a capacity of 2,500 kg which was increased to 10,000 kg in 1948. The cone had an apex of 60° and a diameter of 36 mm.

In 1953, L. Parez (France) constructed the Sol-Essais Static Penetrometer which consisted of a conical point connected to the piston of a hydraulic jack. Continuous readings of the point resistance were made. In the same year, Gidroprockt (USSR) designed a static sounding rig which consisted of rods 33 mm in diameter and a cone with an apex angle of 60° and a diameter of 35.6 mm. Dynamometers were used to measure the point resistance.

Electric penetrometers were devised in various Dutch institutes beginning in 1948 (Fig. 1.2). In 1964, Fugro Consulting Foundation Engineers in the Netherlands started commercial use of the electric penetrometer. This apparatus only measured the point

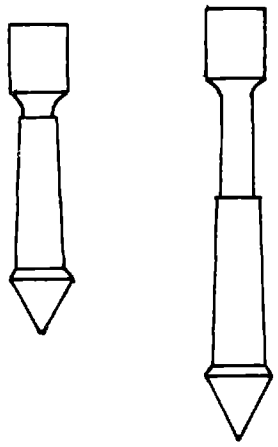

FIG. 1.1. Dutch Mantle Cone

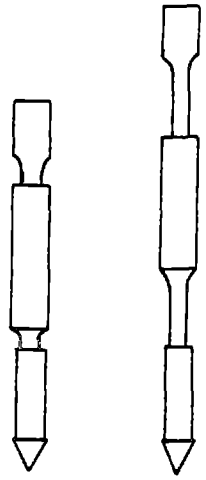

FIG. 1.4. Mantle Mechanical Cone Fitted with a Side Friction Sleeve of the Begemann Type

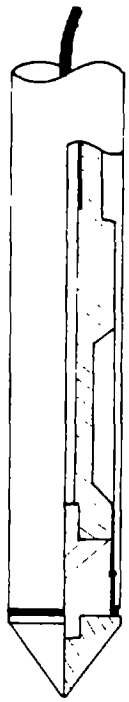

FIG. 1.2. Electric Penetrometer Tip (q_c)

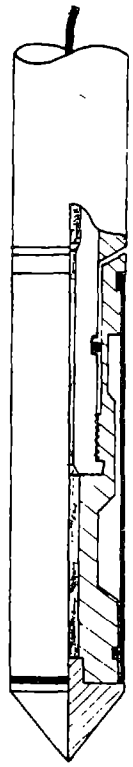

FIG. 1.3. Electric Penetrometer Tip ($q_c + f_s$)

resistance q_c, with an electrically operated cell which contains a number of strain gages arranged to measure the axial stresses. The maximum load was 5000 kg. Later, a sleeve was added to measure the lateral friction. It had a surface area of 150 cm^2 (Fig. 1.3).

In 1969, Begemann fitted a friction sleeve to the mechanical penetrometer which enabled to measure the lateral friction f_s directly, as well as the point resistance q_c (Fig. 1.4).

In 1966, the CEBTP (Centre Experimental du Batiment et des Travaux Publics) in Paris developed an electric static penetrometer (Fig. 1.5). In 1968, an electric cone penetrometer was developed in Australia which could measure both the point resistance on the cone q_c and the frictional resistance f_s on a friction sleeve. This cone had a cross-sectional area of 6 $in.^2$ and an apex angle of 60°.

In 1969, the L.P.C. (Laboratoire des Ponts et Chaussees, in France) developed an electric sounding device (Jezequel, 1969) similar to the Fugro type (Fig. 1.6). Introduction of pore pressure measurement at the tip of the electric penetrometer started in 1975. This step significantly improved the use and interpretation of data from the electric penetrometer.

In 1975, an ASTM standard was published for the quasi-static cone and friction-cone penetration tests of soil (ASTM D-3441-75T). This original version was revised in 1979 (ASTM D-3441-79) and 1986 (ASTM D-3441-86). In 1988, ISSMFE (International Society for Soil Mechanics and Foundation Engineering) proposed a reference test procedure (ISSMFE, 1988).

In the past ten years a number of new specific devices were developed, among which are the following:

* Seismic cone (Campanella and Robertson, 1984; Campanella et al., 1986; Baldi et al., 1988).
* Lateral stress cone (LS-CPT) and Piezo-lateral-stress cell (PLSC), which allow measurement of the lateral stress on the cone shaft (Baligh et al., 1985; Bruzzi, 1987).
* Vibratory cone (V-CPT), which creates the possibility for evaluating the susceptibility of cohesionless deposits to liquefaction (Sasaki et al., 1984; Bruzzi, 1987).

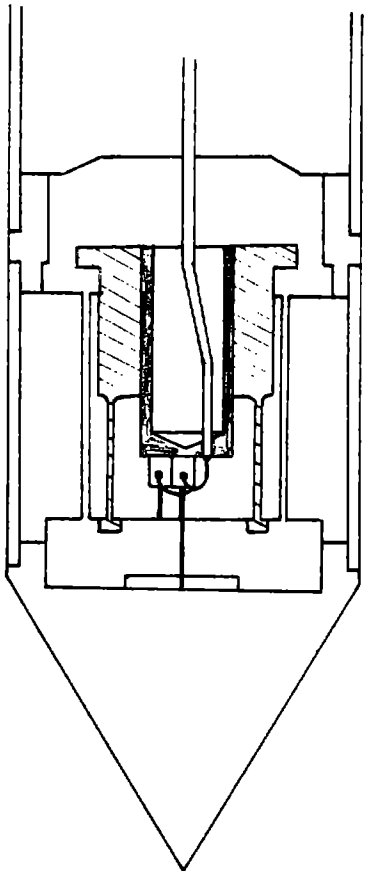

FIG. 1.5. C.E.B.T.P Electric Penetrometer Tip

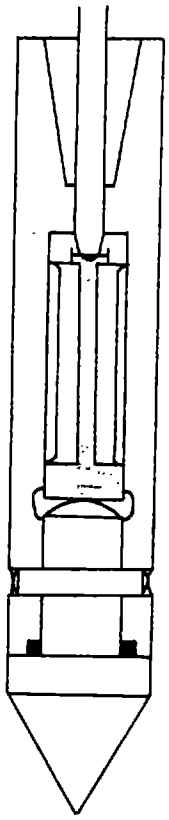

FIG. 1.6. L.C.P.C Electric Penetrometer Tip

1.3 Definitions

CPT and CPTU

CPT usually means: Cone Penetration Test, and includes what has been called Static Penetration Test, Quasi-static Penetration Test and Dutch Sounding Test. A CPT consists of pushing into the soil at a constant rate, a series of cylindrical rods with a cone at the base, and measuring continuously or at selected depth intervals the penetration resistance of the cone and the friction resistance on a friction sleeve. A CPTU (frequently called piezo-cone) consists in measuring the same parameters as in a CPT plus an additional parameter which is the pore water pressure generated near the tip.

Cone Resistance q_c

The cone resistance q_c is the resistance to penetration developed by the cone (see Section 2.1). It is obtained by dividing the ultimate axial force acting on the cone tip Q_c by the horizontal projected area of the base of the cone A_c.

$$q_c = \frac{Q_c}{A_c} \tag{1.1}$$

Friction Resistance f_s

The friction resistance f_s is the resistance to penetration developed by the friction sleeve (see section 2.1). It is obtained by dividing the ultimate frictional force Q_s acting on the sleeve, by its surface area A_s.

$$f_s = \frac{Q_s}{A_s} \tag{1.2}$$

1.4 Soils suited for a CPT

The CPT can be used in soils which are finer than gravelly sands. It is not recommended when cobbles are present because they can damage the equipment. Some cemented soils are not suited for cone testing because they develop a high friction ratio and therefore reduce dramatically the penetration depth. Rocks usually stop the penetration and can cause damage to the cone.

For those soils which are suited for a CPT, Tables 1.2 and 1.3 will help to select the appropriate pushing equipment in order to achieve a given penetration depth.

Table 1.2 - Truck with 20 ton push capability

Soil / Depth ft	Clay			Sand		
	Soft	Stiff	Hard	Loose	Medium	Dense
15	*	*	*	*	*	*
30	*	*	*	*	*	*
60	*	*	*	*	*	*
90	*	*		*	*	
120	*			*		
150	*			*		
200	*					
250	*					
300						

Table 1.3 - Drill rig with 5 ton push capability

Soil / Depth ft	Clay			Sand		
	Soft	Stiff	Hard	Loose	Medium	Dense
5	*	*	*	*	*	
10	*	*		*	*	
15	*	*		*	*	
20	*			*	*	
30	*			*		
40	*			*		
50	*			*		
60	*					
70	*					
80						

Of course, Tables 1.2 and 1.3 can only be used if the geology of the area is known (previous borings) and if the characteristics of the ground layers can be estimated (soft, stiff or hard soil). If none of the above information is available it is difficult to predict whether a CPT can be performed or not.

2. COMPONENTS

2.1 Penetrometer

The following definitions are according to the ISSMFE reference test (ISSMFE, 1988).

A **penetrometer** is a device made of a series of push rods screwed together, with a terminal body called a penetrometer tip. The main types of penetrometer are:

* The electric penetrometer which makes use of a single set of rods and of strain gages built into the penetrometer tip (Fig. 2.1).
* The mechanical penetrometer which makes use of a double set of rods to operate the penetrometer tip (Fig. 2.2).

The word (cone) penetrometer in practice is frequently used for the penetrometer tip. The word cone is also used for this but should be discouraged.

The **penetrometer tip** is made of the active elements that sense the soil resistance, the cone, the friction sleeve, and the porous filter. The recommended standard dimensions of the penetrometer tip and the tolerances are presented in Fig. 2.3. For soft soils a cone tip with a larger end area allows an increase in sensitivity for the measurements. The ASTM standard (1986) allows end areas from 5 to 20 cm^2 to be used, providing they maintain the same tip geometry as the standard cone. The tip and friction sleeve areas must be noted if different from the standard. A cone with a 15 cm^2 end area (44 mm diameter) is now commonly used in the United States (Hekma, 1991).

The **cone** is the cone-shaped end piece of the penetrometer tip on which the end bearing is developed. There are two kinds of cone:

* A simple-cone is a cone which has a cylindrical extension above the conical part (Fig. 2.4).
* A piezo-cone is a cone with a filter located either on the conical part or in the cylindrical extension above the conical part (Fig. 2.5).

The recommended standard dimensions of these cones are presented in Figs. 2.4 and 2.5 as well as the tolerances.

The **friction sleeve** is the section of the penetrometer tip upon which the local side friction resistance to be measured is developed (Fig. 2.3). If the friction sleeve is attached to the penetrometer tip as shown in Fig. 2.7, the penetrometer is called a subtracting penetrometer. In this case, gage 1 measures q_c and gage 2 measures $q_c + f_s$. The friction sleeve can also be attached to the penetrometer tip as shown in Fig. 2.8. In this case, the

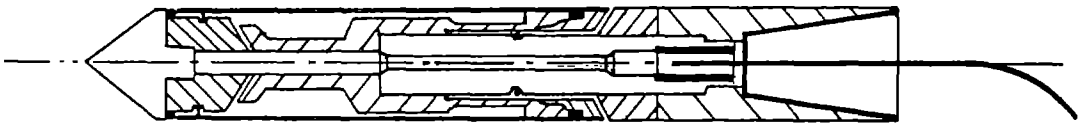

FIG. 2.1. Electric Penetrometer Tip

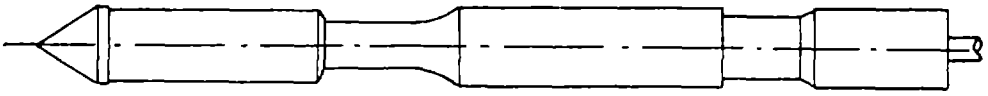

FIG. 2.2. Mechanical Penetrometer Tip

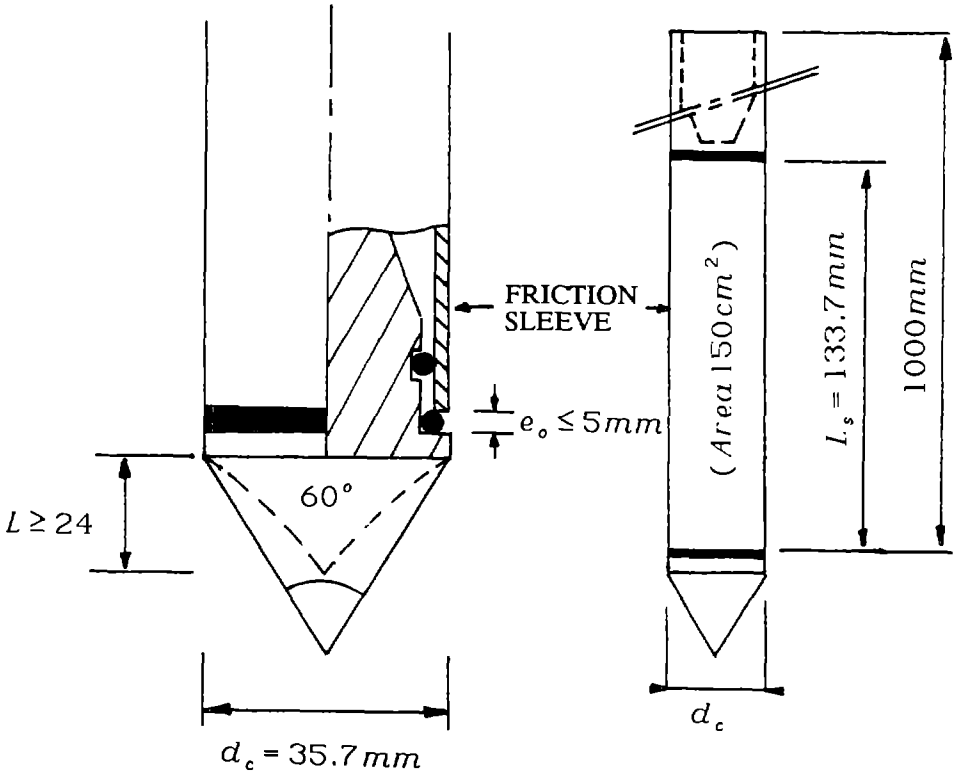

FIG. 2.3. Standard Dimensions of the Electric Penetrometer Tip

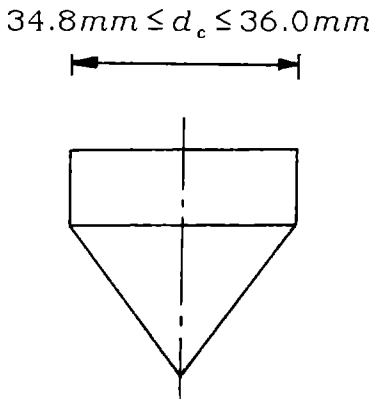

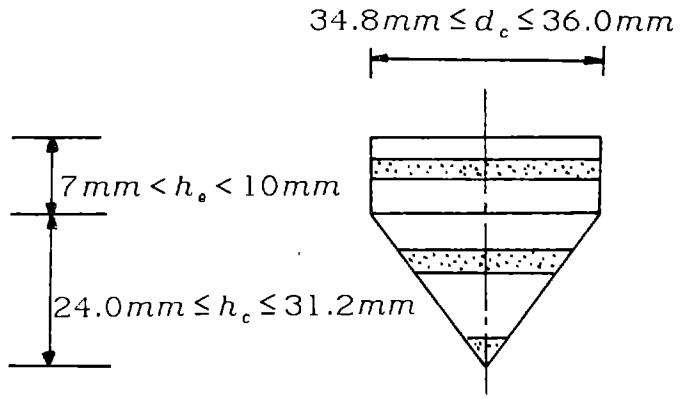

FIG. 2.4. Simple Cone

FIG. 2.5. Piezo-Cone

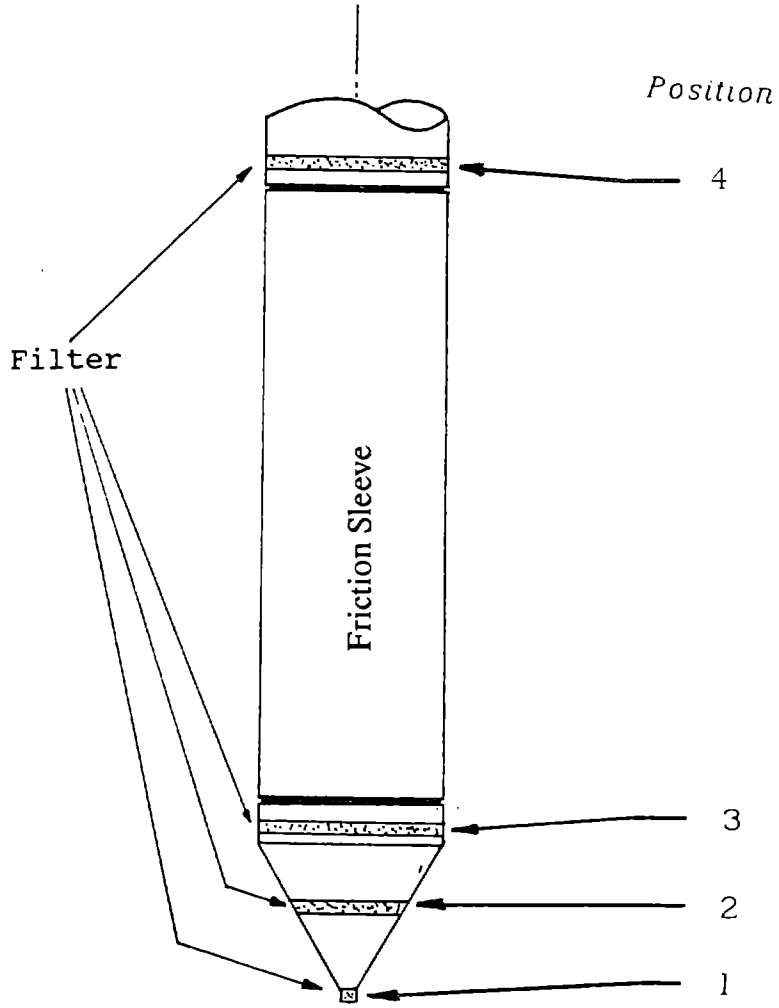

FIG. 2.6. Location of the Porous Filter

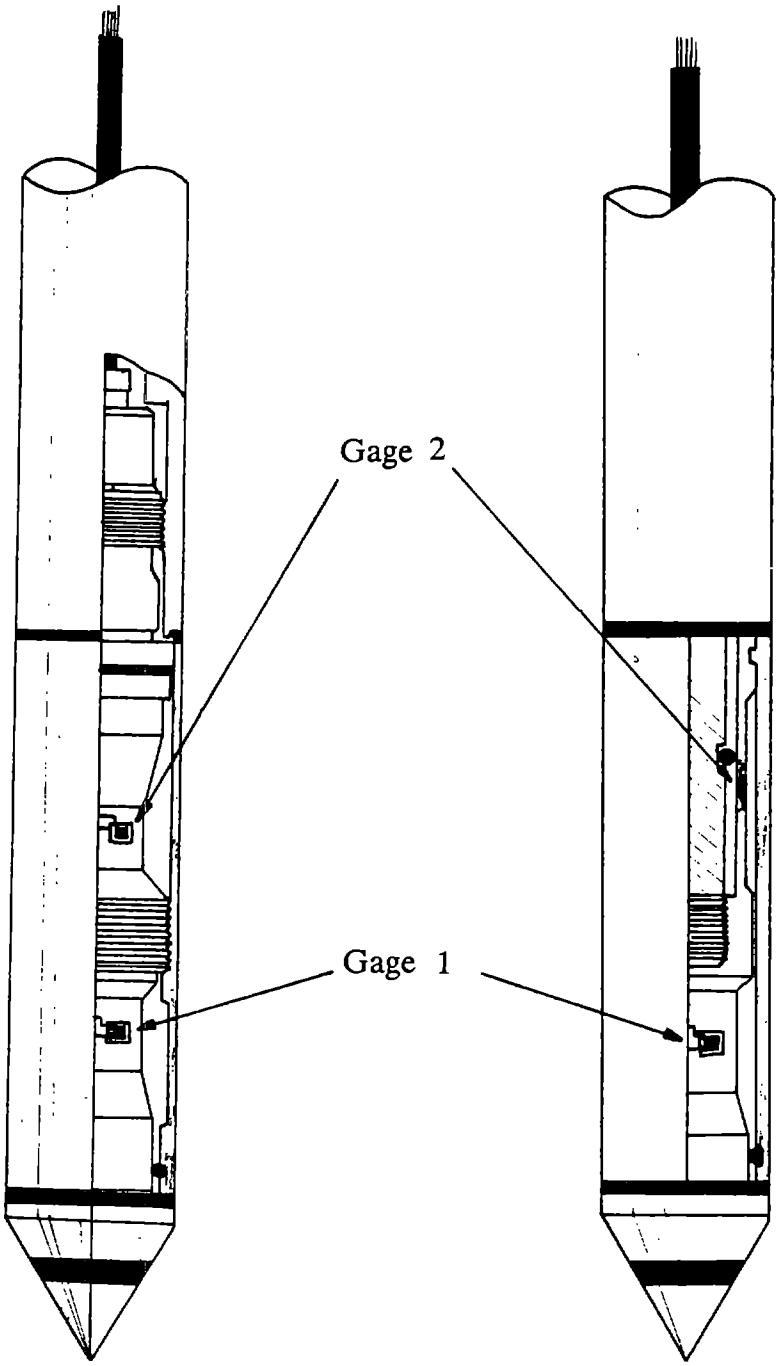

FIG. 2.7. Subtracting Penetrometer **FIG. 2.8. Tension Penetrometer**

penetrometer is called a tension penetrometer with a separate friction load cell; gage 1 measures q_c (load cell in compression) and gage 2 measures f_s (load cell in tension). It is important to know what type of penetrometer is being used in order to reduce the data from a CPT or a CPTU.

The recommended standard dimensions and tolerances of a friction sleeve are the following:

- The diameter of the friction sleeve d_s shall not be less than the actual diameter of the base of the cone d_c. The tolerance is:

$$d_c < d_s < d_c + 0.35 \quad mm$$

- The surface area of the friction sleeve a_s shall be:

$$1.5 \times 10^4 \quad mm^2$$

  The tolerance is:

$$1.47 \times 10^4 \quad mm^2 < A_s < 1.53 \times 10^4 \quad mm^2$$

- The surface roughness r of the friction sleeve in the direction of the longitudinal axis shall verify:

$$0.25 \quad \mu m < r < 0.75 \quad \mu m$$

* In order to measure the pore water pressure the penetrometer tip can be equipped with a **porous filter** which can be made of porous plastic, sintered stainless steel, ceramic, or other porous material. The filter has been placed either at the tip, at mid-height of the cone, immediately behind the cone neck on the cylindrical part, or behind the friction sleeve (Fig. 2.6). So far, the position of the porous filter has not been standardized. However, the ISSMFE (1988) proposed to locate the porous filter immediately behind the cone neck as a reference (position 3 on Fig. 2.6). In order to work properly, the filter and the pore pressure measuring system must be rigid enough to respond immediately to any change in pore pressure. The filter must also have a high permeability to water, yet a high air entry resistance.
* The **push rods** are used for advancing the penetrometer tip to the required test depth. They are made of high strength steel. The standard rods are one meter long with tapered threads. They have the same diameter as the base of the standard tip and sleeve. Their maximum capacity is usually 20 tons. They are screwed together by hand, and there should be no protruding edge at the screw connection between the rods.

  The recommended tolerances are the following:

- The deflection at the mid-point of a 1 meter push rod shall not exceed 0.5 mm for the five lowest push rods, and 1 mm for the remainder.
- For any pair of connected push-rods, the deflection at the joint shall also not exceed these limits.

* Several studies (Heinen, 1973; Joustra, 1974; De Ruiter, 1982) have indicated that the size of the penetrometer affects the results obtained from CPTs. However, it has been shown (Eid, 1987; Sweeney and Clough, 1990) that there is no apparent size effect between 10 and 15 cm^2 cone probes. Also, it should be recognized that correlations (see chapter 6) developed for a standard electric cone may not be valid for a mechanical cone. The values of q_c and f_s measured with an electric penetrometer may be different from the values measured with a mechanical penetrometer, for the same soil (Fig. 2.9). One explanation for the difference between the 2 cone penetrometer q_c values may be as follows. In softer soils ($q_c < 50 kg/cm^2$) the hole squeezes back against the shaft of the mechanical cone (Figs. 1.1 and 1.4) and gives an erroneously high point resistance because of the added friction. For harder soils ($q_c > 50 kg/cm^2$) the lack of horizontal confinement behind the cone tip for the mechanical cone (Figs. 1.1 and 1.4) leads to q_c values lower than with the electric cone. The mechanical cone with friction sleeve (Fig. 1.4) may also give high friction readings due to the friction sleeve bearing on the soil. Because the friction force to be measured is much smaller than the point resistance, the precision on the friction f_s is usually not as good as the precision on the point resistance q_c, especially for the subtracting cone (section 3.1).

2.2 Pushing Equipment

In order to push the penetrometer into the soil, the use of a hydraulic jacking system is required. Usually, the thrust capacity needed for cone testing varies between 5 tons (soft soils) and 20 tons (maximum capacity of the push-rods). The hydraulic rig shall be able to push the rods at a constant rate of penetration, at least a distance of one push rod length (1 meter). The heavier equipment (15 to 20 tons of thrust) can be mounted in a heavy duty truck with a dead weight of 20 tons to provide the necessary reaction. The truck has a working cabin equipped for electrical and mechanical penetration test, and is air-conditioned for the stability of the electrical equipment and dust control, as well as the comfort of the operating crew. A penetration depth of at least 50 ft can be expected when using these trucks in sites not characterized by extensive coarse grained deposits.

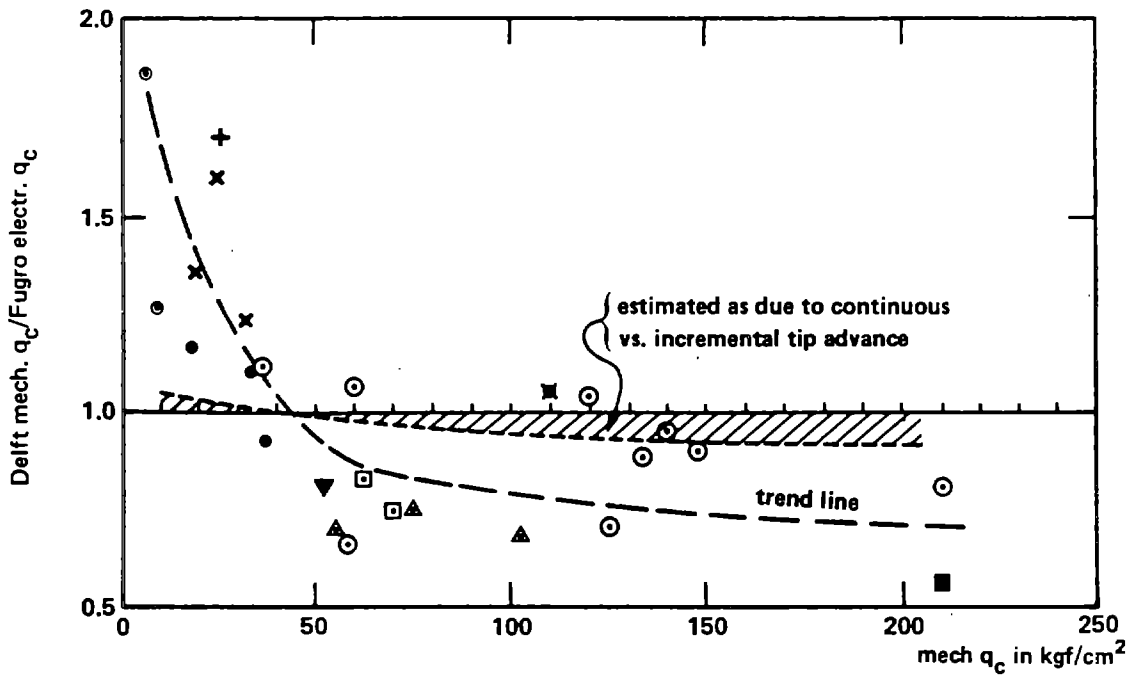

Legend: ⊙ Fugro tests, below WT (Joustra, 1974)
⊡ Delft tests, below WT (Heijnen, 1973)
▲ Kok (1974), below WT
■ U.F., field below WT
✚ U.F., field, below WT, sandy clay
● U.F., field, above WT
▼ U.F., chamber, dry uniform med. sand
⊙ Ft. Pierce, Fla., silty sand below WT
✖ Raleigh, NC, above WT, residual silt
✖ Raleigh, NC, below WT, residual silt

All points represent averages of a layer at least 1.0 m thickness

FIG. 2.9. Comparison Between q_c Otained with Delft Mechanical and Fugro Electric Static Cone Tips (From Schmertmann 1978)

The lighter equipment (5 to 15 tons thrust) can be mounted on light trucks or trailers equipped with earth screw anchors to provide the necessary reaction. Sometimes drill rigs are used to perform a CPT but their capacity is often limited to about 5 tons. When anchored with earth screw anchors (or 5 to 10 ft hollow stem augers) on either side of the drill rig, their capacity can approach that of the cone trucks (20 tons). Also, the drill rig has the advantage of being able to drill through hard layers if necessary, without repositioning the truck.

2.3 Data Acquisition System

The electric penetrometer can be equipped with modern data acquisition systems which allow to print and plot the values of q_c and f_s during a cone sounding.

While the test is performed, the strain gages built in the penetrometer tip send electric analog signals continuously to an amplifier. This amplifier sends the analog amplified signal to a digital converter which transforms the analog signals into digital signals. The digital signal is then interpreted by a computer in order to obtain the q_c versus depth profile and f_s versus depth profile. The pore pressure u can also be recorded and plotted using the same system.

2.4 Selecting the Right Equipment

The cone probes are made with various capacities resulting in different sensitivity. The capacity of the penetrometer tip should be selected based on the soil conditions as follows (Yilmaz, 1991):

Soil Strength	Tip Capacity	$q_c (kg/cm^2)$
Very soft	1 to 2.5 tons	50 to 125
Soft to medium	2.5 to 5 tons	125 to 250
Medium to hard	5 to 10 tons	250 to 500
Dense sand	15 tons and more	> 750

It should be noted that these capacities are of the penetrometer tip, not the jacking system. Typically a high capacity tip (10 tons or more) is used for general profiling. Then if a soft layer is found which requires more detailed information, a lower capacity, more sensitive tip may be used.

The location of the porous filter must also be selected based on soil type and project objectives (Hekma, 1991). Table 2.1 lists preferred filter locations for different soil types. These locations may need to be varied based on special project needs (The Earth Technology Corporation, 1991).

Table 2.1 - Piezo-cone filter locations (from The Earth Technology Corporation, 1991).

Soil Type	Comments on Filter Location
Soft Silt and Clays	Use of a side sensing piezo-cone enables adjustments to be made to the cone tip and sleeve friction measurements to account for pore pressure effects, which could be significant in this type of soil. These adjustments cannot generally be made with tip sensing piezo-cones.
Loose Sands	The measured pore pressure response from tip sensing piezo-cones is more sensitive to small variations in stratigraphy and soil properties, enabling higher resolution stratigraphic profiling. Pore pressure effects on the cone tip and sleeve friction measurements are generally not significant enough to require adjustments.
Dense Sands and Silts	A tip sensing piezo-cone is generally preferable because the filter of a side sensing piezo-cone is often subjected to negative pore pressure (suction) in these soils. Excessive suction on the filter could cause cavitation, and loss of saturation, which would reduce the reliability of subsequent pore pressure measurements.
Stiff Clays	A tip sensing probe may be subjected to pore pressures higher than the capacity of the transducer, which could result in unreliable readings and damage to the transducer. On the other hand, the side sensing probe may be subjected to excessive negative pore pressure. Therefore under these soil conditions, the piezo-cone configuration is best determined on a case-by-case basis.

3. CALIBRATION, MAINTENANCE, SATURATION

3.1 Calibration

Most commonly, electric cone penetrometers measure the cone resistance q_c and the friction resistance f_s by means of load cells built into the penetrometer tip. The load cells are usually made of strain gages interconnected to form a circuit called a wheatstone bridge. These strain gages are rigidly attached to the shaft of the penetrometer tip as shown in Figs. 2.7 and 2.8. When a load is applied to the cone or to the friction sleeve, the shaft length varies and the gages are subjected to the same variation in length. This variation changes the resistance of the strain gages. Therefore the resistances of the load cell are a function of the load applied on the cone tip and on the friction sleeve.

When a constant excitation signal (say 5 volts) is sent to the load cell, the value of the output signal depends on the load cell resistance. The value of the output signal (voltage) is therefore a function of the load applied on the cone and the friction sleeve.

The calibration of each load cell consists of comparing the load cell output (voltage) against the load applied (tons or lbs) and is performed at constant temperature. Temperature variations in the cone may have a significant impact on zero shift (drift). Usually the calibration line is straight plus or minus a very small deviation called non-linearity. The sketch in Fig. 3.1 is an enormous exaggeration to define the terminology (Zuidberg, 1991). The shape of the calibration curves does change during the lifetime of the penetrometer tip.

Several terms characterize this curve:

- The **calibration error** is the difference in percent between the original calibration performed on the new or cleaned penetrometer tip and the one being performed (Fig. 3.1). Studies have shown that the major factor which affects the calibration error is soil ingress into the grooves.
- The **zero load error** is the difference in zero readings before and after the calibration or before and after the sounding (Fig. 3.1).
- **Non linearity** refers to the curvature of the calibration curve.
- **Repeatability** refers to the range of values obtained during a series of calibrations (Fig. 3.1).
- **Hysteresis** refers to the width of the loop in the calibration curve (Fig. 3.1).

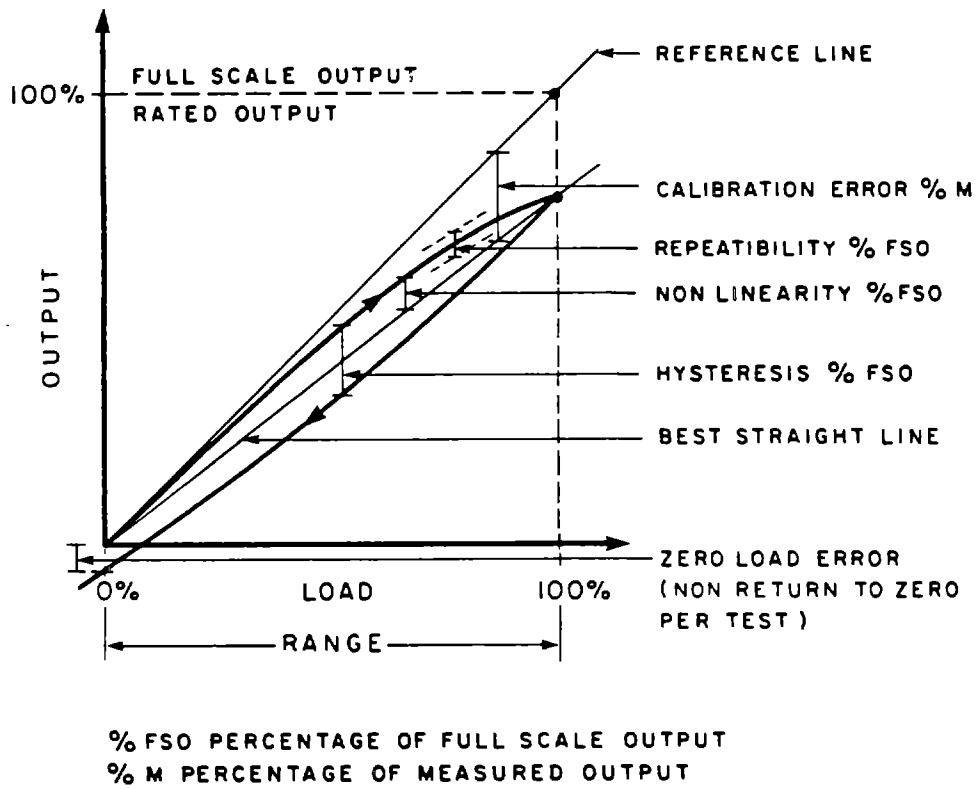

FIG. 3.1. Calibration Curve (. From Schaap and Zuidberg 1982)

The calibration procedures should be followed in order to determine the best straight line fit for the data (Fig. 3.1). These procedures are described below; one exists for the subtracting cone and one for the tension cone. A third type of cone exists which has separate load cells for point and friction resistance with the friction load cell in compression. This type cone is rare and is not discussed here.

Subtracting Penetrometer Tip

The 2 load cells in this type of penetrometer tip are calibrated simultaneously by loading the cone. During loading and unloading the output of load cells 1 and 2 (Fig. 2.7) should be identical. The following calibration procedure is recommended:

1. Multiple preloading and many other procedures are part of the penetrometer manufacturing process and need not be repeated (Zuidberg, 1991). These procedures reduce the hysteresis in the calibration curves. Calibration starts with step 2.
2. Read the initial values V_{oc} and V_{oc+s} of the output voltage from load cell 1 and 2 respectively when no load is applied on the cone.
3. Load the cone progressively and record the value of the output voltage for each applied load and for each load cell.
4. Record the final values of the output voltage V_{fc} and V_{fc+s} from load cell 1 and 2 respectively corresponding to the maximum allowable load L_f on the cone.
5. Unload the cone progressively and record the value of the output voltage for each applied load and for each load cell. Record the zero load error for each load cell. The zero load error during calibration of a cleaned penetrometer tip should be negligible (less than 0.05 % of the full scale output).
6. Plot the calibration curve of output (voltage) versus load (tons or lbs) for each cell.
7. Draw the best straight lines fit for the data, for each load cell.
8. Calculate the slope C_c and C_{c+s} of both lines:

$$C_c = \frac{V_{fc} - V_{oc}}{L_f} \tag{3.1}$$

$$C_{c+s} = \frac{V_{fc+s} - V_{oc+s}}{L_f} \tag{3.2}$$

9. The measured value of the cone resistance q_c is calculated as follows:

$$q_c = \frac{V_c - V_{oc}}{C_c \times A_c} \tag{3.3}$$

where:

V_c = output voltage from load cell 1

V_{oc} = output voltage from load cell 1 when no load is applied on the cone read at the beginning of the sounding.

A_c = cross-sectional area of the cone (~ 10 cm^2).

The measured value of the friction resistance f_s is calculated as follows:

$$f_s = \frac{1}{A_s}\left[\frac{V_{c+s} - V_{oc+s}}{C_{c+s}} - \frac{V_c - V_{oc}}{C_c}\right] \tag{3.4}$$

where:

V_{c+s} = output voltage from load cell 2.

V_{oc+s} = output voltage from load cell 2 when no load is applied on the cone, read at the beginning of the sounding.

A_s = area of the friction sleeve (= 150 cm^2).

Tension Penetrometer Tip

The load cells of this type of penetrometer tip are calibrated separately. Load cell 1 (Fig. 2.8) is calibrated by loading the cone and load cell 2 (Fig. 2.8) is calibrated by loading the friction sleeve.

The following calibration procedure is recommended:

1. Multiple preloading and many other procedures are part of the penetrometer manufacturing process and need not be repeated (Zuidberg, 1991). These procedures reduce the hysteresis in the calibration curves. Calibration starts with step 2.
2. Read the initial value V_{oc} (or V_{os}) of the output voltage from load cell 1 (or load cell 2) when no load is applied on the cone (or the sleeve).
3. Load the cone (or the sleeve) progressively and record the value of the output voltage for each load applied for load cell 1 (or load cell 2).
4. Record the final value of the output voltage V_{fc} (or V_{fs}) from load cell 1 (or load cell 2) corresponding to the maximum allowable load L_{fc} on the cone (or L_{fs} on the sleeve).
5. Unload the cone (or the sleeve) progressively and record the value of the output voltage for each applied load and for load cell 1 (or load cell 2).

Record the value of the zero load error for load cell 1 (or load cell 2).

6. Plot the calibration curve of output (volts) versus load (tons or lbs) for each cell.
7. Draw the best straight line fit for the data, for each load cell.
8. Calculate the slope C_c and C_s of both lines.

$$C_c = \frac{V_{fc} - V_{oc}}{L_{fc}} \tag{3.5}$$

$$C_s = \frac{V_{fs} - V_{os}}{L_{fs}} \tag{3.6}$$

9. The measured value of the cone resistance q_c is:

$$q_c = \frac{V_c - V_{oc}}{C_c \times A_c} \tag{3.7}$$

where:

V_c = output voltage from load cell 1.

V_{oc} = output voltage from load cell 1 when no load is applied on the cone read at the beginning of the sounding.

A_c = cross-sectional area of the cone (~ 10 cm^2).

The measured value of the friction resistance f_s is:

$$f_s = \frac{V_s - V_{os}}{C_s \times A_s} \tag{3.8}$$

where:

V_s = output voltage from load cell 2.

V_{os} = output voltage from load cell 2 when no load is applied on the friction sleeve read at the beginning of the sounding.

A_s = area of the friction sleeve.

The load cells shall be calibrated at least every 3 months. Also, regular inspection and maintenance of the penetrometer tip help to reduce the calibration error.

3.2 Maintenance

Before each sounding, inspection shall be made for wear of the cone, the friction sleeve, and the shaft of the penetrometer tip. Also, the seals between the different elements of a penetrometer tip shall be inspected to determine their condition, checked for the presence of soil particles, and cleaned. The penetrometer should also be checked to assure that it is not bent.

The penetrometer tip dimensions shall be checked regularly to ensure that they do not exceed the tolerances set out in chapter 2.

For an electric penetrometer tip, the zero load error should be checked by observing the zero load output before and after each test. If the zero load error exceeds 1% of the full scale output the penetrometer tip should be checked, cleaned, and re-calibrated.

Also, if the calibration error (see section 3.1) exceeds 2 to 3% of the original calibration value, the penetrometer tip should be checked, cleaned, and recalibrated.

3.3 Saturation of the Filter Element (CPTU)

It is crucial to have a complete saturation of the pore pressure element system in order to produce high quality, reliable pore pressure recordings. Before each sounding, the piezo-cone should be saturated as follows:

1. The recommended procedure (Robertson and Campanella, 1988) is to saturate the filter elements in the laboratory by placing them under a high vacuum with a suitable saturating fluid in an ultra-sonic bath for approximately 3 hours. De-aired glycerin is often used as the saturating fluid since it retains saturation better than water. However, other liquids are also used. High vacuum will allow the saturating fluid to boil at low temperature, which will improve saturation, and avoid damage to the filter element due to high temperature.
2. Once saturated, the filter elements should be placed in a container filled with the saturating fluid in order to maintain saturation during transportation of the filter into the field.
3. Flush all voids in the cone, using a plastic syringe filled with saturating fluid and a hypodermic needle.
4. Assemble the penetrometer tip and maintain it in saturating fluid until the test is ready to be performed. To do so, the penetrometer tip can be placed in a container filled with the saturating fluid.
5. The piezo-cone is then pushed into the upper layers of the soil deposit. If the water table is not at the ground surface, it can be difficult to maintain the saturation. To avoid this problem, it is recommended to drill a hole down to the water table. Then, the saturated piezo-cone is lowered in this hole with a thin protective rubber sleeve placed over the cone. The penetrometer tip is then pushed into the soil and punches the rubber sleeve.
6. Repeat the saturation procedure before each sounding and change the filter elements if damaged.

Note: The response of the pore pressure measuring system can be checked by simple laboratory tests.

4. RUNNING THE TEST

4.1 Procedure

1. If using a continuous electric cable, pre-thread it through the push rods.
2. Set up the thrust machine for a thrust direction as near as vertical as practical.
3. Often, the upper zone (1 meter) of the soil is constituted of very stiff material, and gravel or random fill can be encountered. To avoid damage to the cone, in this case it is recommended to first push a solid steel "dummy cone" of 15 cm^2 area into this zone.
4. If performing a CPTU, saturate the porous filter as explained in section 3.3.
5. After an initial short penetration test hole so that the tip temperature is at the soil temperature, retract the tip and record the zero load readings (voltage) with the penetrometer tip hanging freely in air or in water, but out of the direct sunlight.
6. Push the penetrometer into the soil at a constant rate of 20 mm/sec with a tolerance of $\pm$ 5 mm/sec. Between these tolerances, a constant rate shall be maintained during the entire stroke.
7. Record the cone resistance q_c, the friction resistance f_s, and the pore pressure u, at intervals of 3 cm (0.1 ft). The depths shall be measured with an accuracy of at least 0.1 m.
8. At the end of the sounding obtain a final set of zero load readings, as in step 5 above, and check them against the initial set. Discard the sounding and repair or replace the tip if this check is not satisfactory for the accuracy required (see section 5.3).
9. After retrieval of the cone penetrometer, it is usually required to grout the hole with cement-bentonite or an equivalent slurry.

4.2 Problems that May Occur During the Test

1. <u>Reaction force exceeded</u>

   This problem can occur commonly during a test depending on the geographical area (Tables 1.2 and 1.3) and may be due to the presence of a very hard layer. Usually, the earth anchors yield or the dead weight lifts off; this can be avoided with hydraulic regulators or pressure relief valves.

One way to prevent this from happening is to reduce the friction along the rods. A friction reducer should always be used with the standard 10 cm^2 cone; it is usually made of an enlarged ring around the rods near the tip. It shall be located at least 400 mm above the base of the cone or 300 mm above the top of the friction sleeve. One advantage of the larger 15 cm^2 cone is that it needs no friction reducer because the probe diameter is larger than the push pipe diameter. Another way to reduce friction along the rods is to use drilling mud pumped down the inside of the cone rods and injected into the soil behind the tip.

One can also avoid this problem by using a heavier equipment or larger earth anchor.

If none of the previous remedial action works, it is necessary to retrieve the penetrometer and to drill through the hard layer.

2. Push Rod Buckling

   In very loose or soft soils such as swamps or backwater organic deposits, silty hydraulic fill, or loose sand, rods can buckle when being pushed into the soil. One way to avoid this problem is to set casing or push rod guides through the soft layer. Another way is to limit the thrust applied on the rods.

3. Rapid Change in Inclination

   If the CPT equipment was not leveled at the beginning of the test, the inclination will keep on increasing with depth. Also, if the cone encounters cobbles, gravels, or sloping bedrocks, there might be a rapid change in penetrometer tip inclination. The way to detect this problem is to install an inclinometer inside the penetrometer tip and to record the inclination continuously with depth. When the inclination reaches 10°, especially if this angle is reached in less than 1 m, the cone tip can be damaged. In this case, the only suitable remedial action is to retrieve the penetrometer and start again. Inclination of the push rods may cause serious errors in the depth record of the CPT. Fig. 4.1 shows an example of the possible error due to bending of the cone rods.

4. Damage to the Equipment

   Experience shows that as long as the pushing thrust is below 10 tons, it is rare that any damage occurs to the cone or to the rods.

4.3 CPTU Dissipation Test Procedure

The piezo-cone test (CPTU) has the potential of providing estimates of the in situ coefficient of consolidation from dissipation tests (section 6.12). A dissipation test can be performed at any depth as follows:

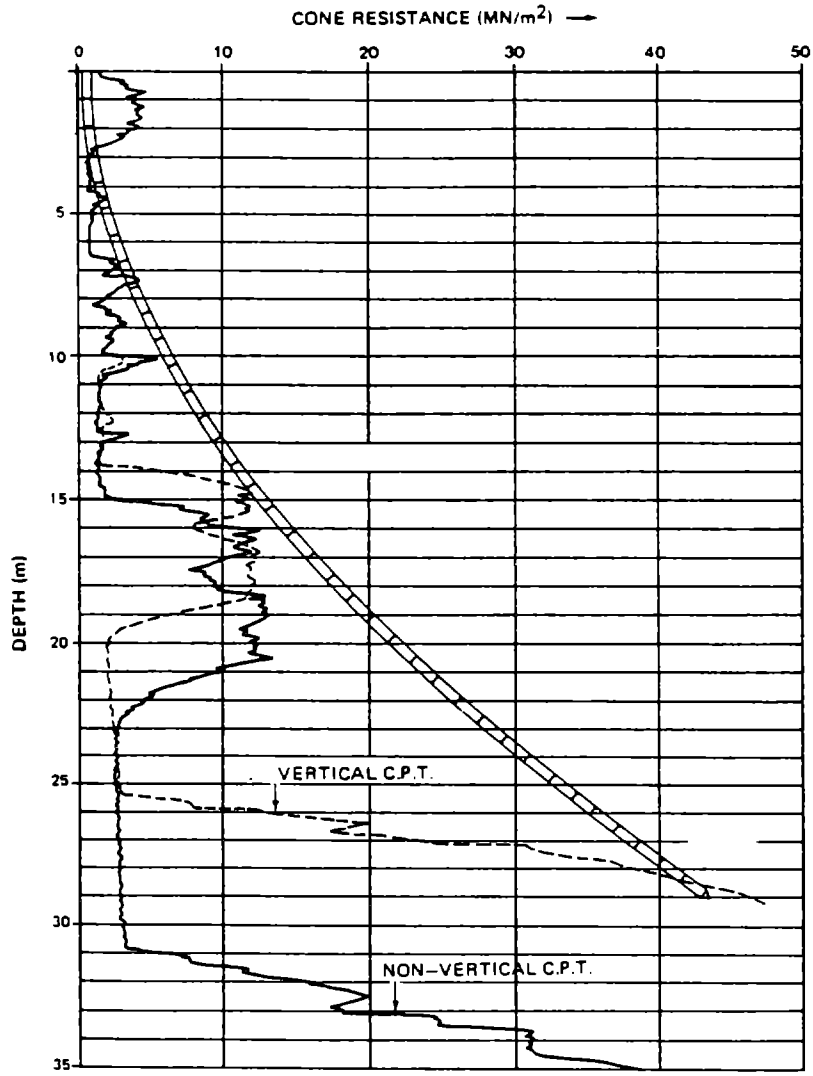

FIG. 4.1. Effect of Cone Inclination on CPT Profile (From de Ruiter 1981)

1. Stop the penetration of the penetrometer by completely releasing the load on the push rod. As soon as the penetrometer stops, the excess pore pressure u_e around the cone will start to dissipate.
2. Record the total pore pressure $u_T = u_o + u_e$ at 0, 1, 2, 4, 8, 16, 30 seconds, 1, 2, 4, 8, 16, 30 min in order to obtain reasonably spaced data points for the dissipation curve.
3. While performing the test, plot the normalized excess pore pressure ($\Delta u / \Delta u_o$) versus log time (dissipation curve).

   where: Δu = excess pore pressure above hydrostatic at time t = t.

   Δu_o = excess pore pressure above hydrostatic at time t = 0.
4. Continue the test until a predetermined percentage of the hydrostatic pore pressure is reached (50% or 80%), or alternatively at a set time. Fig. 4.2 gives an idea of the time required to reach 50% dissipation based on fines content.

NOTE: Tests performed with different porous filter locations have resulted in wide scatter in the predicted coefficient of consolidation. Also, the measured value of the pore pressure depends on the porous filter location (Table 2.1).

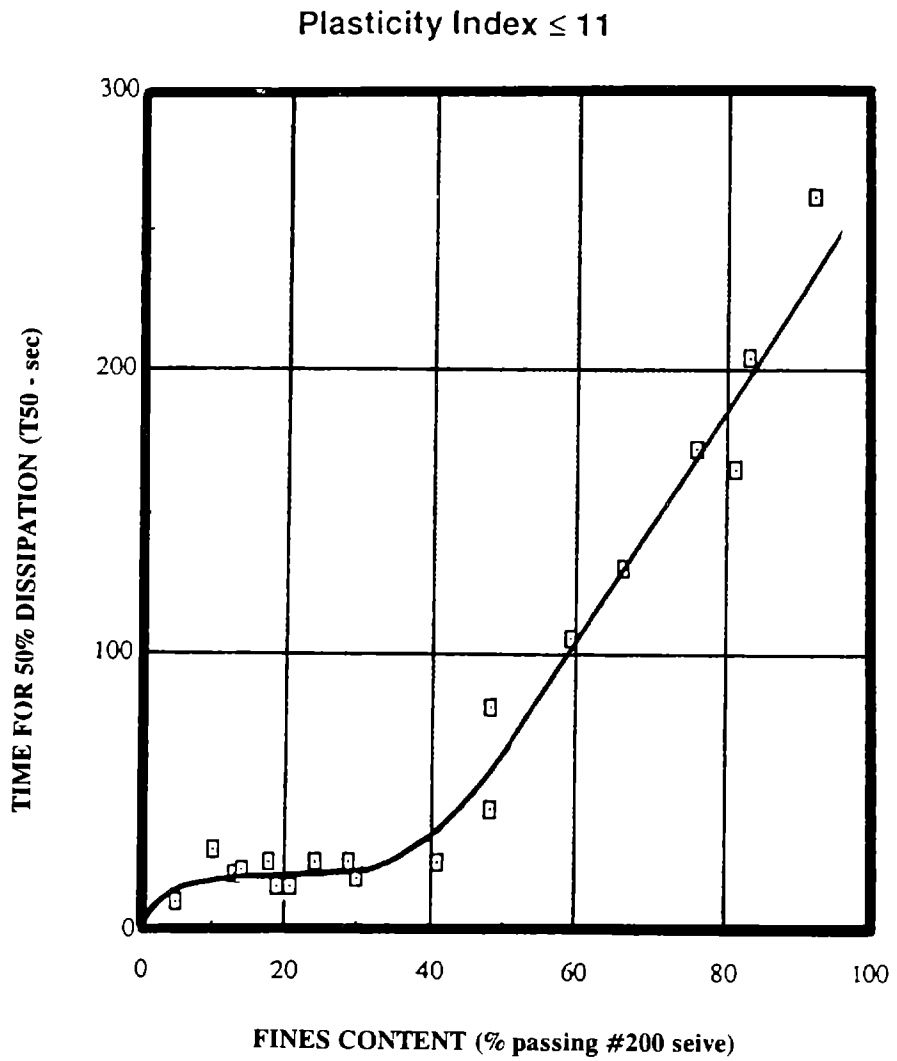

FIG. 4.2 Correlation Between Fines Content and 50% Dissipation Time for 10 cm^2 CPT (after Robertson, et al., 1992)

5. REDUCING THE DATA

5.1 Data Reduction

The data collected during the test consists of the values of the output voltage from load cell 1 and 2 (Figs. 2.7 and 2.8) recorded regularly with depth. When a CPTU is performed the pore pressure u is also available. These data may be reduced and corrected in order to obtain the corrected cone resistance q_T developed by the soil and acting on the cone tip, the corrected friction resistance f_T developed by the soil and acting on the friction sleeve, and the corrected pore pressure u_T.

5.1.1 Pore pressure u_T

The pore pressure u measured during a CPTU depends upon the location of the porous filter (see section 2.4). In all cases the location of the porous filter should be clearly mentioned in the report. The following equation is a relation between the pore pressures at various locations on the cone (Senneset, et al., 1989).

$$u_T = u_o + K(u - u_o) \tag{5.1}$$

where:

u_T = pore pressure behind the cone tip (position 3 on Fig. 2.6).

u = pore pressure on the cone tip (position 1 or 2 on Fig. 2.6).

u_o = hydrostatic or initial in situ pore pressure,

K = adjustment factor from Table 5.1.

The values of the K factor may vary considerably from those in Table 5.1. Local correlation is necessary to obtain reliable values. In general, this correction procedure is discouraged; instead direct measurement of the pore pressure at the desired location is encouraged.

5.1.2 Cone resistance q_T

In section 3.1, the values of the output voltage from load cell 1 are used to obtain the measured value of the cone resistance q_c (equation 3.3 or 3.7, section 3.1).

When using a piezo-cone below the water table, this q_c value may be corrected to account for the area effect as explained in the following. The pore pressure u_T acts behind the cone over an area equal to the difference between the cross section area A_N and the cross section area A_q. Therefore, the measured tip resistance q_c is lower than the true resistance of the soil q_T acting on the front face of the cone tip; indeed, the pressure u_T applied over the area $A_N - A_q$ will have a tendency to push the cone into the soil. The relationship between q_T and q_c is:

TABLE 5.1. Empirical Values of K for Adjustment of Pore Pressures (from Senneset, 1989)

	FILTER LOCATION	
Soil type	Cone face, mid-height	Cone tip
Normally consolidated clay	0.6 - 0.8	0.7 - 0.9
Slightly overconsolidated, sensitive clays	0.5 - 0.7	0.6 - 0.8
Heavily overconsolidated clays	0 - 0.3	0.1 - 0.3
Loose, compressible silts	0.5 - 0.6	0.5 - 0.7
Dilatant, dense silts	0 - 0.2	0.1 - 0.3
Loose, silty sands	0.2 - 0.4	0.5 - 0.7

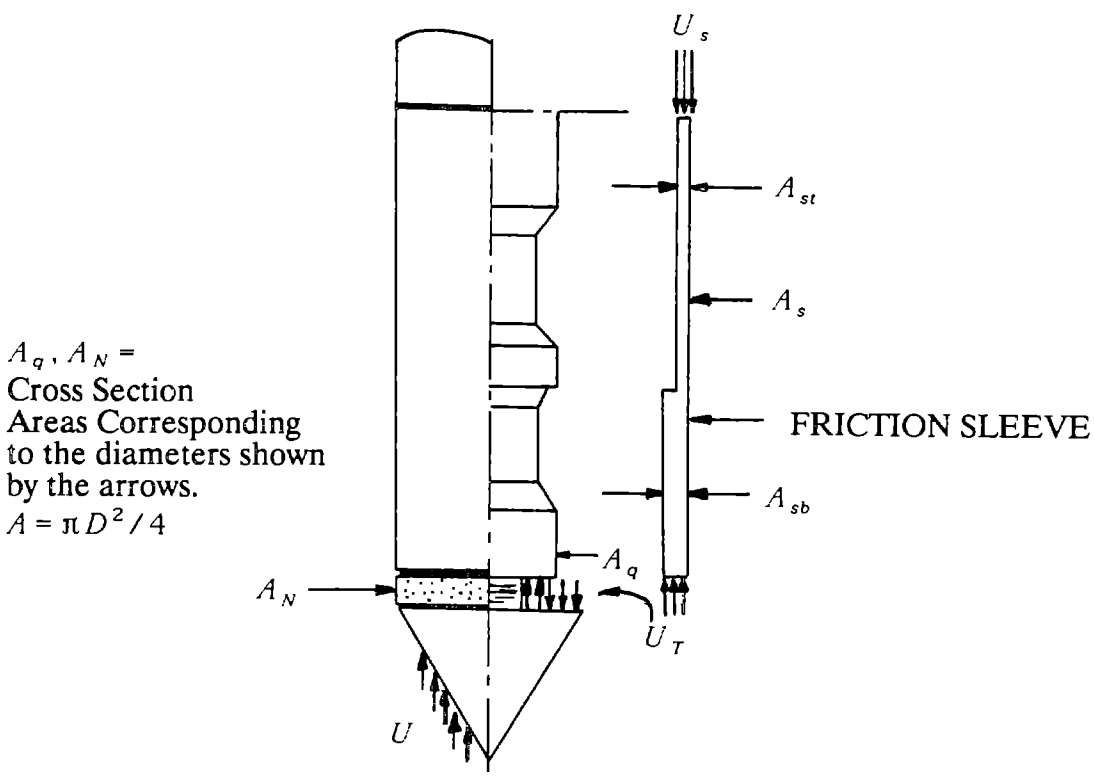

FIG. 5.1. Correction of Measured Cone Resistance for Pore Pressure Effects (after Senneset et al., 1989)

$$q_T \cdot A_N = q_c \cdot A_N + u_T(A_N - A_q)$$

$$q_T = q_c + u_T(1 - a) \tag{5.2}$$

where:

a = A_q / A_N = net area ratio, typical value ~ 0.8

u_T = pore pressure at the depth considered, measured behind the cone tip.

This correlation is particularly important for soft soils because it represents a significant percentage of q_T. This correction is only approximate however; indeed, u_T is measured with a stiff fluid pressure measuring system, the slit is not deaired, and the internal volume is variable (Zuidberg, 1991).

5.1.3 Friction resistance f_T

In section 3.1, the values of the output voltage from load cells 1 and 2 are used to obtain the measured value of the friction resistance f_s (equations 3.4 and 3.8, section 3.1). When using a piezo-cone below the water table this f_s value may be corrected to account for the unequal area effect as explained in the following. As shown in Fig. 5.1 the pore pressures act on the end areas of the friction sleeve. These end areas may not be equal in size and pore pressures may be different at both ends of the sleeve thus causing an unbalanced force to occur during penetration. This force may represent a significant correction in soft clays where f_s and q_c are small. The recorded friction resistance f_s will be larger than the true friction resistance f_T. Senneset, et al., (1989) proposed for a subtracting cone.

$$f_T = f_s - (1 - K_s b) \cdot C \cdot u_T \tag{5.3}$$

where:

b = sleeve end area ratio, $A_{st} / A_{sb} \leq 1$.

A_{st} = cross section area at top of sleeve.

A_{sb} = cross section area at bottom of sleeve.

C = sleeve area ratio $A_{sb} / A_s < 1$.

A_s = surface area of sleeve.

u_T = total pore pressure at the bottom of the friction sleeve (position 3 on Fig. 2.6).

K_s = u_s / u_T ~ 0.6 - 0.8 in soft clays.

u_s = total pore pressure at top of friction sleeve (position 4 on Fig. 2.6).

In cohesionless, coarse soils, this correction is practically negligible. Furthermore, Zuidberg (1991) states that the reservations concerning correction of q_c using u_T mentioned in section 5.1.2 apply even more for f_s. He believes that f_s correction is a purely theoretical exercise and that f_s should not be interpreted directly, but only used for the ratio R_f (section 5.1.4). Even though f_s is not a very repeatable value, R_f has shown to be a good denominator for soil type, however, still to be used with care.

5.1.4 Friction ratio R_f

The friction ratio R_f is equal to the ratio of the friction resistance over the cone resistance ($R_f = f_s / q_c \times 100\%$) at the same depth. In order to calculate R_f, one must account for the fact that the center of the friction sleeve is approximately 4 in. (10 cm) behind the cone tip. Indeed, at a time t, the recorded values of $q_c(t)$ and $f_s(t)$ are not measured at the same depth. So, if the rate of penetration is 2 cm/sec, the friction ratio at a given depth is:

$$R_f = \frac{f_s(t + 5\,\text{sec})}{q_c(t)} \tag{5.4}$$

It is common to compare f_s with the average of q_c measured over the depth where f_s is measured (Zuidberg, 1991).

5.2 Data Presentation and Report

5.2.1 Data presentation

The CPT and CPTU results should be reported on graphs (Fig. 5.2). The following plots shall be given:

<u>CPT</u>

1. Cone resistance q_c versus depth.
2. Friction resistance f_s versus depth.
3. Friction ratio $R_f (= f_s / q_c \times 100\%)$ versus depth.

<u>CPTU</u> In addition to 1, 2, 3 above the following is given:

4. Corrected cone resistance q_T versus depth.
5. Corrected friction resistance f_T versus depth.
6. Friction ratio, $f_T / q_T \times 100\%$ versus depth.
7. Corrected pore pressure u_T versus depth.
8. $B_q = \Delta u / (q_T - \sigma_{vo})$ versus depth, where $\Delta u = u_T - u_o$, u_o = hydrostatic pressure, σ_{vo} = total vertical stress.

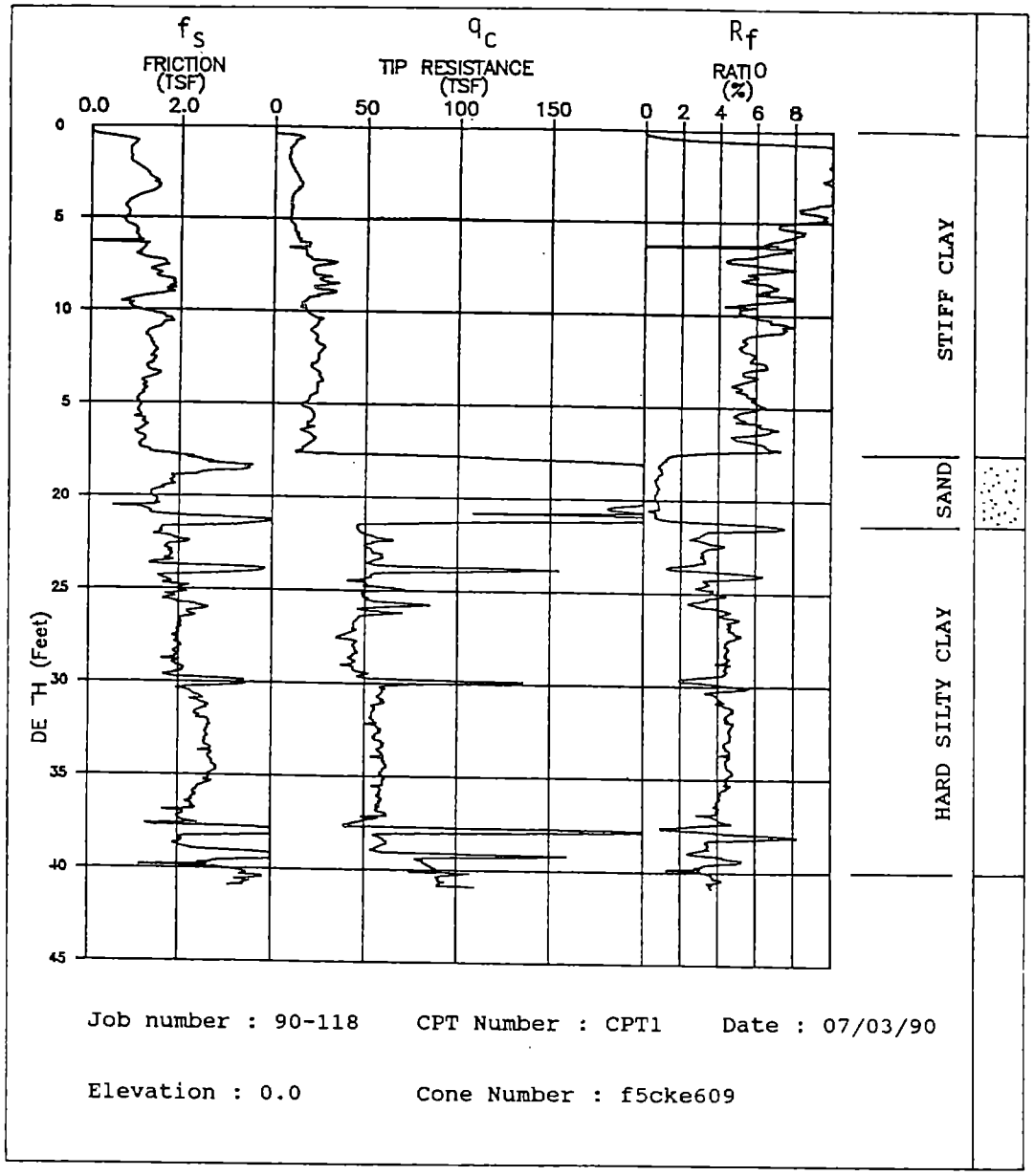

FIG. 5.2. Data Presentation for a CPT

The following information shall be reported on the graphs.

1. The date and the time of the test, and the name of the firm.
2. The number of the test and its location.
3. Any abnormal interruption of the reference procedure (chapter 4).
4. The identification number of the penetrometer tip.

5.2.2 Report

The report should include all the informations and plots described in section 5.2.1. In addition, the following informations should be included:

1. Refusal criteria (rod buckling, total capacity exceeded, target depth achieved).
2. The dates and reference numbers of the calibration certificates for the measuring devices.
3. The zero readings of all sensors before and after the test.
4. The maximum test inclination.
5. A clear indication of the location of the porous filter.
6. The name of the operator who performed the test.

5.3 Precision and Accuracy of the Measurements

The accuracy of the CPT method is estimated as follows (ASTM D 3441-86):

- Mechanical tips: Standard deviation of 10% for q_c and 20% for f_s
- Electrical tips: Standard deviation of 5% for q_c and 20% for f_s

The electric cone accuracy is influenced by the zero load error and the calibration error (see section 3.1). The zero load error should in general not exceed 0.5% to 1% of the full scale output, and in soft soil this error should be less than 0.5% of the full scale output.

The accuracy of the measurement of q_c also depends on the type of soil. If the soil is very soft the cone resistance q_c will be small and will be obtained with less accuracy than in stiff soils. The ISSMFE (1988) reference test procedure requires the precision of the measurement to be less than 5% of the measured value or 1% of the maximum of the measured resistance in the layer under consideration, whichever is greater.

6. INTERPRETATION OF THE DATA

6.1 Stratigraphy

Stratigraphy evaluation is the CPT's primary purpose and there is no other conventional geotechnical tool which can match the CPT for layer definition and low cost per foot. The problem in the past has been that engineers plan a CPT investigation just like they would for borings, which is wrong. Borings are for retrieving soil samples and the CPT is for stratigraphy and simplified parameter evaluation. Therefore, perform the CPT at the site before the borings. Define soil layers in the office using CPT data and determine where to retrieve the few important soil samples during the subsequent limited boring program. Plan to use all of these expensive boring soil samples for laboratory tests, either index tests (i.e. sieve, PI, etc.), or quality tests (i.e. consolidometer, triaxial, etc.). Do not take boring soil samples for the sake of stratigraphy because the CPT is better and less expensive.

An important but little known observation is that some over-consolidated clays have the potential for classifying as loose sand using any CPT classification. Therefore when a loose sand layer is detected based on CPT data and the general site geology is not known, a soil sample from that layer should be retrieved for verification.

Examples of CPT profiles and possible interpretation are given in Figs. 6.1, 6.2 and 6.3 (Schmertmann, 1978). During the profile interpretation it must be kept in mind that the cone penetrometer resistance q_c will go through a smooth transition at layer interfaces. According to Schmertmann (1978) the transition zone extends about 7 CPT diameters on either side of the interface (Fig. 6.4). This transition zone thickness varies with the soil stiffness. Therefore, in very stiff layers thinner than approximately 60 cm (2 ft), and soft layers thinner than approximately 20 cm (8 in.), the q_c reading will not reach its full value. It should also be noted that a spike may appear on the profile every time the downward push is released, another rod is added, and the downward push is re-applied.

Also, the development of stratigraphic profiles requires looking not only at material type but also at the magnitude and signature of the cone readings in each material type to assess continuity. For example, the location of rising and falling resistances within a layer resulting from a deposition history is an important clue to the continuity of that particular layer. This profiling step always needs to be done in the primary idealization of the site.

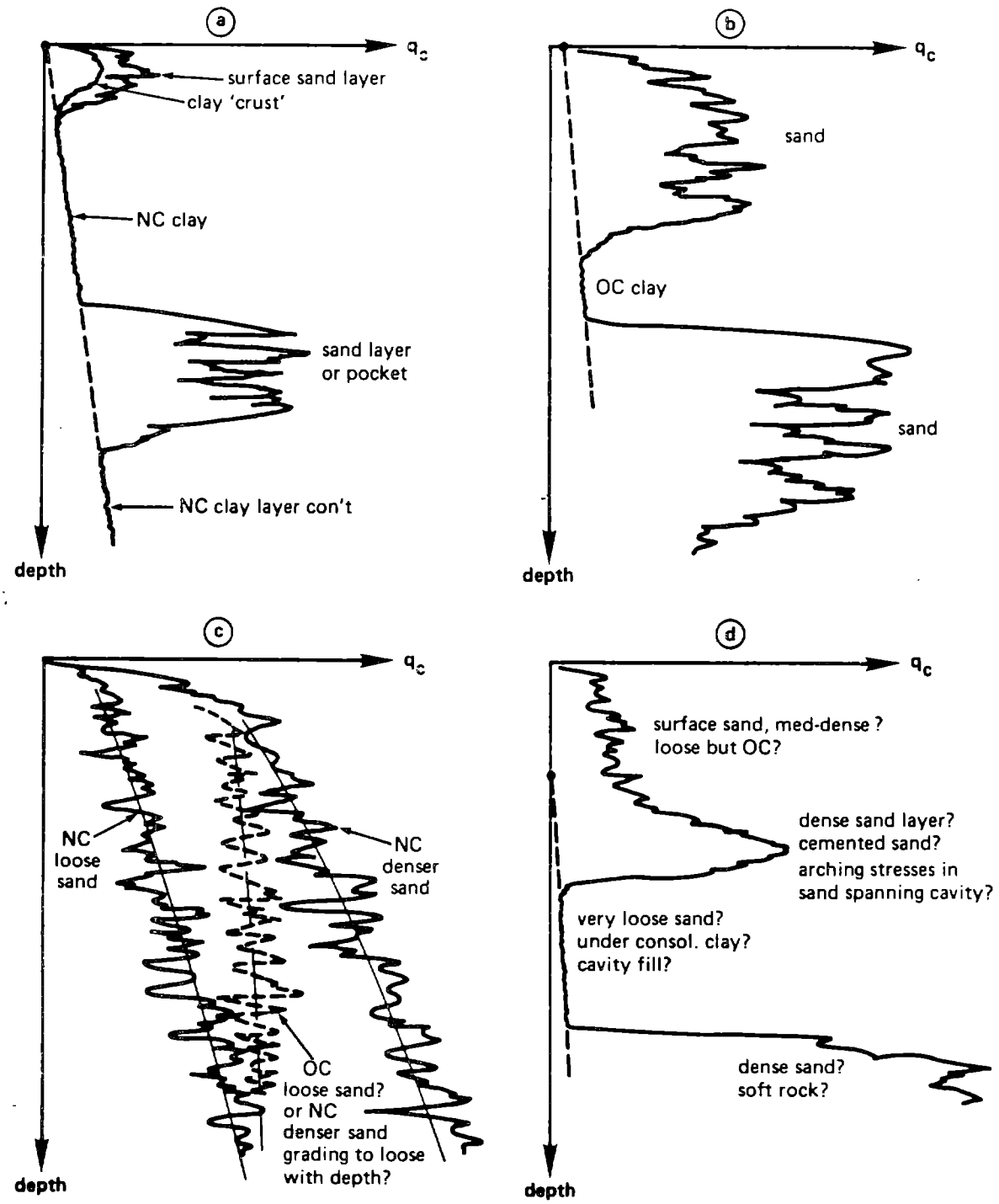

FIG. 6.1. Simplified Examples of q_c-Log Profiles Showing Likely and Possible Interpretations for Soil Types and Conditions (from Schmertmann, 1978)

In the first place one can determine quickly the trend of the layers in the vertical and horizontal directions.

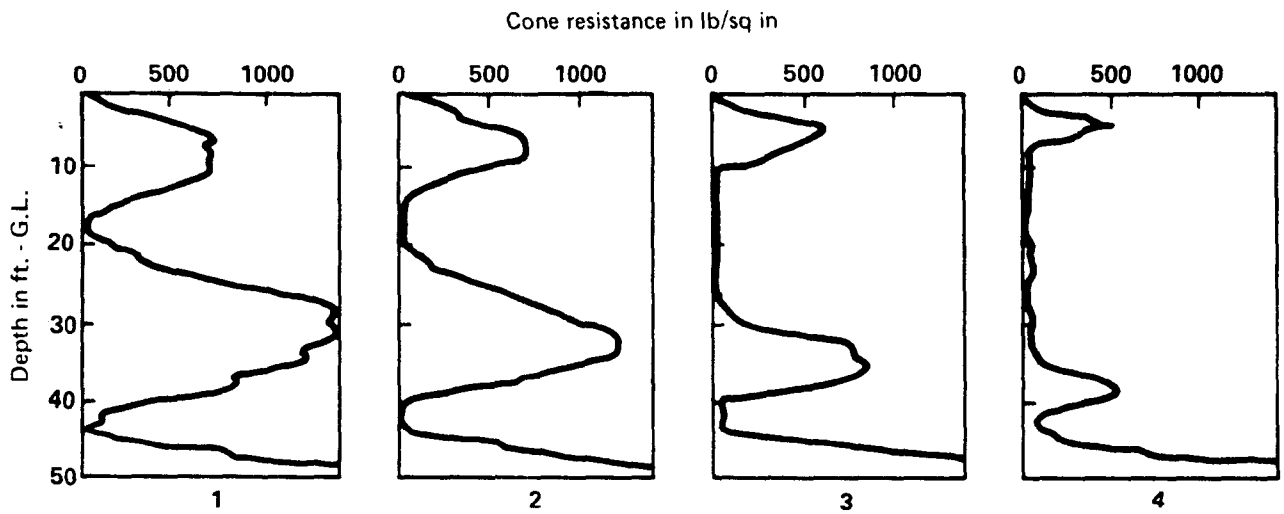

This will be seen from the following simple example. In this case, a light building could be founded on the upper sand layer, although it will be immediately clear that more settlement will take place at sounding 4 than at sounding 1 owing to the greater thickness of the soft layers. For heavier buildings, a pile foundation will be necessary because of its small thickness at position 4 and its rather poor quality at 2 and 3. The piles should be placed in the third sand layer.

FIG. 6.2. Example (from Begemann, 1963) Showing the Use of CPT q_c Profiles to Discover the Variation in Thickness and Quality of Potential Pile Bearing Layers Across a Site (from Schmertmann, 1978)

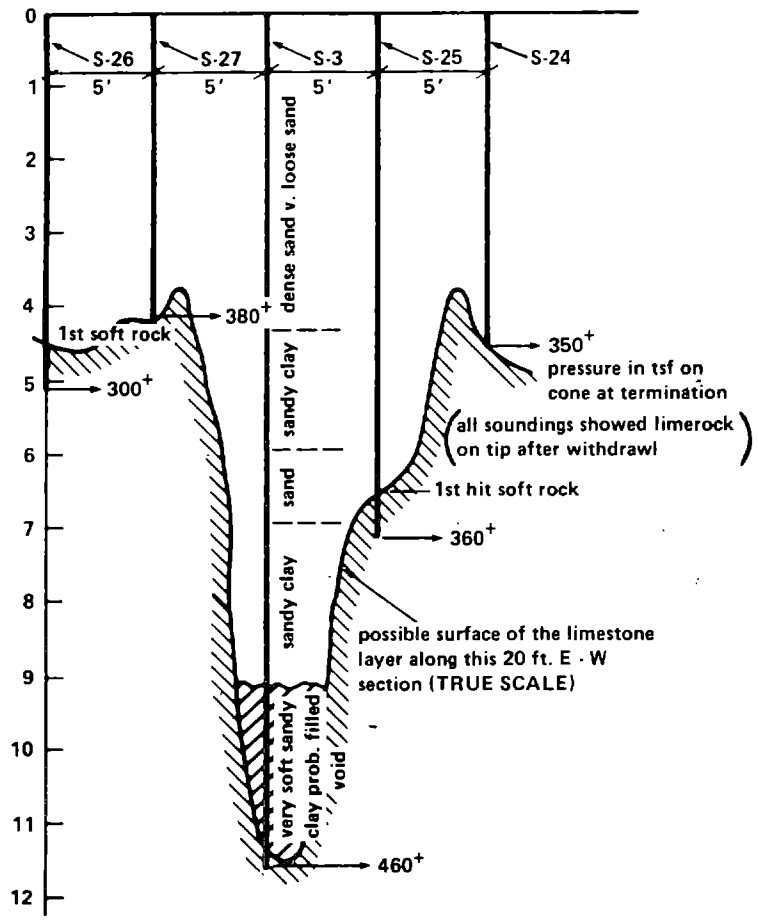

Note: Soundings S-24, -25, -26 and -27 made with Dutch mantle cone tip, advanced without gage readings, for the purpose of quickly better defining the nature of the rock surface and the likely geometry, in section, of any cavities above this rock.

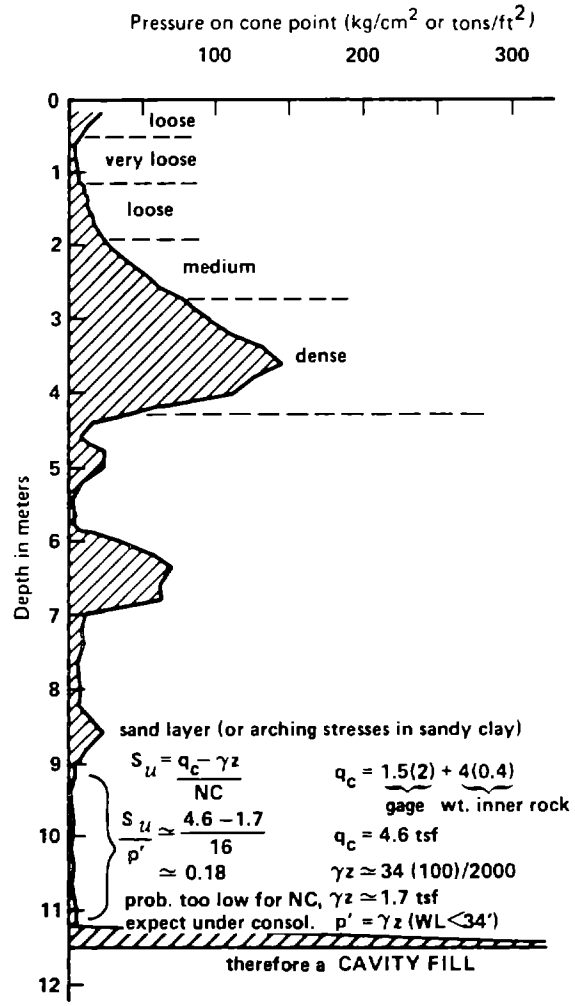

Above: Cone bearing log of S-3. Also illustrates calculated low s_u/p' ratio indicating probable cavity fill.

FIG. 6.3. Example of the Use of Static Cone Soundings to Quickly Check Rock Surface Profile and Confirm Pothole and Probably Underconsolidated Clay Nature of Cavity Fill (from Schmertmann, 1978)

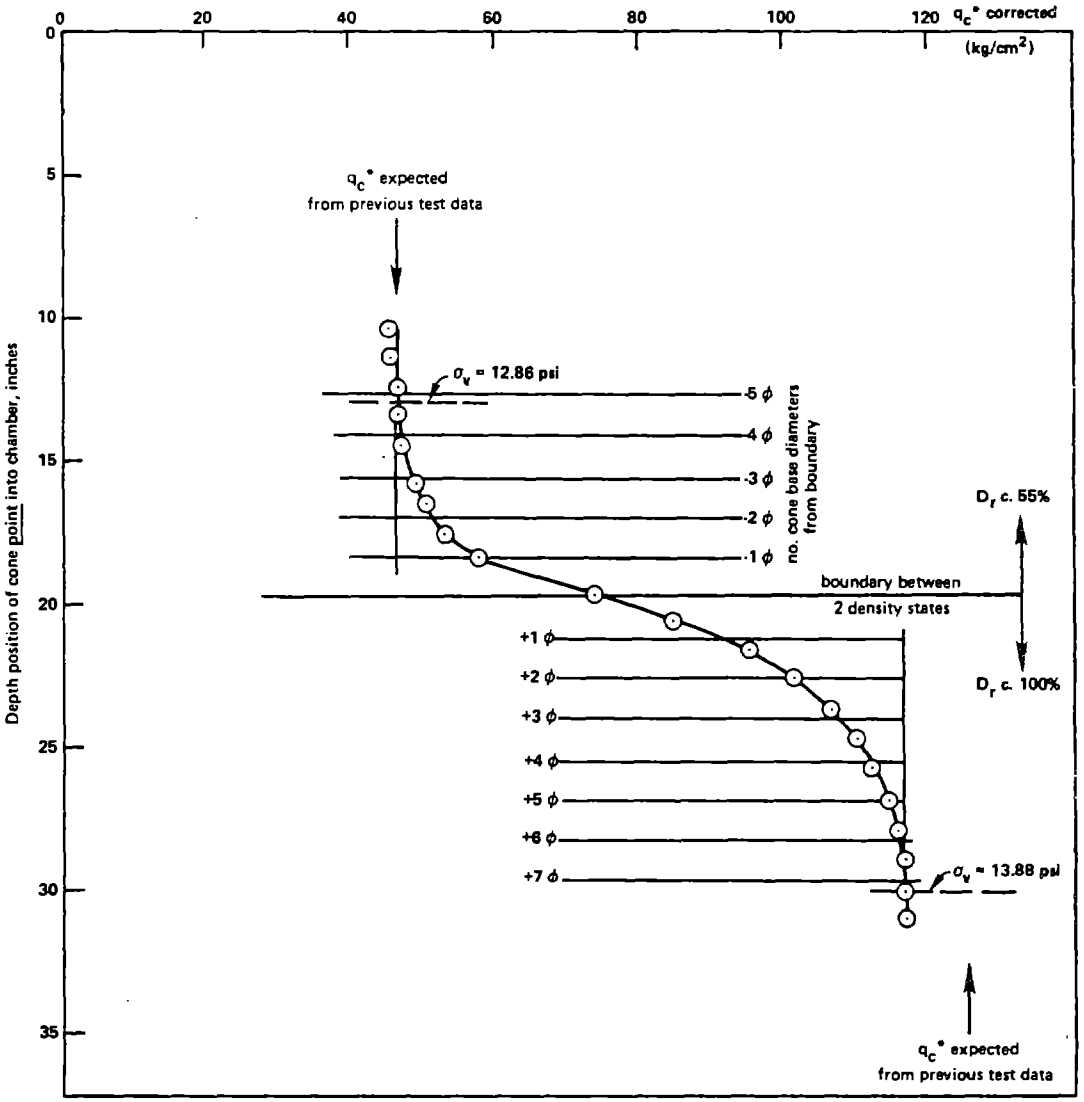

FIG. 6.4. Penetration of Fugro-Type Tip Through Loose to Dense Sand Boundary (q_c During Cone Advance Only) (from Schmertmann, 1978)

There is a growing use of the piezo-cone for stratigraphy evaluation. The pore pressure record provides a much more sensitive means to detect thin soil layers. This could be very important in determining consolidation rates in a clay with thin sand seams. The piezo-cone also has the potential to provide consolidation rate parameters.

6.2 In Situ Horizontal Stress

It is very difficult to obtain a reliable measure of the in situ horizontal stress at rest σ_{ho} because any tool designed to measure σ_{ho} directly disturbs the soil in the process. With the CPT, any attempt to obtain σ_{ho} has to be based on correlations between CPT parameters and quality direct measurements of σ_{ho}. The scarcity of such quality data and the correlation aspect of the methods lead to poor reliability.

Masood (1988) proposed a method which seems to give results within a reasonable range; tests at two sites in California reported by Masood et al. (1988) gave K_o values comparing well with those determined by other in situ tests. The approach is based on the use of the sleeve friction f_s, the overconsolidation ratio OCR (see section 6.9) and the vertical effective stress σ'_{vo}. Fig. 6.5 is then entered with f_s/σ'_{vo} and OCR in order to obtain K_o. Then,

$$\sigma'_{ho} = K_o \sigma'_{vo} \tag{6.1}$$

In view of the precision and accuracy of f_s, this method can only be considered as a rough guess.

The purpose of the lateral stress cone (section 1.1) is to obtain a better estimate of σ'_{ho}, but at present this is still an uncertain approach.

6.3 Soil Classification

Several soil classification charts based on the CPT or the CPTU data have been proposed. They make use of the measured cone resistance q_c and either the friction ratio R_f or the pore pressure ratio B_q. These charts should only be used as guides, and it may happen that a soil will fall within different zones of classification on each chart. In this case, engineering judgement as well as local experience may help to correctly classify the soil behavior type. In all cases the CPT and these classification charts should be used with the recovery of a minimum number of samples in order to ensure reliability of classification, unless the work is performed in a well defined region with much previous experience.

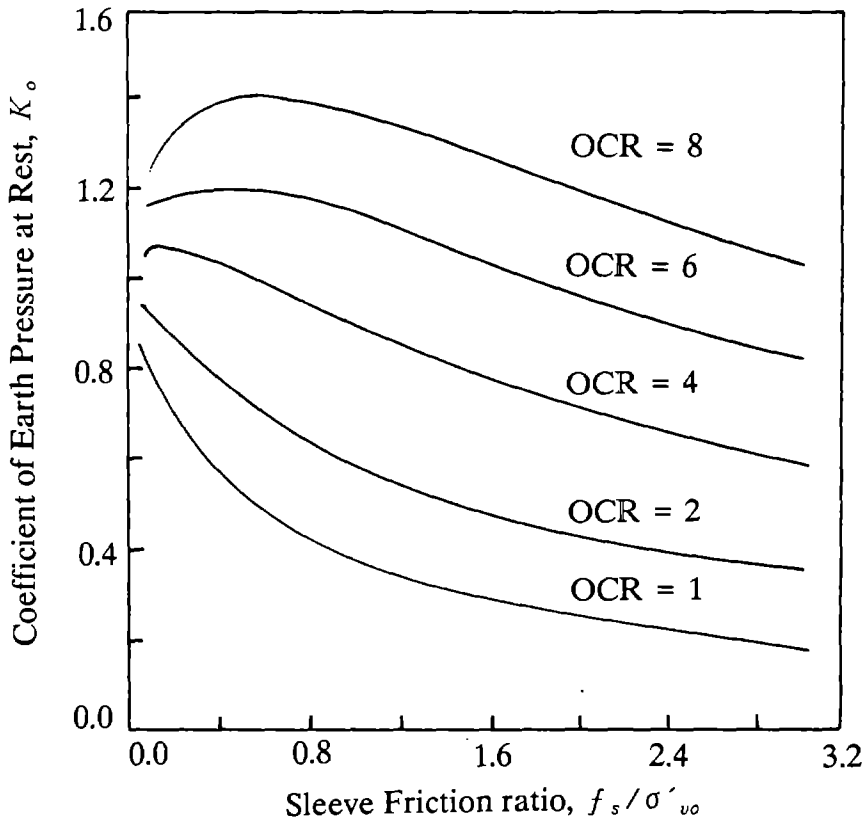

FIG. 6.5. K_o **as a Function of CPT Sleeve Friction and Overconsolidation Ratio (from Masood, 1988)**

CPT - In 1981, Douglas and Olsen proposed a chart which makes use of q_c and R_f. The friction ratio is R_f: $R_f = f_s/q_c \ x \ 100\%$ or $f_s/q_T \ x \ 100\%$. The chart provides a better understanding of the factors influencing the parameters q_c and R_f (Fig. 6.6). A simplified version of this chart was presented by Douglas in 1984 (Fig. 6.7). This chart makes use of the cone resistance q_{cl} normalized for overburden pressure and is recommended for use. The parameter q_{cl} is calculated by using the formula:

$$q_{cl} = q_c(1 - 1.25\log_{10}\sigma'_{vo}) \qquad (6.2)$$

where σ'_{vo} (tsf) is the effective overburden pressure. The use of q_{cl} instead of q_c will help to classify the soil with more accuracy because it accounts for the fact that q_c will increase with depth in a uniform deposit. The use of q_c alone in this case might lead to a gradual change in the soil's apparent classification as the penetration of the CPT increases.

CPTU - Experience shows as discussed at the end of section 2.1 that friction sleeve measurements depend to a certain extent on the cone design, and are sometimes less accurate and reliable than the tip resistance measurement (Robertson and Campanella, 1988). To overcome these problems, and to improve the method of classification, several authors proposed to use the pore pressure ratio B_q (calculated from the CPTU data) in addition to q_T and R_f. These parameters are defined as follows; q_T is the total cone resistance corrected for unequal pore pressure effects (section 5.1.2):

$$q_T = q_c + u_T(1 - a) \qquad (6.3)$$

where a = net area ratio A_q/A_N and u_T is the pore pressure measured behind the tip. The definitions of A_q and A_N are given on Fig. 5.1 and in section 5.1.2.
The pore pressure ratio is B_q: $B_q = \Delta u/(q_T - \sigma_{vo})$, where Δu = excess pore pressure $= u_T - u_o$ and σ_{vo} = total vertical stress.

The chart by Robertson (1990) is recommended (Fig. 6.8). When the value of q_T and B_q are not available, Fig. 6.8 can still be used to provide a reasonable estimate of soil type. In this case Fig. 6.8 is entered with q_c (from a CPT) instead of q_T (Robertson, 1985). The corrected tip q_T is only important in soft clays and silts where the cone resistance is low and pore pressures are high (Robertson, 1990). In all cases the f_s is used.

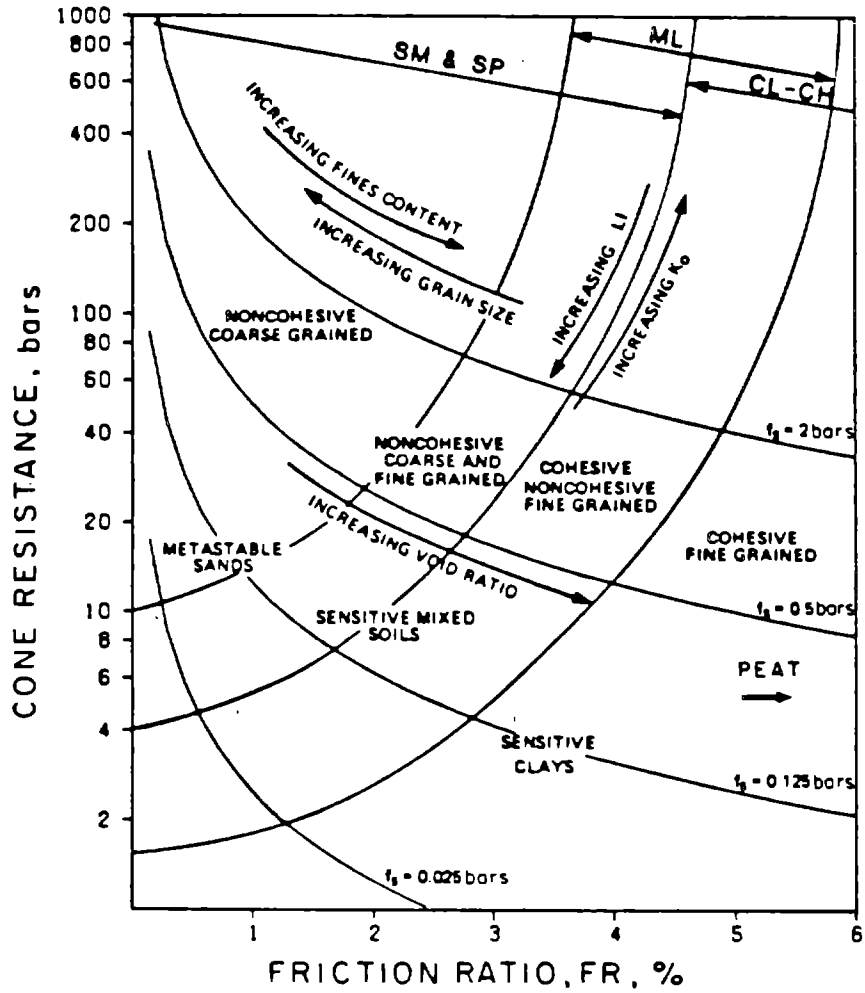

1 bar = 100 kPa ≈ 1 kg/cm²

FIG. 6.6. CPT Soil Behavior Chart (from Douglas and Olsen, 1981)

$$q_{cl} = q_c(1 - 1.25\log_{10}\sigma'_{vo})$$

with $\sigma'_{vo}, q_c, q_{cl}$ in bars or tsf.

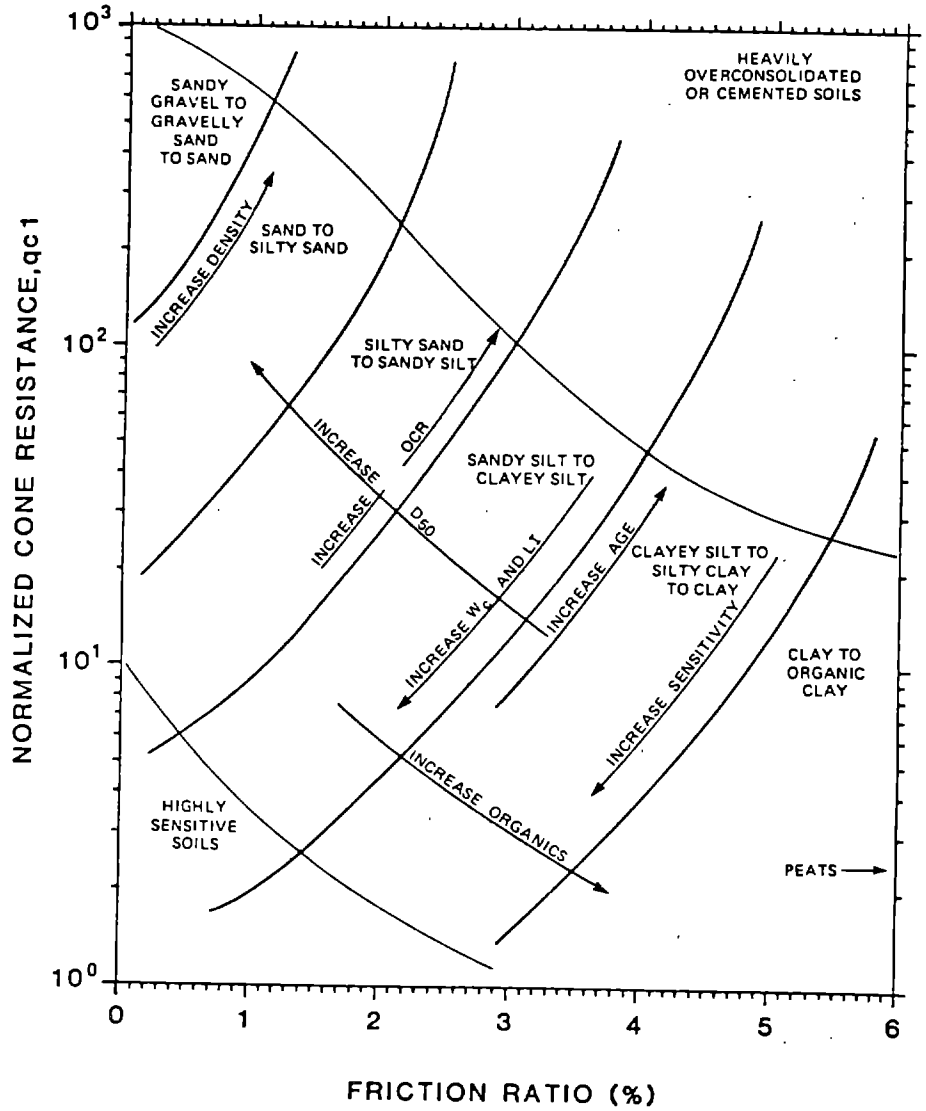

FIG. 6.7. Simplified Soil Behavior Type Classification Chart (from Douglas, 1984)

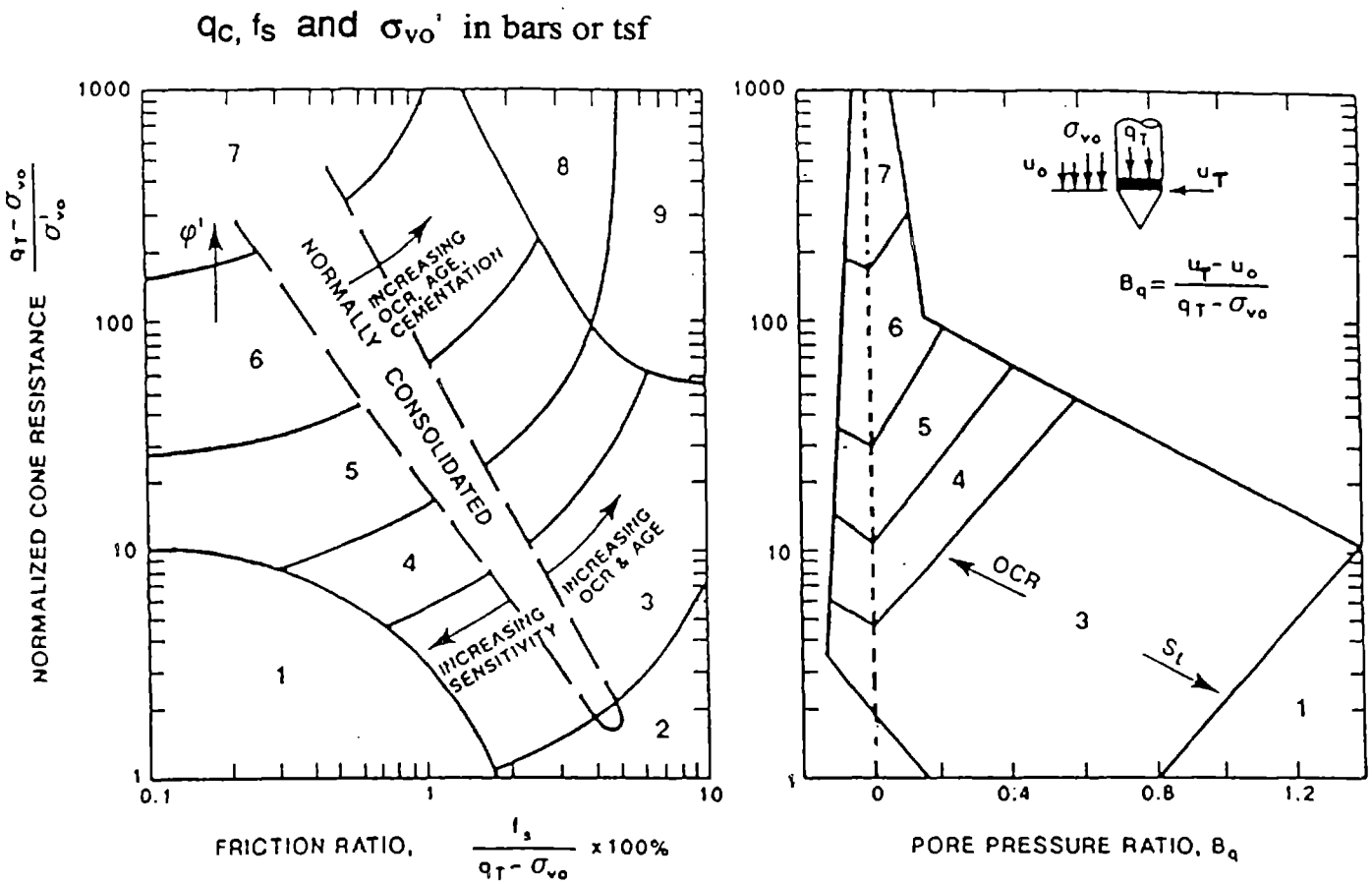

1. Sensitive fine grained
2. Organic soils - peats
3. Clays - clay to silty clay
4. Silt mixtures - clayey silt to silty clay
5. Sand mixtures - silty sand to silty silt
6. Sands - clean sand to silty sand
7. Gravelly sand to sand
8. Very stiff sand to clayey sand (heavily overconsolidated or cemented)
9. Very stiff fine grained (heavily overconsolidated or cemented)

FIG. 6.8. Soil Behavior Type Classification Charts for CPT (after Robertson, 1990)

6.4 In Situ Density Dr

Chamber tests on sands (Schmertmann, 1978; Baldi et al., 1981; Villet and Mitchell, 1981) show that the compressibility and the grain size of the material are the main factors which influence the determination of Dr from CPT measurements. So far, the method proposed by Baldi et al. (1986) seems to give relatively accurate results, although it is only recommended for normally consolidated, uncemented, unaged quartz sands of moderate compressibility (R_f of about 0.5%) with $K_o = 0.45$ (Robertson and Campanella, 1988). Fig. 6.9 shows Baldi's relationship between Dr, vertical effective stress (σ'_{vo}), and cone resistance (q_c). The coefficients C_0, C_1, C_2 in the equation on Figure 6.9 are regression coefficients for the curves shown and R is the parameter indicating the goodness of fit.

Lunne and Christoffersen (1983) recommend reducing q_c for overconsolidated sands (q_{coc}) to an equivalent normally consolidated resistance (q_{cnc}) by estimating the OCR and using the following equation:

$$\frac{q_{coc}}{q_{cnc}} = 1 + 0.75\left(\frac{K_{ooc}}{K_{onc}} - 1\right) \tag{6.4}$$

$$\frac{K_{ooc}}{K_{onc}} = OCR^{.45} \tag{6.5}$$

Jamiolkowski et al. (1985) proposed a chart which can be used as a guide to adjust the correlation by Baldi et al. (1986) for sands that may be more or less compressible (Fig. 6.10).

For those soils which are not quartz sands, Fig. 6.11 based on the soil classification chart by Douglas and Olsen (1981) shows general trends for relative density. This chart uses q_{c1}, the cone resistance normalized for overburden pressure using the following equation:

$$q_{c1} = q_c(1 - 1.25\log_{10}\ \sigma'_{vo}) \quad \text{with} \quad \sigma'_{vo} \quad \text{in} \quad \text{tsf} \tag{6.6}$$

6.5 Friction Angle ϕ'

Several correlations have been proposed between the cone resistance q_c and the peak friction angle ϕ' measured in triaxial tests. Unfortunately, these correlations cannot account for soil compressibility which influences the cone resistance.

Lunne (1991) recommends estimating ϕ' from the following three different approaches and choosing the ϕ' value that is most conservative for the problem at hand.

First, use a correlation between Dr and ϕ', or run triaxial tests after finding Dr from section 6.4.

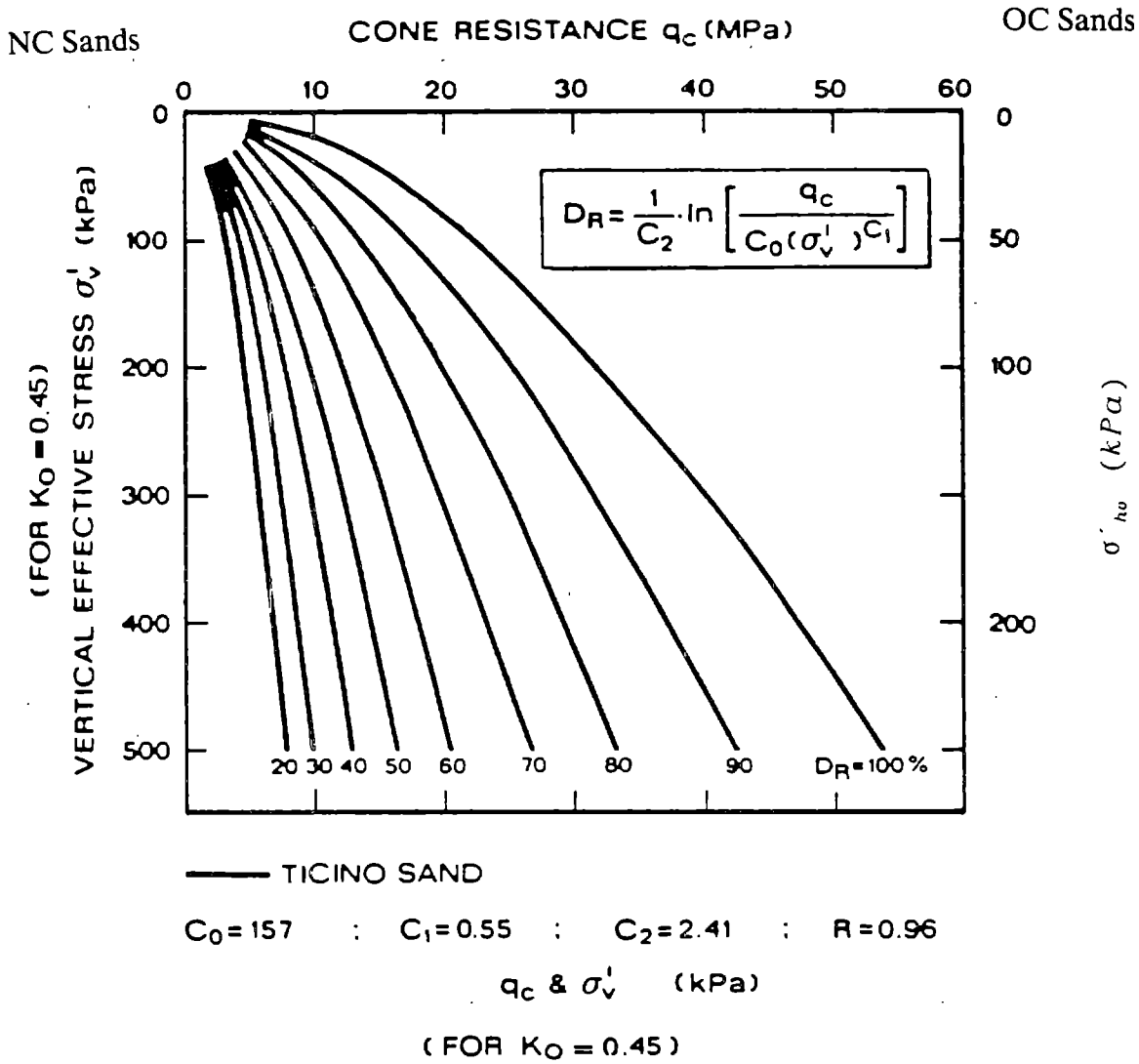

FIG. 6.9. Relative Density Relationship for N.C., Moderately Compressible, Uncemented, Unaged Quartz Sands (from Baldi et al., 1986)

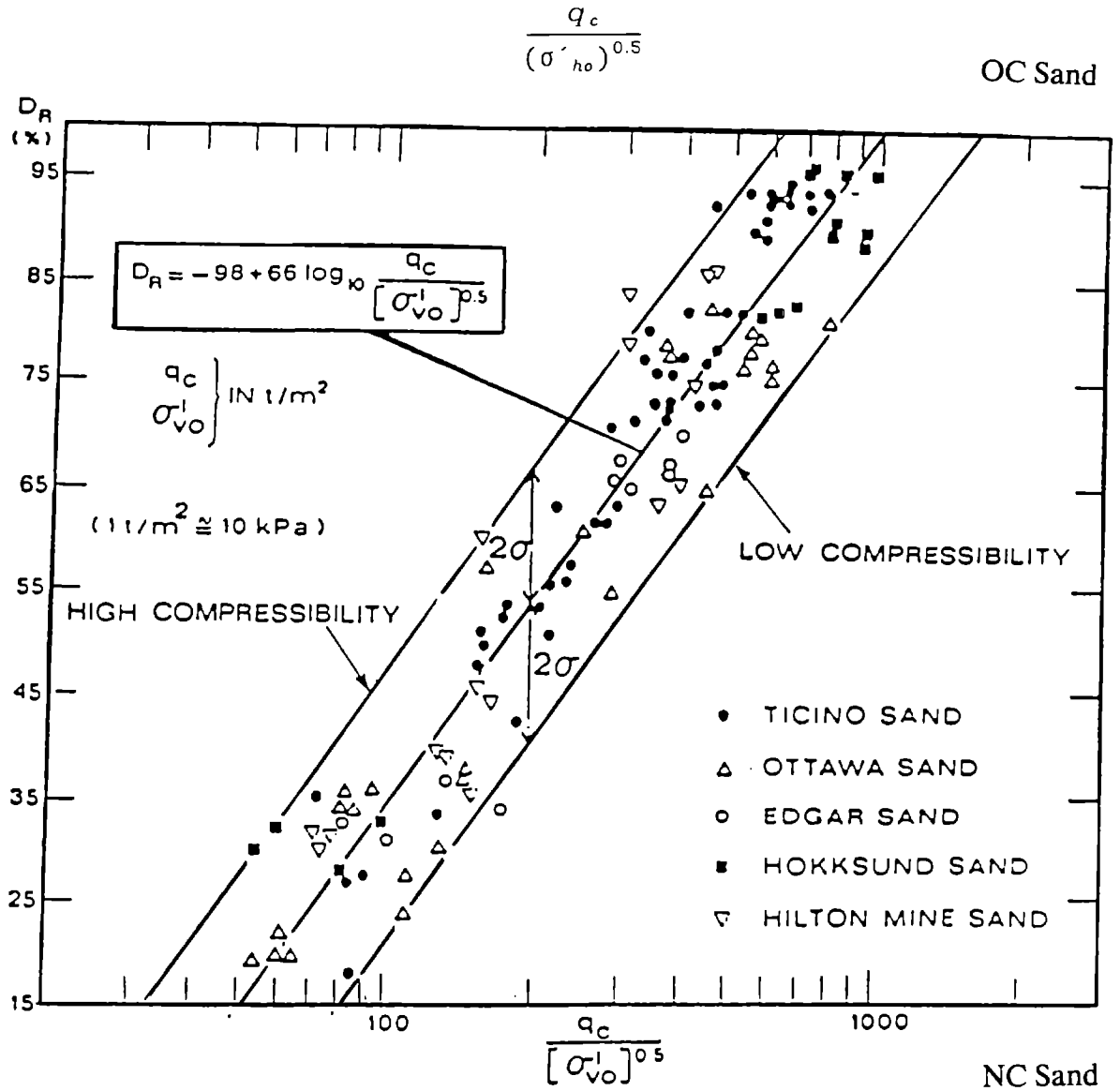

FIG. 6.10. Influence of Compressibility on N.C., Uncemented, Unaged, Predominantly Quartz Sands (after Jamiolkowski et al., 1985)

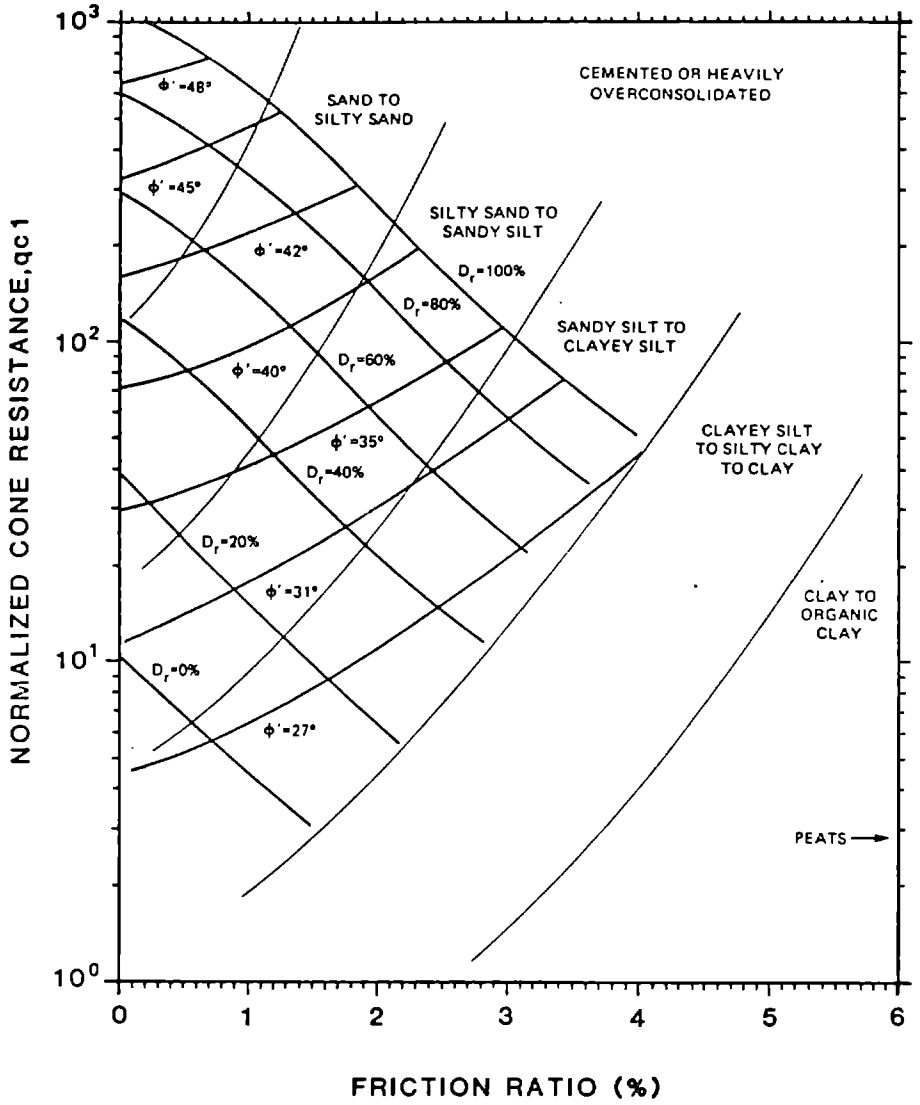

FIG. 6.11. Expanded Soil Behavior Type Classification Chart with Equivalent Overburden Normalized Friction Angle and Relative Density Trends (from Douglas, 1984)

Second, for moderately compressible (R_f of about 0.5%), normally consolidated, uncemented, predominantly quartz sands, the empirical correlation proposed by Robertson and Campanella (1983) can be expected to provide reasonable estimates of ϕ' (Robertson and Campanella, 1988). However, this method may underestimate ϕ' when R_f is higher than 0.5%, or overestimate ϕ' if the sand is overconsolidated. To use this method it is necessary to measure q_c and estimate σ'_{vo}. Then, one can enter Fig. 6.12 to obtain the peak friction angle ϕ'.

For sands which are not moderately compressible, Fig. 6.13 will help to adjust the results from Fig. 6.12.

Third, use Durgunoglu and Mitchell (1975) approach

They proposed that q_c could be estimated for cohesionless soils by

$$q_c = \rho g B N_{\gamma q} E_{\gamma q} \tag{6.7}$$

where

ρ = soil mass density

g = acceleration of gravity

B = diameter of cone

$N_{\gamma q}$ = bearing capacity factor for the surcharge-friction term and can be calculated by

$$N_{\gamma q} = \frac{\cos(\psi-\delta)}{\cos\delta}\frac{(1+\sin\phi_{ps}\sin(2\gamma-\phi'_{ps}))}{\cos\phi'_{ps}\cos(\gamma-\phi'_{ps})}\{\frac{\cos^2(\gamma-\phi'_{ps})}{4\cos^2\psi\cos^2\theta}I_\theta$$

$$+\frac{3\cos(\gamma-\phi'_{ps})\cos^2\beta}{4\cos\psi\cos\phi'_{ps}}e^{2\theta_o\tan\phi'_{ps}}\left(m-\frac{2}{3}m'\right)-K\frac{\cos\psi\cos\phi'_{ps}}{\cos(\gamma-\phi'_{ps})}$$

$$\cdot(m-m')^2\cdot(m+2m')+K\frac{\cos\psi\cos\phi'_{ps}}{\cos(\gamma-\phi'_{ps})}m^3\}-\frac{\tan\psi}{4} \tag{6.8}$$

$$m = D/B \tag{6.9}$$

$$m' = \frac{\sin\beta\cos(\gamma-\phi'_{ps})}{2\cos\psi\cos\phi'_{ps}}e^{\theta_o\tan\phi'_{ps}} \tag{6.10}$$

$$\tan\gamma = (\sin\phi'_{ps}+\sqrt{1+2\cos\phi'_{ps}})/(2+\cos\phi'_{ps}) \tag{6.11}$$

$$\psi = 90^\circ-\alpha \tag{6.12}$$

$$\theta_o = 180^\circ-(\psi+\gamma)+\beta \tag{6.13}$$

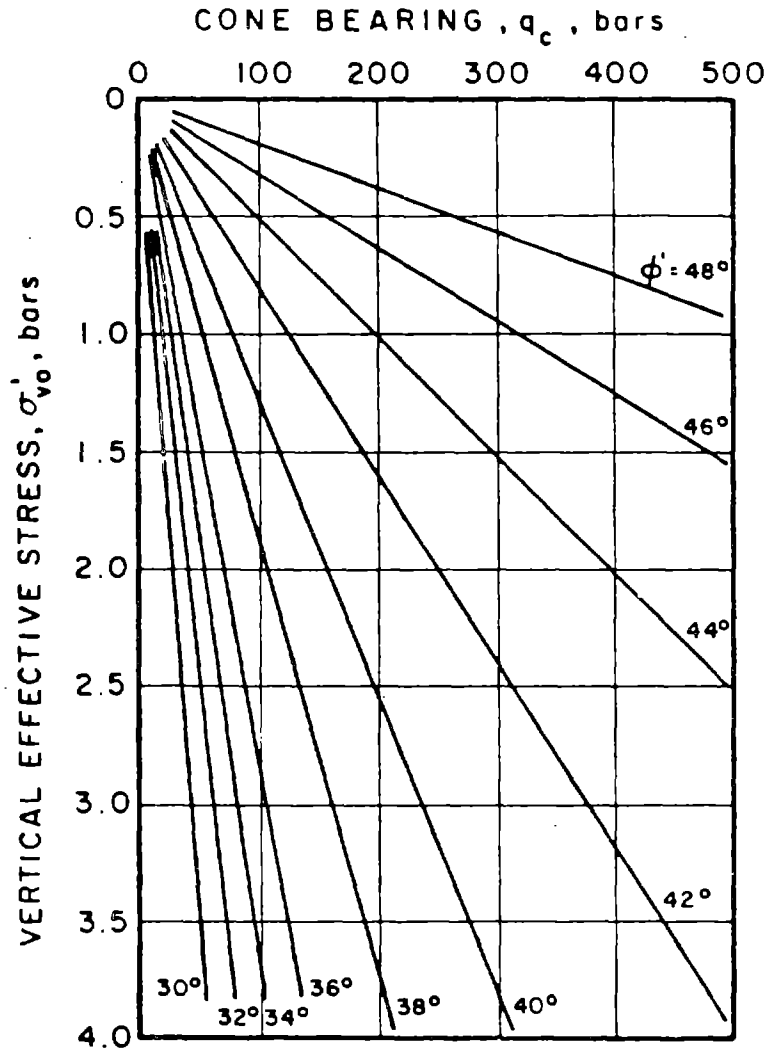

FIG. 6.12. Proposed Correlation Between Cone Bearing and Peak Friction Angle for Uncemented Quartz Sands (from Robertson and Campanella, 1983)

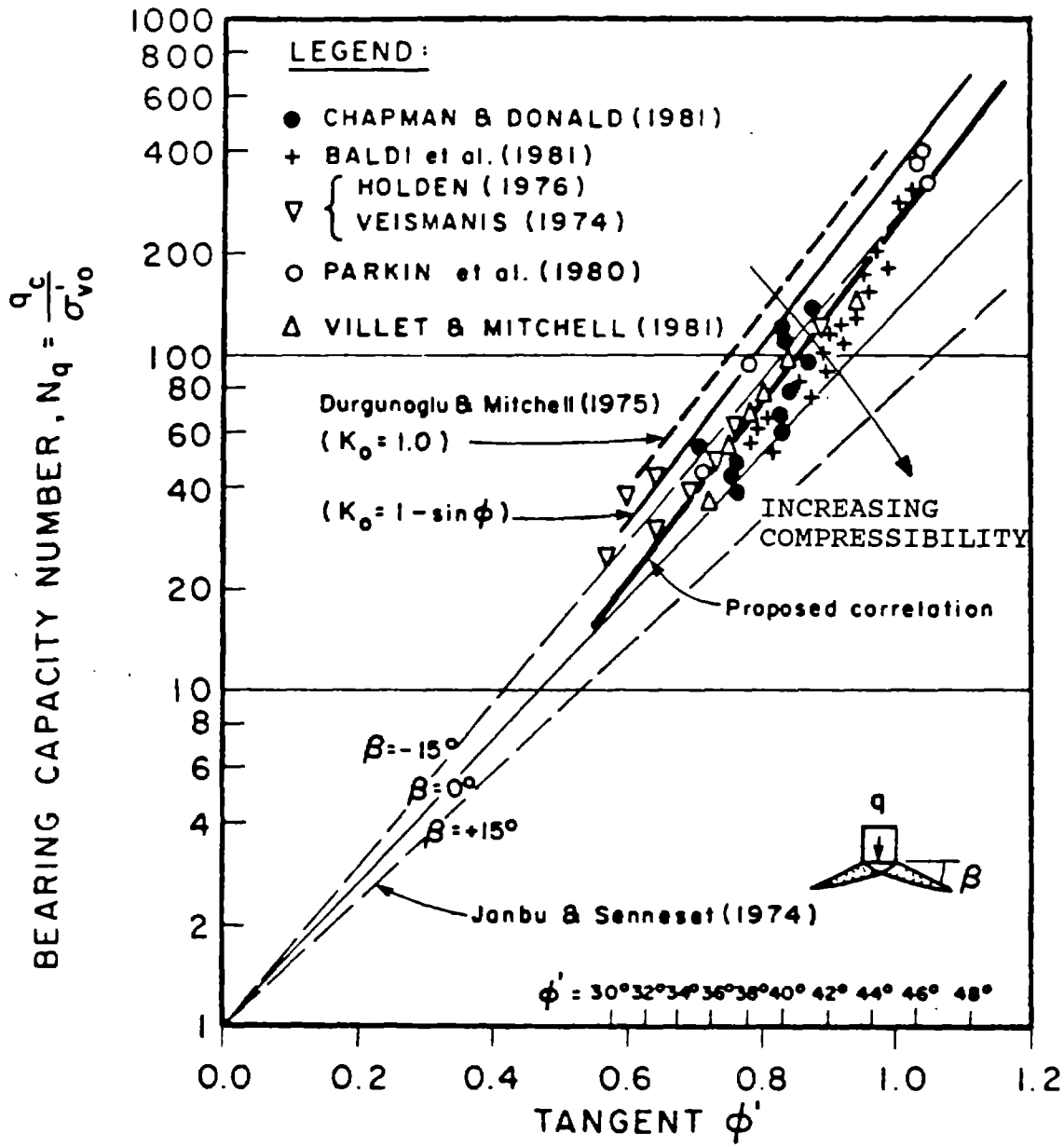

FIG. 6.13. Relationship Between Bearing Capacity Number and Friction Angle from Large Calibration Chamber Tests (from Robertson and Campanella, 1983)

$$I_\theta = \frac{1}{1+9\tan^2\phi'_{ps}}\{3\tan\phi'_{ps}\left\{e^{3\theta_o\tan\phi'_{ps}}\cos\beta - \cos(\theta_o-\beta)\right\}$$

$$+\left\{e^{3\theta_o\tan\phi'_{ps}}\sin\beta + \sin(\theta_o-\beta)\right\}\} \qquad (6.14)$$

where

$\psi, \alpha, \beta, \gamma, \delta$ = angles defined on Fig. 6.14,

M = ratio of penetrometer depth D to cone diameter B,

M' = ratio of distance between cone tip and vertical tangency of the failure surface to cone diameter,

θ_o = defines logarithmic failure surface angle,

K = coefficient of lateral earth pressure,

$\phi'_{\gamma s}$ = drain, plane strain, friction angle,

$E_{\gamma q}$ = shape factor which can be calculated as

$$E_{\gamma q} = (1.0 - 0.4B/L) + \frac{1.5}{B/D + \frac{1.5}{(0.6+\tan^6\phi'_{ps})B/L}} \qquad (6.15)$$

The solution of these equations to obtain ϕ involves an iterative procedure starting with an initial guess.

Fig. 6.11, based on the soil classification chart by Douglas and Olsen (1981), may also be used to estimate ϕ' as a function of q_{cl}, where

$$q_{cl} = q_c \ [1 - 1.25 \ \log_{10} \ \sigma'_{vo}] \qquad \text{(with } \sigma'_{vo} \text{ in tsf)} \qquad (6.16)$$

6.6 Constrained Modulus, M

Definition - Most correlations between in situ test results and the drained constrained modulus, M, refer to the tangent modulus, as found from oedometer tests, where an increase in pressure Δp is applied and results in a relative change in volume $\Delta V/V$.

$$M = \frac{1}{m_v} \quad \text{from oedometer tests} \qquad (6.17)$$

where m_v = volumetric compressibility = $(\Delta V/V/\Delta p)$.

Sand - Several correlations have been published in order to estimate the constrained tangent modulus of sands; these correlations are generally of the form:

$$M = \alpha q_c \qquad (6.18)$$

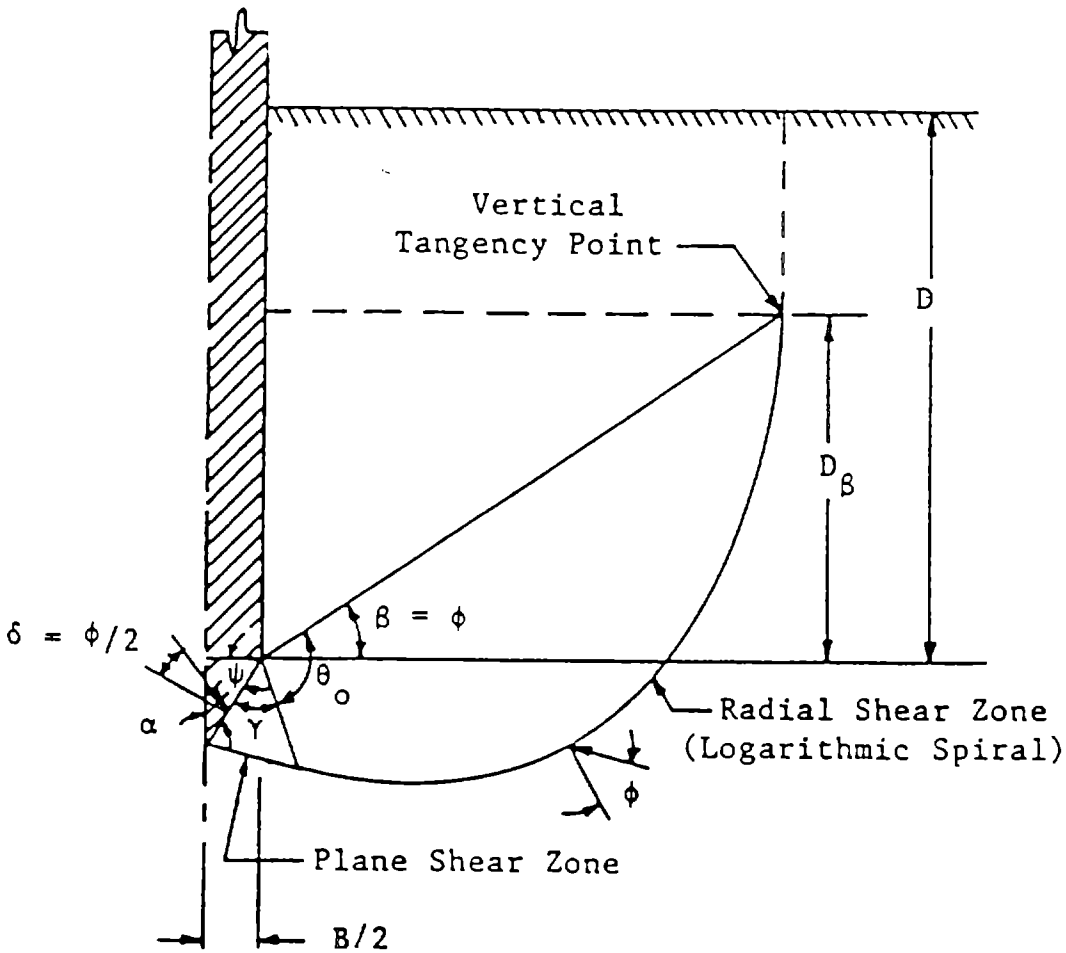

FIG. 6.14. Relationship of Bearing Capacity Parameters, Symbols Used and Assumed Failure Planes (after Durgunoglu and Mitchell, 1975)

The parameter α depends on the overconsolidation ratio OCR, the effective stress level, and the relative density Dr, for a given sand. (Figs. 6.15 and 6.16).

In 1983, Robertson and Campanella published a chart based on the cone resistance q_c, and the vertical effective stress σ'_{vo} to estimate the constrained tangent modulus of normally consolidated, uncemented quartz sands.

For overconsolidated sand the previous chart cannot be used since α increases with OCR for a given sand. In this case, it is recommended to use the chart by Jamiolkowski et al. (1988) (Fig. 6.16) which includes the influence of the overconsolidation ratio OCR, the mean effective stress and the relative density Dr. The coefficient C_0, C_1, C_2 in the equation on figure 6.16 are regression coefficients for the curves shown and R is the parameter indicating the goodness of fit. To use this chart in practice, it is necessary to estimate the value of the OCR, σ'_{vo}, K_o and Dr. Then σ'_m can be computed using

$$\sigma'_m = \frac{1}{3} \sigma'_{vo} (1 + 2K_o) \tag{6.19}$$

and Fig. 6.16 can be used with OCR, Dr and σ'_m in order to obtain M.

<u>Clays under Undrained Behavior</u> - So far the methods that have been proposed to predict the constrained modulus M of clays under undrained behavior lead to results that may be in error by $\pm 100\%$ (Robertson and Campanella, 1988). Therefore, the following method should only be used to provide a rough estimate of M.

In 1975, Mitchell and Gardner presented Table 6.1 for correlation between the cone resistance q_c and the constrained modulus M where

$$M = \alpha q_c \tag{6.20}$$

The α values are adapted from Sanglerat (1972).

<u>Note</u> - A small strain constrained modulus can also be measured by using compression wave data from the seismic cone penetrometer.

6.7 Young's Modulus, E

<u>Sand</u> - Since soils are nonlinear materials, the soil modulus depends on the spherical and deviatoric components of the stress tensor. Robertson and Campanella (1983) acknowledged this fact and presented a relationship between the cone resistance and the drained secant moduli at 25% (E_{25}) and 50% (E_{50}) of the failure deviator stress level, for different levels of vertical effective stress σ'_{vo}. More recently, Berardi et al. (1991) recommended Fig. 6.17 which shows the ratio of E (0.1%) to q_c as a function of q_c normalized with respect to the square root of σ'_{vo}. E (0.1%) is the modulus for a normal strain equal to 0.1%.

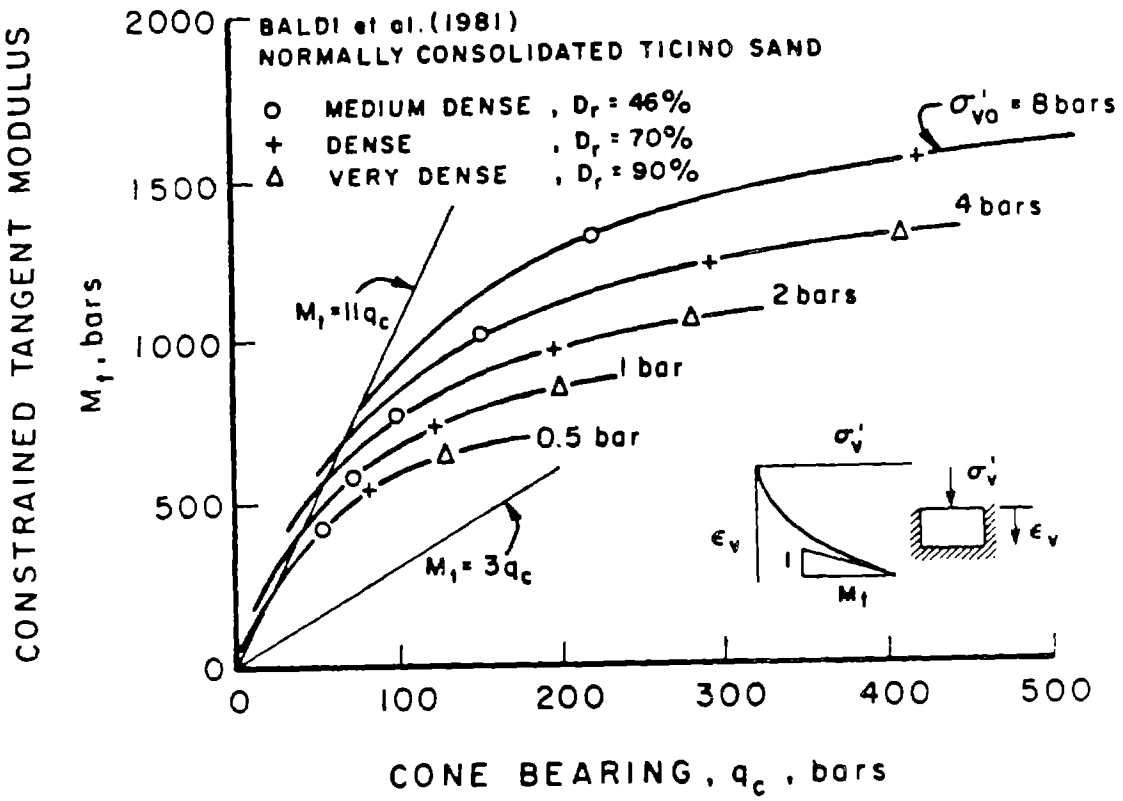

FIG. 6.15. Relationship Between Cone Bearing and Constrained Modulus for N.C., Uncemented Quartz Sands (based on data from Baldi et al., 1981) (from Robertson and Campanella, 1983)

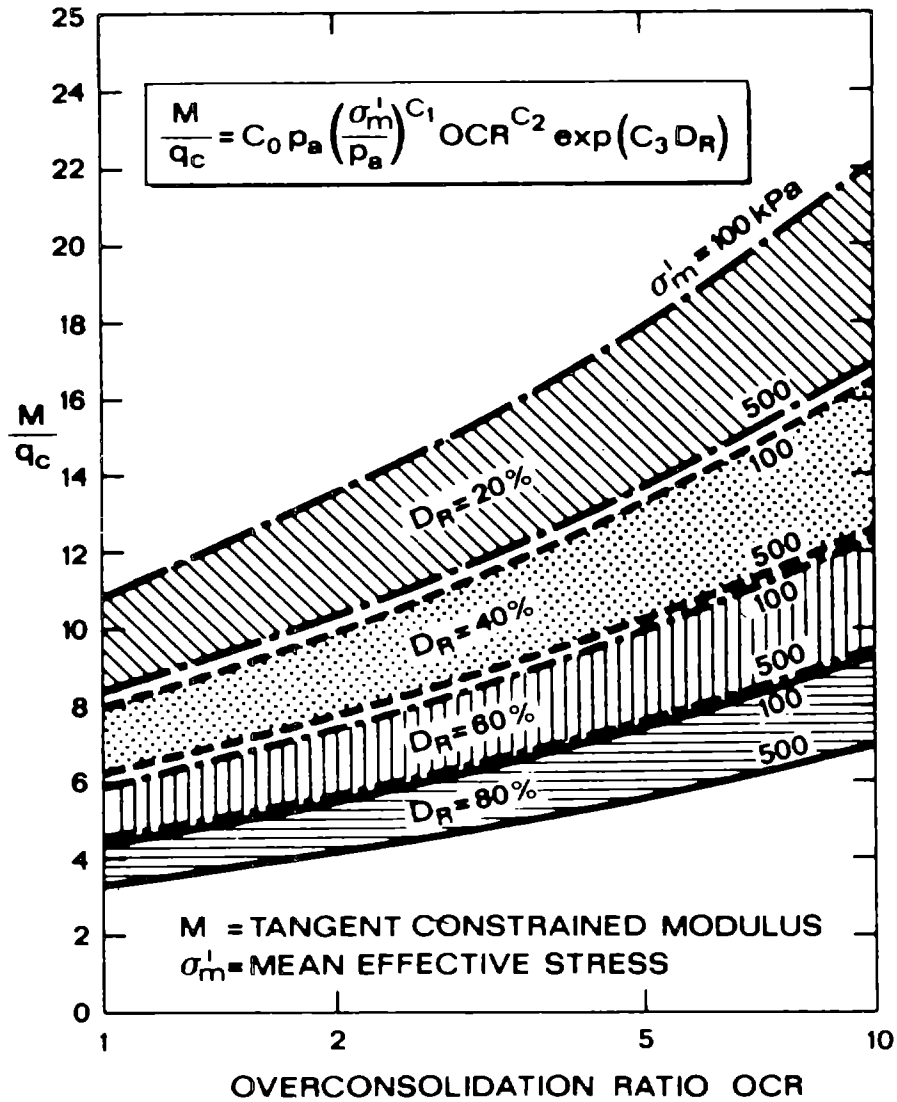

$C_0 = 14.48$; $C_1 = -0.116$; $C_2 = 0.313$; $C_3 = -1.123$; $R = 0.95$
$p_a = 1$ bar $= 98.1$ kPa

FIG. 6.16. Constrained Modulus of Sand from Cone Penetration Resistance (from Jamiolkowski et al., 1988)

Table 6.1 - Estimation of constrained modulus, $M = \alpha \cdot q_c$, for clays. (adapted from Sanglerat, 1972) (after Mitchell and Gardner, 1975)

q_c (bar)	α	Soil type
$q_c < 7$ $7 < q_c < 20$ $q_c > 20$	$3 < \alpha < 8$ $2 < \alpha < 5$ $1 < \alpha < 2.5$	Clay of low plasticity (CL)
$q_c > 20$ $q_c < 20$	$3 < \alpha < 6$ $1 < \alpha < 3$	Silts of low plasticity (ML)
$q_c < 20$	$2 < \alpha < 6$	Highly plastic silts and clays (MH, CH)
$q_c < 12$	$2 < \alpha < 8$	Organic silts (OL)
$q_c < 7$ $50 < w < 100$ $100 < w < 200$ $w > 200$	 $1.5 < \alpha < 4$ $1 < \alpha < 1.5$ $0.4 < \alpha < 1$	Peat and organic clay (P_t, OH)

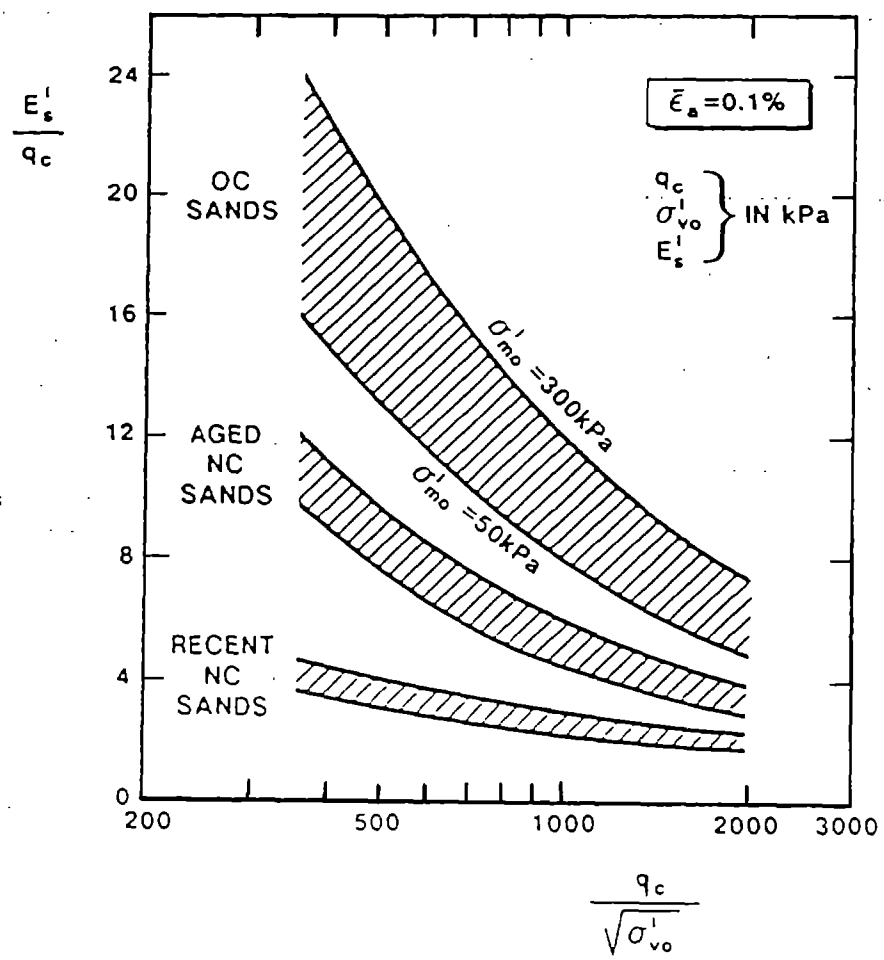

FIG. 6.17. Evaluation of Drained Young's Modulus from CPT for Silica Sands (from Berardi et al., 1991)

Clay - Robertson and Campanella (1988) recommended the use of Fig. 6.18, based on work done by Ladd et al. (1977), which shows the variation of the undrained Young's modulus E_u divided by the undrained shear strength S_u as a function of the stress level for seven different cohesive soils. The recommended procedure is:

- o Estimate the undrained shear strength S_u (see section 6.11).
- o Estimate the overconsolidation ratio OCR (see section 6.9).
- o Using Fig. 6.18, estimate E_u from the stress level appropriate to the problem.

A knowledge of the plasticity index PI would help in this determination.

6.8 Maximum Shear Modulus, G_{max}

The maximum shear modulus G_{max}, or G_o in the figures, corresponds to very small strains.

Sand - In 1985, Jamiolkowski et al. argued that G_{max} and q_c are both functions of the same variables: density and effective vertical and horizontal stresses. Therefore, confidence can be placed on the estimate of G_{max} from q_c. Robertson (1990) proposed a correlation (Fig. 6.19) for normally consolidated, uncemented silica sands, where the maximum shear modulus G_{max} is a function of the cone resistance q_c and the vertical effective stress σ'_{vo}.

To use this method in practice, it is necessary to measure q_c and calculate σ'_{vo}.

Also available is a relationship proposed by Imai and Tonouchi (1982) between q_c and the SPT N value (Fig. 6.19):

$$G_{max} = 125N^{0.611} \quad with \quad N = \frac{q_c}{4.5} \tag{6.21}$$

with G_{max} and q_c in bars and N in blows per foot.

Jamiolkowski et al. (1988) proposed a relationship between G_{max}, q_c, Dr and the mean effective stress σ'_m.

$$\frac{G_{max}}{q_c} \simeq 30.1\, p_a \left(\frac{\sigma'_m}{p_a}\right)^{-0.08} \exp(-1.84Dr)$$

where p_a = 98.1 kPa and Dr is a fraction of one (i.e. not percent). This relationship is valid only for Fig. 6.20 which shows the experimental data from which this was derived.

Clay - It appears that no accurate correlation is available at this time (1990), for finding G_{max} from CPT results in clay. Fig. 6.21 from Robertson (1990) is presented as a guide.

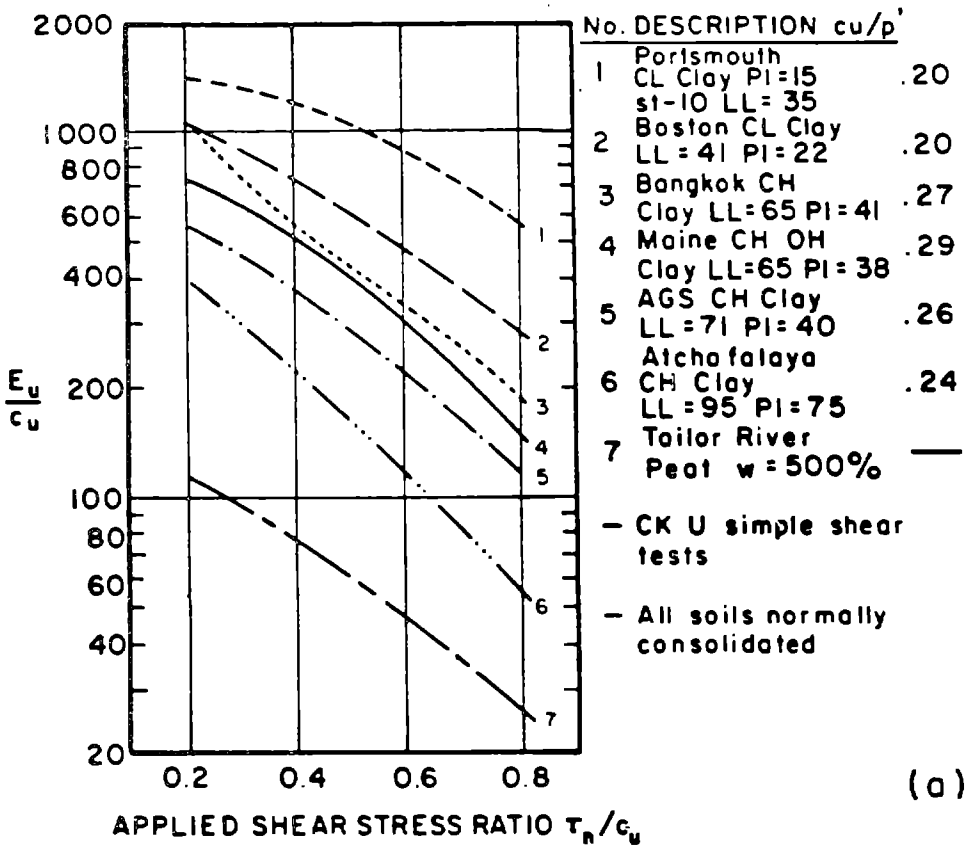

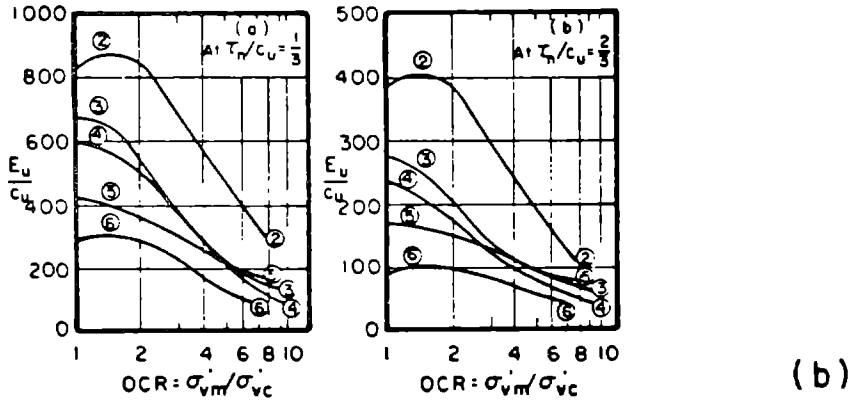

FIG. 6.18. Selection of Soil Stiffness Ratio for Clays (adapted from Ladd et al., 1977) (from Robertson and Campanella, 1983)

IN THIS FIGURE, $G_{max} = G_o$

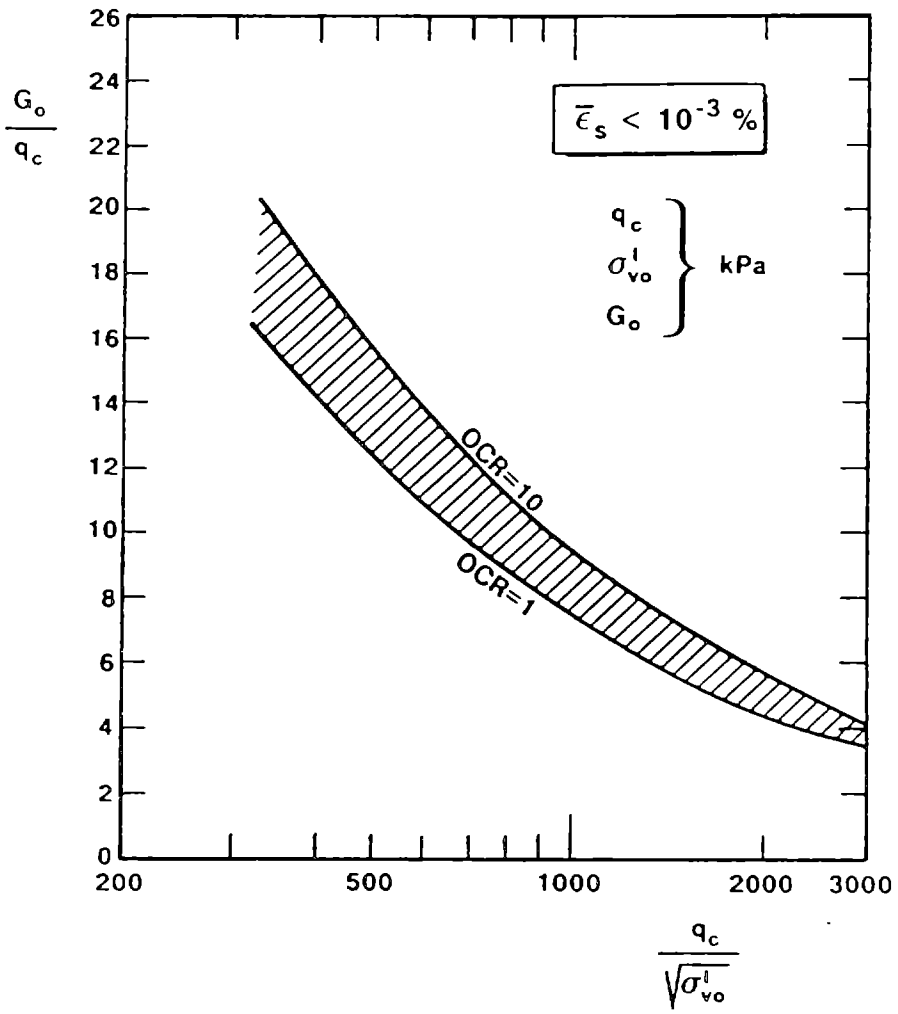

FIG. 6.19. Evaluation of Small Strain Shear Modulus from CPT for Uncemented Silica Sand (from Robertson, 1990)

IN THIS FIGURE, $G_{max} = G_o$

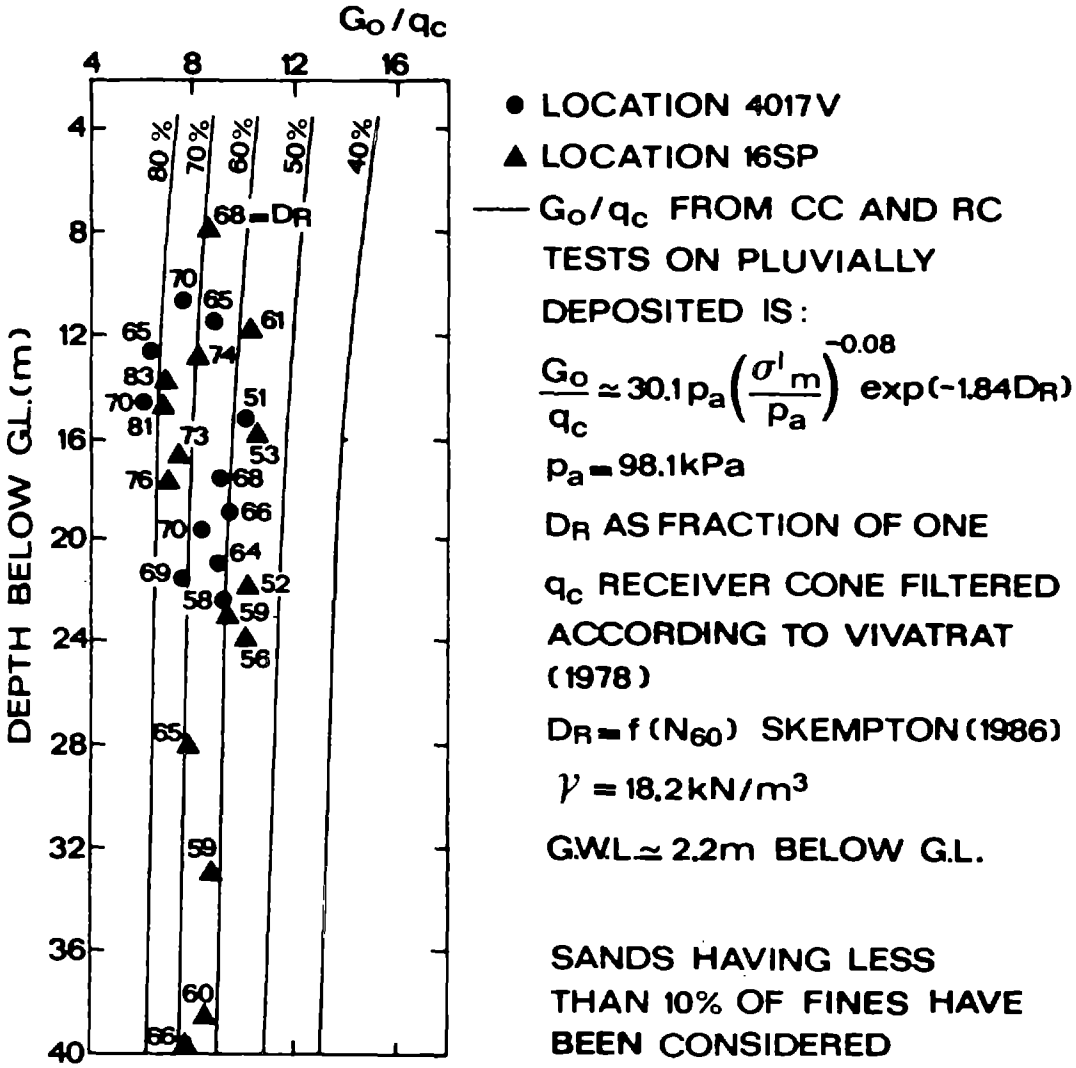

FIG. 6.20. Correlation of G_{max} vs q_c from Seismic Cone in Po River Sand (from Jamiolkowski et al., 1988)

IN THIS FIGURE, $G_{max} = G_o$

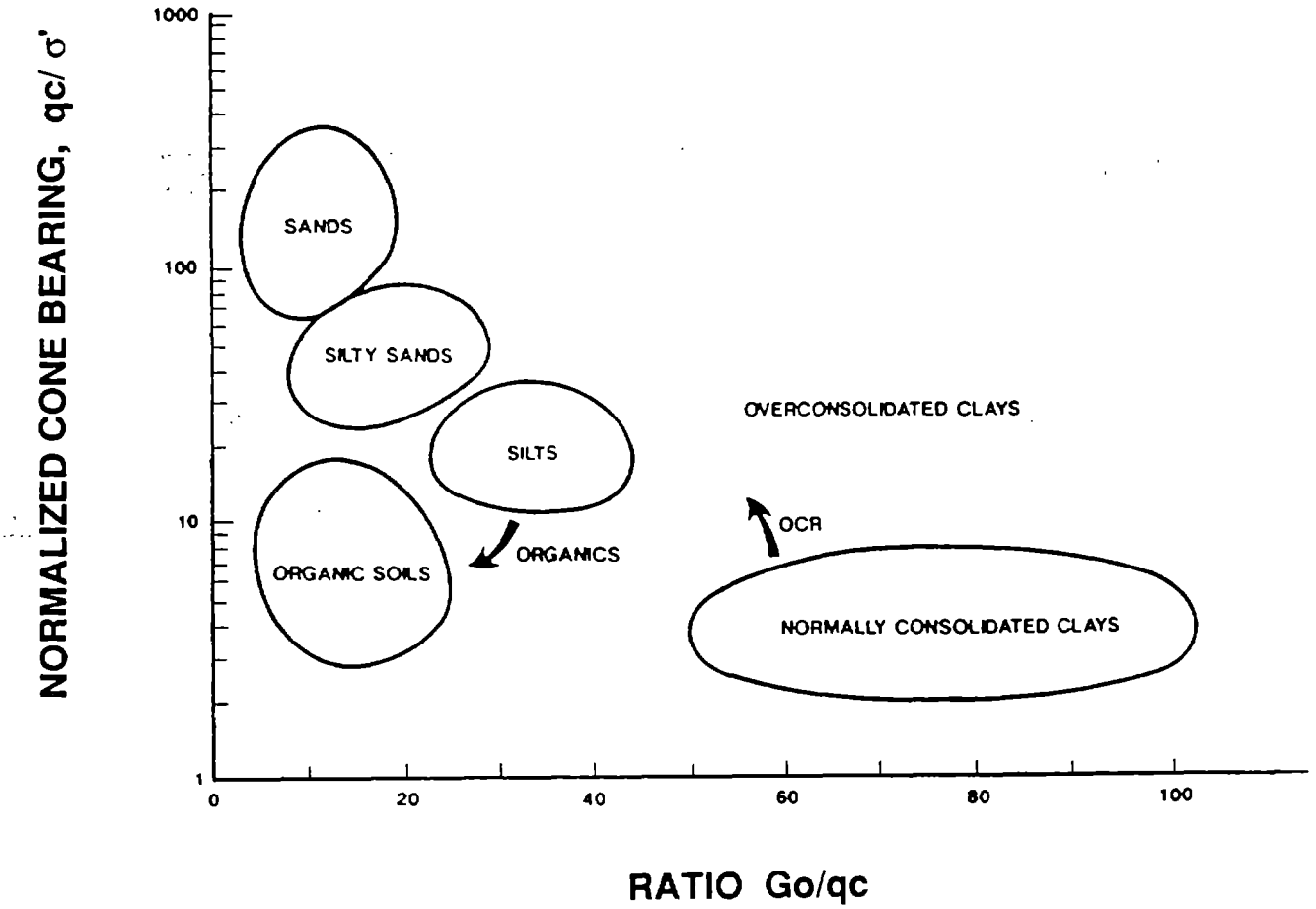

FIG. 6.21. Correlation Between Small Strain Modulus, q_c and Soil Type (from Robertson, 1990)

Recently, the seismic cone has been used to obtain G_{max} using elasticity theory which relates G_{max} to soil density ρ and shear wave velocity v_s by

$$G_{max} = \rho v_s^2 \tag{6.22}$$

6.9 Stress History

Sand - So far, it is not possible to distinguish the stress history from cone penetration data during drained penetration (Robertson and Campanella, 1988). Moreover, the cone may give the same profile for a dense normally consolidated sand and a loose overconsolidated sand. Although some correlations have been proposed for sands, they are not useable in practice.

Therefore, other means of investigation must be used to find the overconsolidation ratio of sand.

Clay - Schmertmann (1978) presented a method of estimating the overconsolidation ratio OCR for clays. This is illustrated in Fig. 6.22.

- o Estimate the actual undrained shear strength of the soil S_u (see section 6.11).
- o Estimate vertical effective stress σ'_{vo}.
- o Compute S_u/σ'_{vo}
- o Use $(S_u/\sigma'_{vo})_{nc}$ = 0.33 as a reasonable average.
- o Estimate OCR using Fig. 6.22.

If the plasticity index is known, $(S_u/\sigma'_{vo})_{nc}$ can be computed from

$$\frac{S_u}{\sigma'_{vo}} = 0.11 + 0.0037 I_p \tag{6.23}$$

The above equation should only be used as an approximation in preliminary design (Fig. 6.23).

More recently Robertson (1990) presented a simplified version of this approach as shown in Fig. 6.24.

Lunne et al. (1989) presented correlations between all the piezo-cone parameters q_c, f_s, and u and the OCR as shown in Fig. 6.25. All the available parameters should be used to obtain estimates of OCR, the difference in the values obtained being the uncertainty in the estimate.

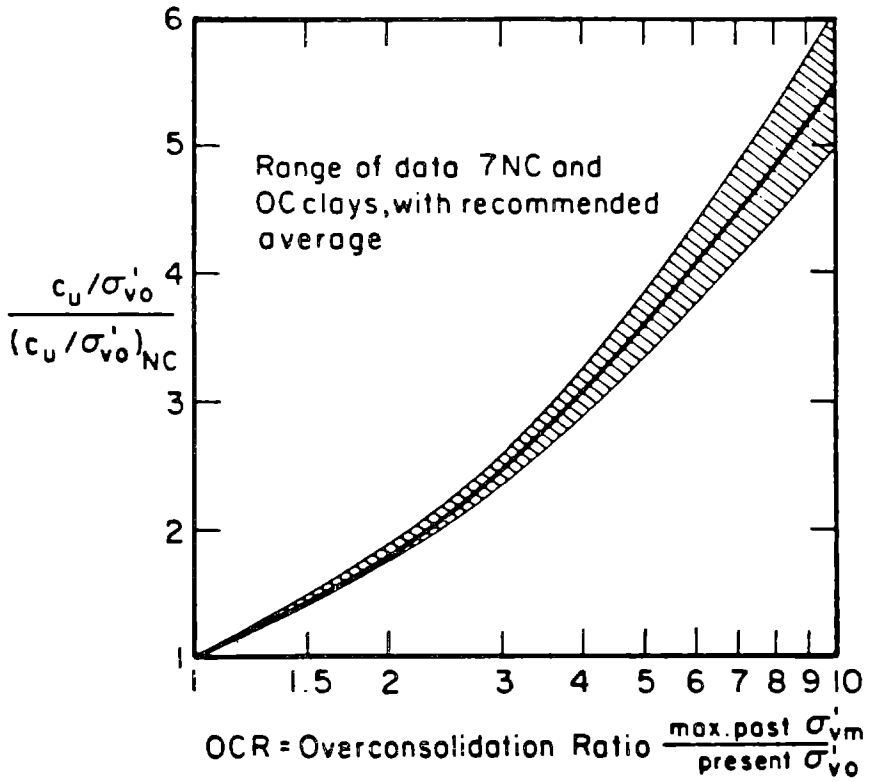

FIG. 6.22. Normalized S_u/σ'_{vo} Ratio vs. OCR for Use in Estimating OCR (From Schmertmann 1978)

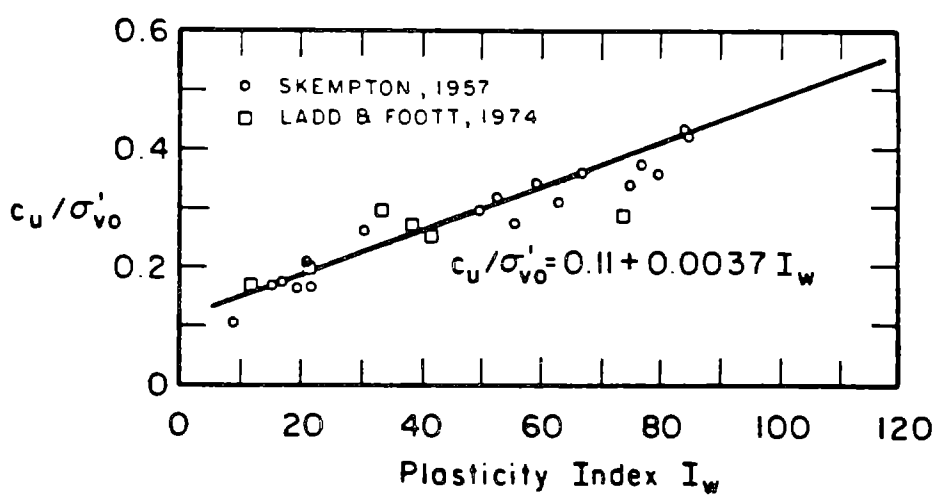

FIG. 6.23. Statistical Relation Between S_u/σ'_{vo} Ratio and Plasticity Index, for Normally Consolidated Clays (From Robertson and Campanella 1983)

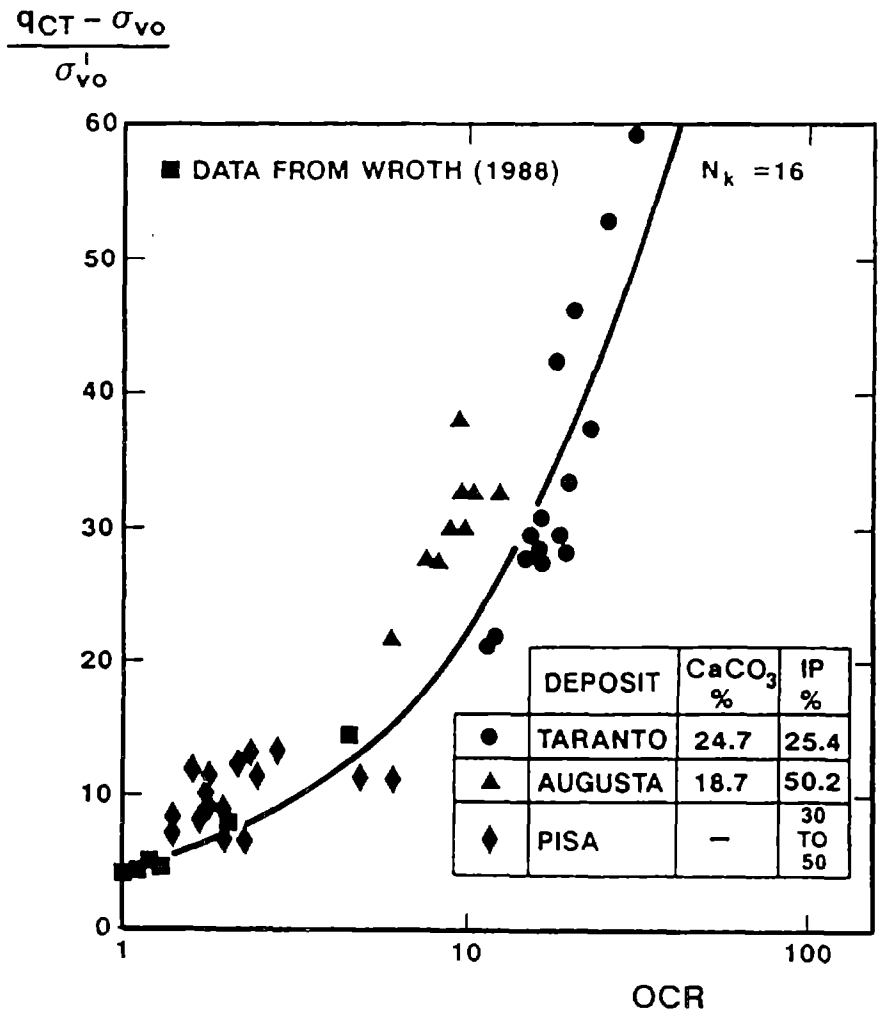

FIG. 6.24. Stress History (OCR) from CPT (from Robertson, 1990)

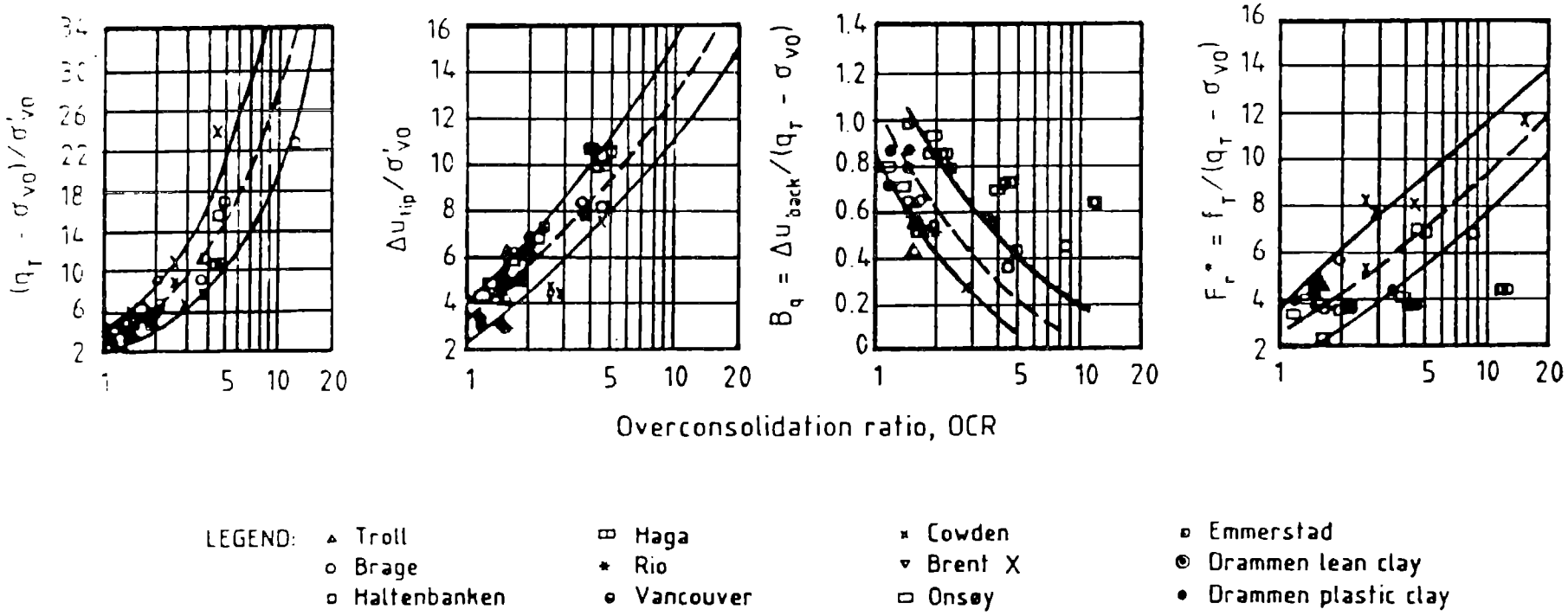

FIG. 6.25. Correlation of OCR to Piezo-cone Parameters (from Lunne et al., 1989)

6.10 Sensitivity

The sensitivity S_t of a clay is the ratio of the undisturbed strength to the remolded strength. Several researchers have found that the sleeve friction f_s is closely related to the remolded shear strength (Robertson and Campanella, 1988).

In 1978, Schmertmann suggested that S_t should be obtained from:

$$S_t = \frac{N_s}{R_f} \tag{6.24}$$

where R_f is the friction ratio in percent and N_s is a constant. Comparisons with sensitivity values from field vane tests suggest that $N_s = 6$ should be used for an initial estimate of S_t.

6.11 Undrained Shear Strength

The most common relationship to estimate the undrained shear strength of clays S_u from cone penetrometer data is:

$$S_u = \frac{(q_c - \sigma_{vo})}{N_k} \tag{6.25}$$

where N_k is called the cone factor and σ_{vo} is the in situ vertical stress where q_c is measured. When possible, the use of q_T in place of q_c in equation 6.25 will reduce the scatter from one cone to another. The cone factor N_k, which varies mainly between 10 and 20 should preferably be obtained from empirical correlation with the strength test used in that area. When local correlations are not available, Robertson and Campanella (1988) recommended to use $N_k = 15$ for preliminary assessment of S_u. However, since N_k is sensitivity dependent, N_k should be reduced to around 10 when dealing with a sensitive clay ($8 < S_t < 16$).

The above method may not give good results in soft clays, mainly because the cone resistance will be too small to be measured with accuracy. To overcome this problem, S_u can be correlated with the excess pore pressure Δu_o measured during continuous penetration. Indeed Δu_o is measured with good accuracy in soft clay, using a piezo-cone. Campanella, et al. (1985) proposed two charts (Fig. 6.26) to estimate S_u using:

$$S_u = \frac{\Delta u_o}{N_{\Delta u}} \tag{6.26}$$

where $N_{\Delta u}$ is a parameter which varies with the overconsolidation ratio OCR, the sensitivity S_t, and stiffness ratio G/S_u. Note that the value of G for the G/S_u ratio can be obtained with the seismic cone (Campanella & Robertson, 1984).

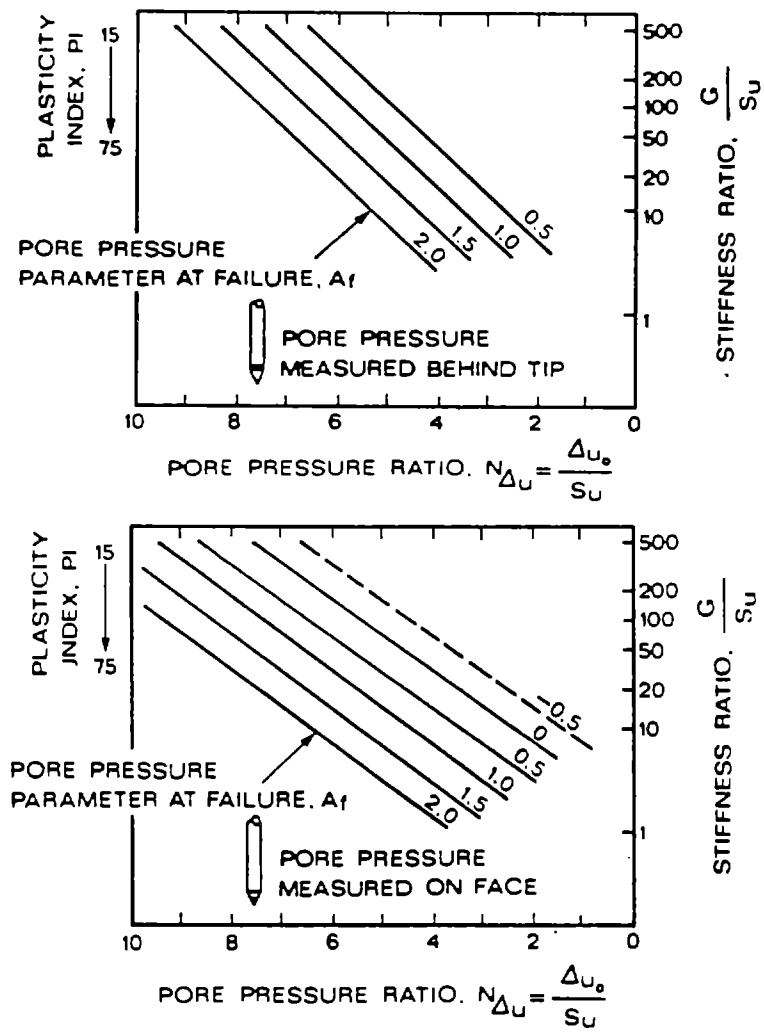

FIG. 6.26. Proposed Charts to Obtain S_u from Excess Pore Pressure, Δu, Measured During CPTU (From Campanella et al. 1985)

TABLE 6.2. A_f Values for Clays (From Robertson and Campanella 1988)

SATURATED CLAYS	A_f
Very sensitive to quick	1.5 - 3.0
Normally consolidated	0.7 - 1.3
Lightly overconsolidated	0.3 - 0.7
Highly overconsolidated	-0.5 - 0.0

To use these charts in practice, it is necessary to estimate the value of S_t (see section 6.10) and OCR (see section 6.9). Then an appropriate value of A_f can be estimated from Table 6.2. Finally, Fig. 6.26 will give the value of $N_{\Delta u}$.

Note: Since it is necessary to know S_u in order to find OCR (see section 6.9) the previous method can only be used if OCR is estimated using another means of investigation than the CPTU, or by an iterative procedure.

6.12 Coefficient of Consolidation, Permeability.

Some methods have been proposed to derive the coefficient of consolidation C_h from the in situ measurement of the dissipation of excess pore pressure; the piezo-cone is the device used most often for such measurements. The most comprehensive method was developed by Levadoux and Baligh (1986), but is only applicable to sedimentary clays with overconsolidation ratio OCR less than 3. The following procedure to evaluate C_h is recommended (Robertson and Campanella, 1988):

1. Run a CPTU dissipation test.
2. Plot the normalized excess pore pressure $(\Delta u)/(\Delta u_o)$ versus log time. In this ratio, Δu = excess pore pressure above hydrostatic at time $t = t$, and Δu_o = excess pore pressure above hydrostatic at time $t = o$.
3. Estimate the pore pressure parameter at failure, A_f (table 6.2) and calculate $I_R = G/S_u$ ($\simeq E/3S_u$ as a first approximation). If no data exists, assume A_f = 0.8 and I_R = 100.
4. Compare the previous curve with the theoretical curves (Fig. 6.27).
5. If the shapes are similar, calculate:

$$C_h = \frac{R^2 T}{t} \qquad (6.27)$$

   where T = time factor (Fig. 6.27), R = radius of cone, t = time to reach a given value of $(\Delta u(t))/(\Delta u_o)$.

   Note: Time factor plots for other pore pressure stone locations have been proposed by Baligh and Levadoux (1980).
6. If one assumes that the soil compressibility is isotropic, then C_v can be calculated using

$$C_v = C_h \times \frac{K_v}{K_h} \qquad (6.28)$$

   Where K_v/K_h can be estimated using Table 6.3.

7. The permeability K_H and K_v can be obtained from the relationship between permeability and coefficient of consolidation: $K_h = C_h \gamma_w / M$ or $K_v = C_v \gamma_w / M$. The parameter M is the constrained modulus discussed in section 6.6.

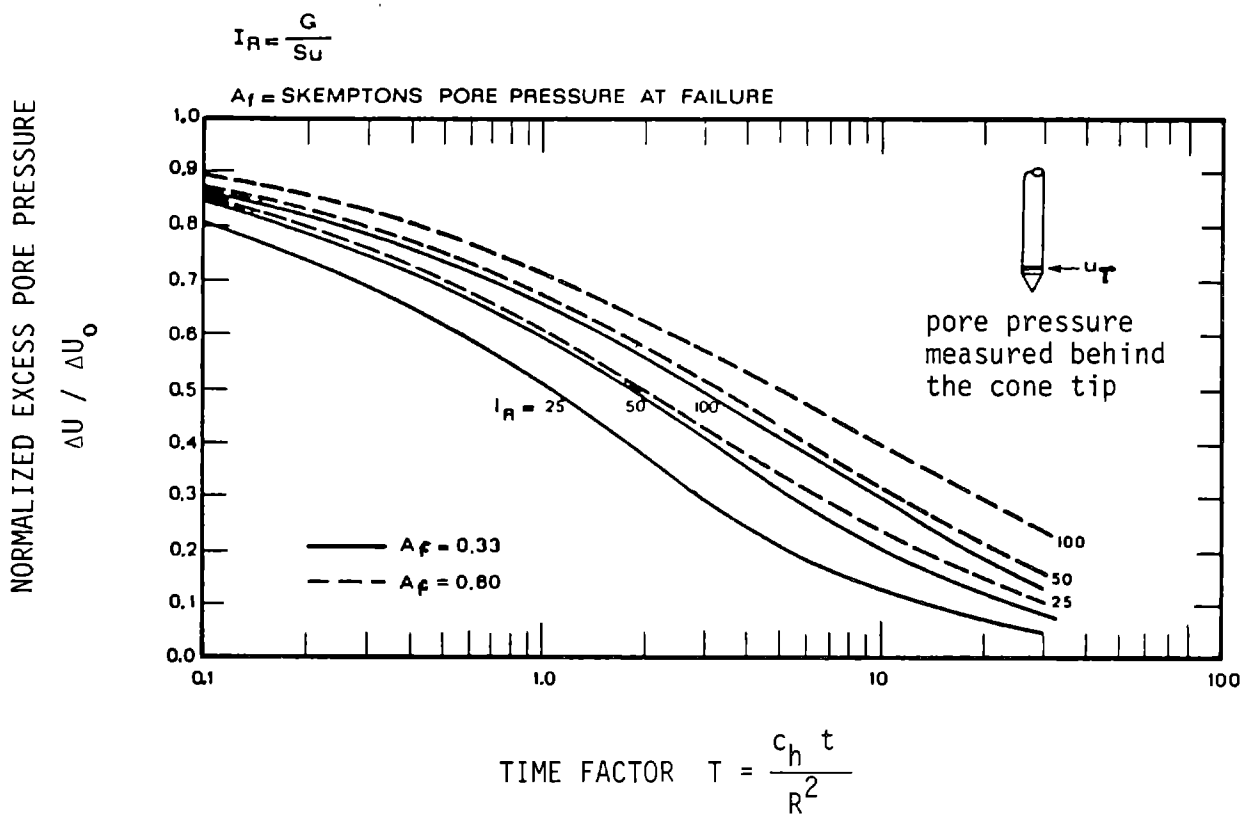

FIG. 6.27. Theoretical Curves for Cylindrical Pore Pressure Dissipation for Various Stiffness Ratios (from Battaglio et al., 1981)

Table 6.3 - Anisotropic permeability of clays (after Baligh and Levadoux, 1980).

	Nature of Clay	k_h / k_v
1.	No evidence of layering.	1.2 ± 0.2
2.	Slight layering, e.g., sedimentary clays with occasional silt dustings to random lenses.	2 to 5
3.	Varved clays in north-eastern U.S.	10 ± 5

6.13 Liquefaction

At present, it is difficult to establish reliable correlations between liquefaction potential and CPT data, because of the scarcity of field data.

The correlations by Robertson and Campanella (1985) and Shibata and Teparaksa (1988) can be used to estimate the liquefaction potential of clean sands. They are not recommended for very coarse sands or gravelly sands (Lunne et al., 1989) and should be used only as an estimate of liquefaction potential. To use these methods in practice the following procedure is recommended.

1. Estimate the vertical effective stress σ'_{vo}.
2. Using Fig. 6.28, calculate the overburden correction factor C and compute $Q_c = C q_c$ where q_c is the cone resistance.
3. Estimate the mean grain size using Fig. 6.29 and a knowledge of q_c and R_f.
4. Use Fig. 6.30 to estimate the cyclic stress ratio, τ_{cy} / σ'_{vo} to cause liquefaction of the soil.
5. Estimate the average cyclic stress ratio τ / σ'_{vo} induced by the design earthquake (Tokimatsu and Tashimi, 1983):

$$\frac{\tau}{\sigma'_{vo}} = 0.1(M-1)\frac{a_{max}}{g}\frac{\sigma_o}{\sigma'_{vo}}(1-0.015Z) \qquad (6.29)$$

where:

M = earthquake magnitude.

a_{max} = acceleration in the sand layer being considered.

g = acceleration due to gravity.

σ_o = total overburden pressure on the sand layer being considered.

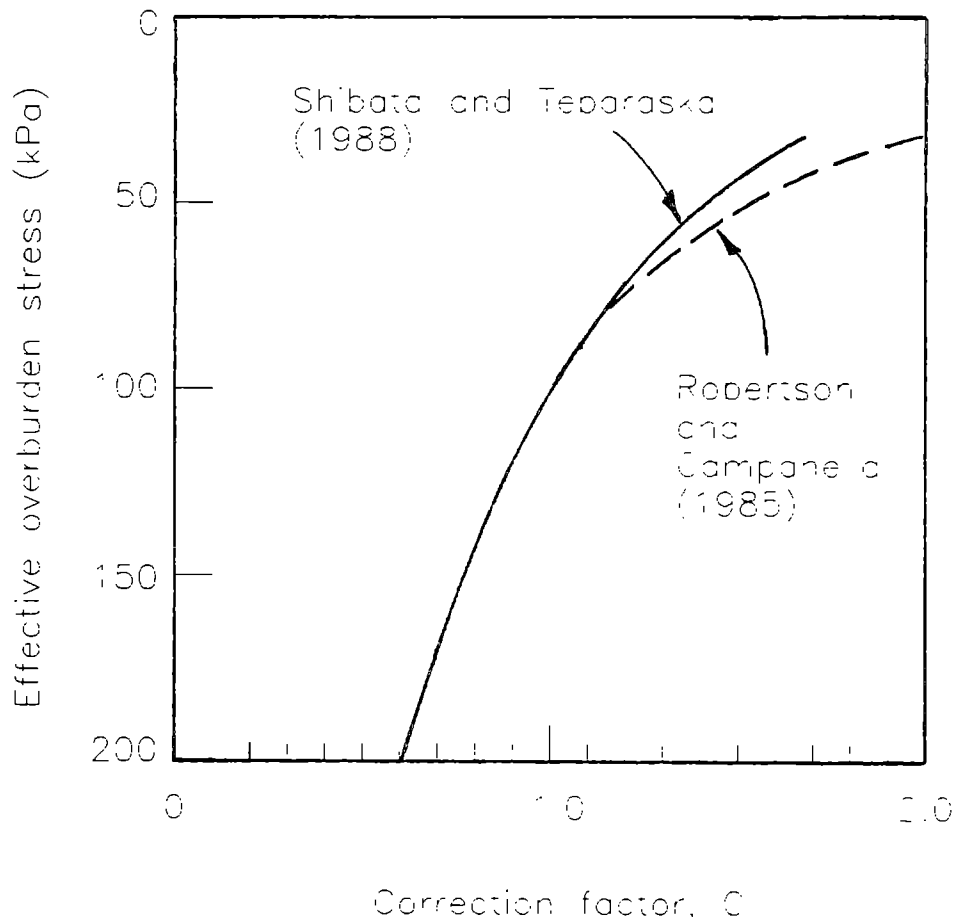

FIG. 6.28. Correction Factor for Cone Resistance to Predict Liquefaction Potential of Sand (from Lunne et al., 1989)

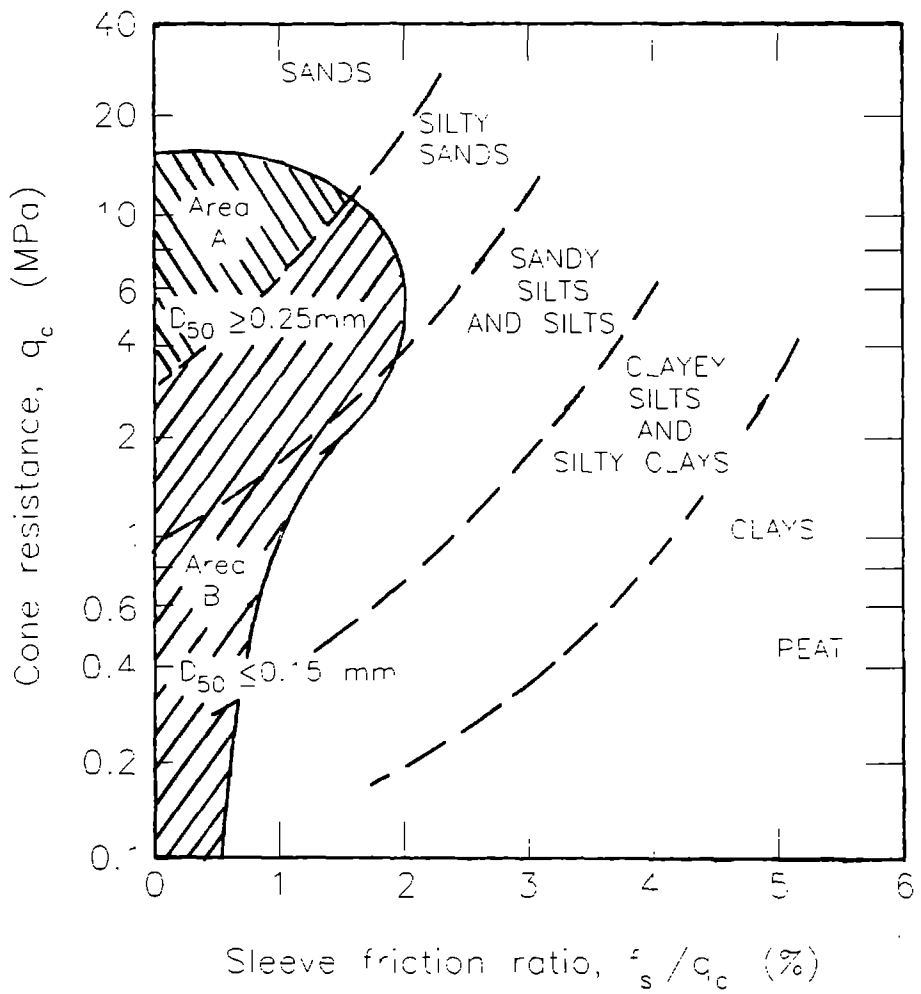

FIG. 6.29. Approximate Grain Size from Cone Resistance and Sleeve Friction (from Robertson and Campanella, 1985)

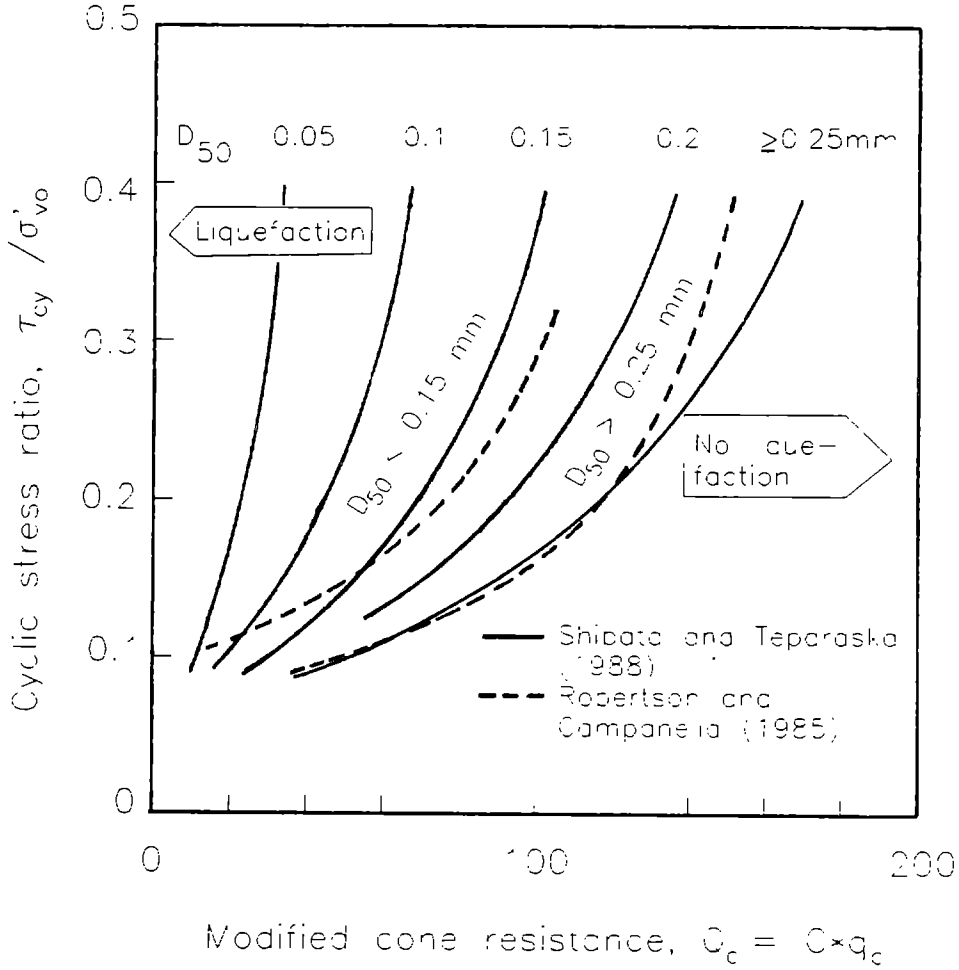

FIG. 6.30. Liquefaction Potential from Cone Resistance (from Lunne et al., 1989)

σ'_{vo} = initial effective overburden pressure on the sand layer being considered.

z = depth, in meters.

An alternative for step 5 would be to use the seismic cone in order to obtain a small strain shear modulus G_{max} and use G_{max} together with the appropriate computer program in order to obtain the τ/σ'_{vo}, ratio for a given earthquake excitation.

6. Compare τ_{cy}/σ'_{vo} to τ/σ'_{vo} to see if liquefaction is likely to occur under the design earthquake.

Teparaksa (1991) presented an equation for critical cone resistance $(q_c)_{cr}$, below which liquefaction is likely to occur:

$$(q_c)_{cr} = C_2\left[50 + 200\left\{\frac{(\tau/\sigma'_{vo}) - 0.1}{(\tau/\sigma'_{vo}) + 0.1}\right\}\right] \tag{6.30}$$

where

C_2 = correction factor

= 1.0 for clean sand with D_{50} > 0.25 mm

= D_{50} (mm)/0.25 mm for fine grained soils with D_{50} > 0.25 mm.

Using equation 6.30 a $(q_c)_{cr}$ profile may be generated. If the actual q_c profile falls below the (q_c) profile, there is a chance of liquefaction. This (q_c) profile may also be used for verification of soil improvement techniques against liquefaction. Yet, another approach is presented by Robertson et al. (1992) based on normalized shear wave velocity.

6.14 Comparison with SPT

Robertson (1990) presented a correlation between the ratio of q_c/N as a function of the mean grain size, D_{50} (Fig. 6.31).

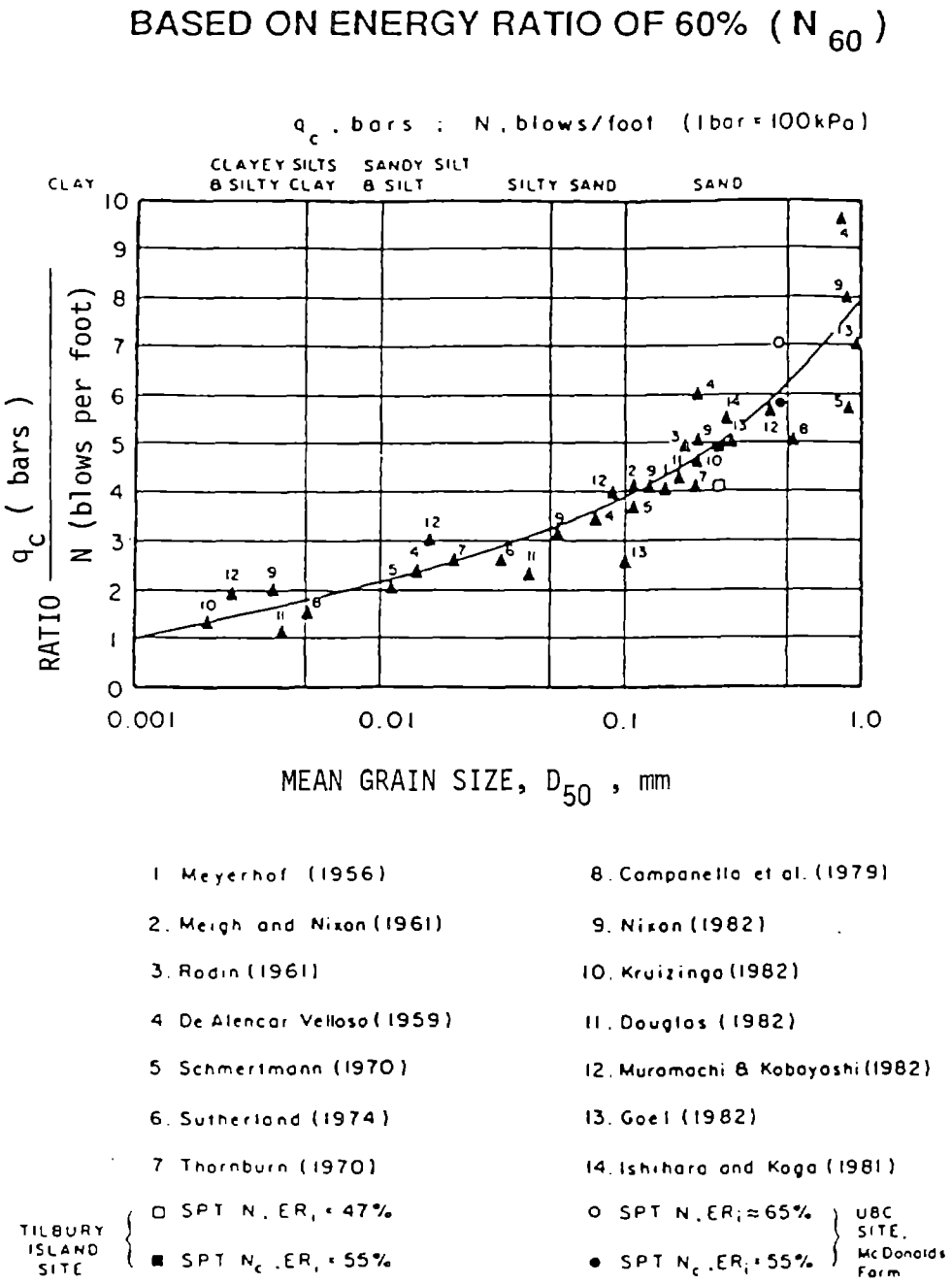

FIG. 6.31. Variation of q_c/N with Mean Grain Size (after Robertson et al., 1983)

7. DESIGN EXAMPLES AND APPLICATIONS

7.1 Design of Shallow Foundations

7.1.1 Sand

7.1.1.1 Bearing capacity: Procedure

1. The Terzaghi bearing capacity equation for cohesionless soils is:

$$q_u = K_q \gamma D N_q + \frac{1}{2} K_\gamma \gamma B N_\gamma \qquad (7.1)$$

where:

q_u = ultimate bearing capacity, in tsf.

γ = effective unit weight of the soil.

D = depth of embedment of the footing.

$\bar{q}_c$ = equivalent cone tip bearing: $\bar{q}_c = \sqrt{q_{c1} \times q_{c2}}$, tsf.

q_{c1} = average cone tip bearing q_c from 0 to 0.5B below the footing.

B = footing width.

q_{c2} = average cone tip bearing q_c from 0.5 to 1.5B below the footing.

N_γ and N_q are the bearing capacity factors. Schmertmann (1978) recommends to estimate N_γ and N_q from

$$N_\gamma = N_q = 1.25\bar{q}_c \quad \text{with} \quad \bar{q}_c \quad \text{in} \quad tsf \qquad (7.2)$$

Another way to obtain N_γ and N_q is to estimate ϕ' from q_c and use the conventional values of N_γ and N_q (Terzaghi and Peck, 1967).

K_q and K_γ are two correction factors which account for the load inclination, the footing shape, the depth of embedment, the inclination of the base, and the inclination of the ground surface (section 7.1.1.3).

An appropriate factor of safety is used to obtain the safe bearing pressure, usually 3. As a check, the method by Meyerhof (1956) and Awkati (1970) may be used.

2. Meyerhof (1956) proposed:

$$q_u = \bar{q}_c \frac{B}{40}\left(1 + \frac{D}{B}\right) \qquad (7.3)$$

where:

q_u = ultimate bearing capacity in tsf.

B = width of the footing in feet.

D = depth of embedment in feet.

$\bar{q}_c$ = average cone resistance within a depth B below the footing in tsf.

A factor of safety of 3 is recommended by Meyerhof to obtain the safe bearing pressure.

3. Awkati (1970) proposed to use Fig. 7.1 in order to estimate the ultimate bearing capacity of shallow footings on sand. A factor of safety of 3 may be used to obtain the safe bearing capacity.

7.1.1.2 Bearing Capacity: Precision of Procedures 1 to 3

Plate loading tests have been performed to check the relationship proposed by Meyerhof (1956). The results are presented in Fig. 7.2. Meyerhof (1956, 1957) found that the observed ultimate bearing capacities are conservative for small footing width; they are about twice the estimated values in the case of 1 ft wide footings. However, the proposed relationship is considered reasonable for the larger footing width 1.5 ft < B < 3.5 ft. Larger footings may have smaller bearing capacities than predicted by this method. No extensive data base study is known to have been done to evaluate the precision of procedures 1 and 3. However, procedure 1 is the classical method to estimate the bearing capacity on sand.

7.1.1.3 Bearing capacity: Eccentric load, inclined load, footing shape, depth of embedment, base and ground inclination

The previous design rules refer to the case of a vertical load applied at the center of a shallow strip footing around which the ground surface is horizontal. When dealing with an eccentric load, an inclined load, depth of embedment, base and ground inclination, and different footing shapes, Vesic (1975) proposed to apply the reduction factor K_q and K_γ to N_q and N_γ, respectively:

$$K_q = i_q \cdot s_q \cdot d_q \cdot b_q \cdot g_q \tag{7.4}$$

$$K_\gamma = i_\gamma \cdot s_\gamma \cdot b_\gamma \cdot g_\gamma \tag{7.5}$$

where i, s, d, b, g are individual correction factors related to inclined load, footing shape, depth of embedment, base and ground inclination.

* <u>Load eccentricity:</u>

  Load eccentricity decreases the ultimate vertical load that a footing can withstand. This effect is accounted for in bearing capacity analysis by reducing

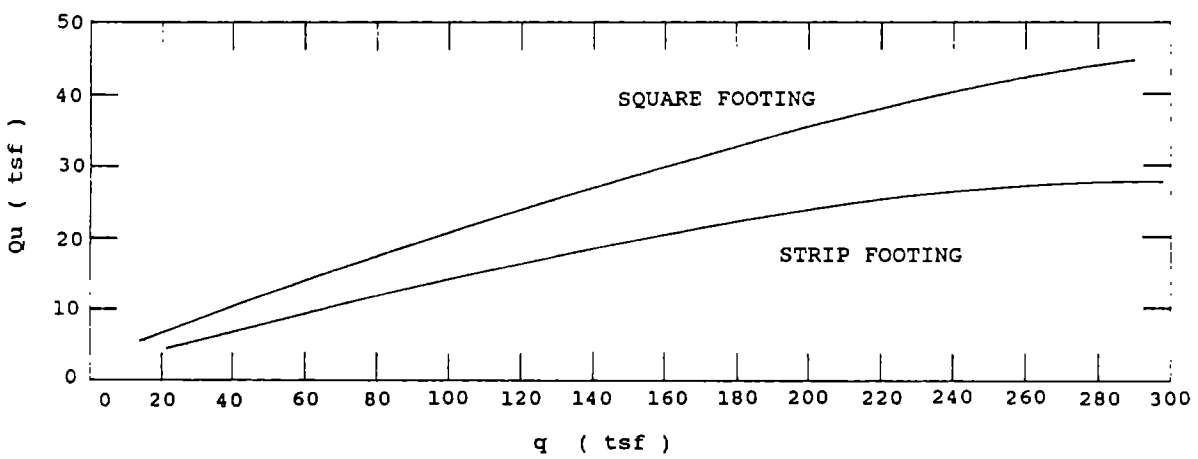

This chart is valid for a footing with an embedment, h, defined as:

h > 1.5' + B' / 2 when B, the minimum width of the footing is < 3'

h > 4' + when B, the minimum width of the footing is > 3'

FIG. 7.1. Chart for Estimating the Ultimate Bearing Capacity of Shallow Footing on Sand Using Average q_c Over Depth 1.5B Below Footing (From Awkati 1970)

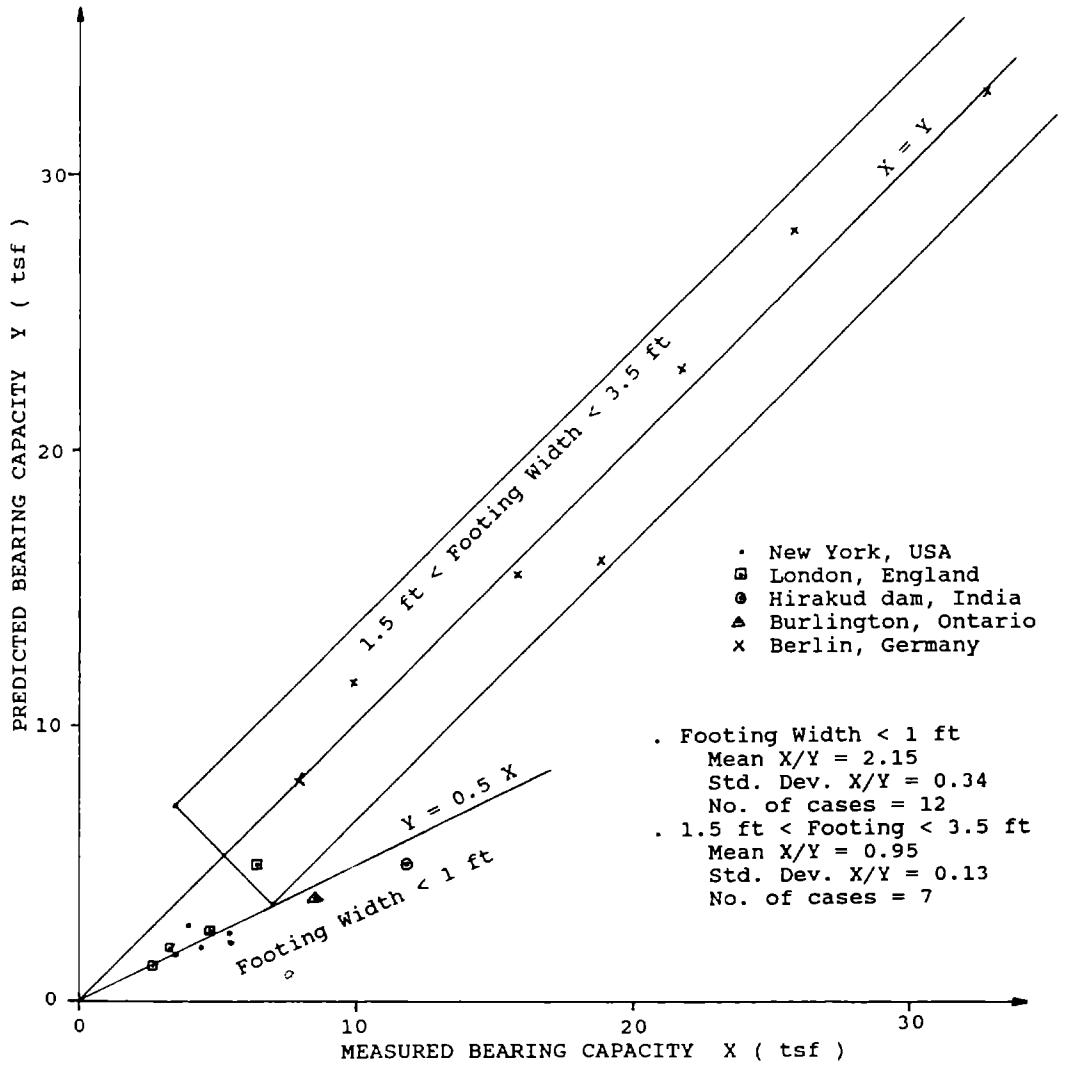

FIG. 7.2. Comparison of Estimated and Observed Bearing Capacity of Shallow Foundation on Sand (Modified After Meyerhof 1956, 1957)

the width B an amount $2e_2$ and the length L an amount $2e_1$, where e_1 and e_2 are the eccentricities along the length and width, respectively. The reduced dimensions of the footing are:

(See Fig. 7.3a for the definition of e_1 and e_2.)

$$L' = L - 2e_1 \tag{7.6}$$

$$B' = B - 2e_2 \tag{7.7}$$

The CPT design rules are then applied to the $B' \times L'$ footing.

* Inclined load:

$$i_q = \left(1 - \frac{H}{Q}\right)^m \tag{7.8}$$

$$i_\gamma = \left(1 - \frac{H}{Q}\right)^{m+1} \tag{7.9}$$

Q is the projection of the load resultant on the axis perpendicular to the footing, and H is the projection of the load resultant on the plane of the footing (see Fig. 7.4).

$$m = m_L \cos^2\theta + m_B \sin^2\theta \tag{7.10}$$

where:

$$m_L = \frac{2 + \frac{L'}{B'}}{1 + \frac{L'}{B'}}$$ L' and B' are defined as before.

$$m_B = \frac{2 + \frac{B'}{L'}}{1 + \frac{B'}{L'}}$$ L' and B' are defined as before.

θ is the angle between the long axis of the footing and H (see Fig. 7.4).

* Shape factors:

1. Rectangular

$$s_q = 1 + \left(\frac{B'}{L'}\right)\tan\phi \tag{7.11}$$

$$s_\gamma = 1 - 0.4\frac{B'}{L'} \tag{7.12}$$

2. Circular

$$s_q = 1 + \tan\phi \tag{7.13}$$

$$s_\gamma = 0.6 \tag{7.14}$$

where: ϕ is the friction angle of the sand.

B' and L' are defined as before.

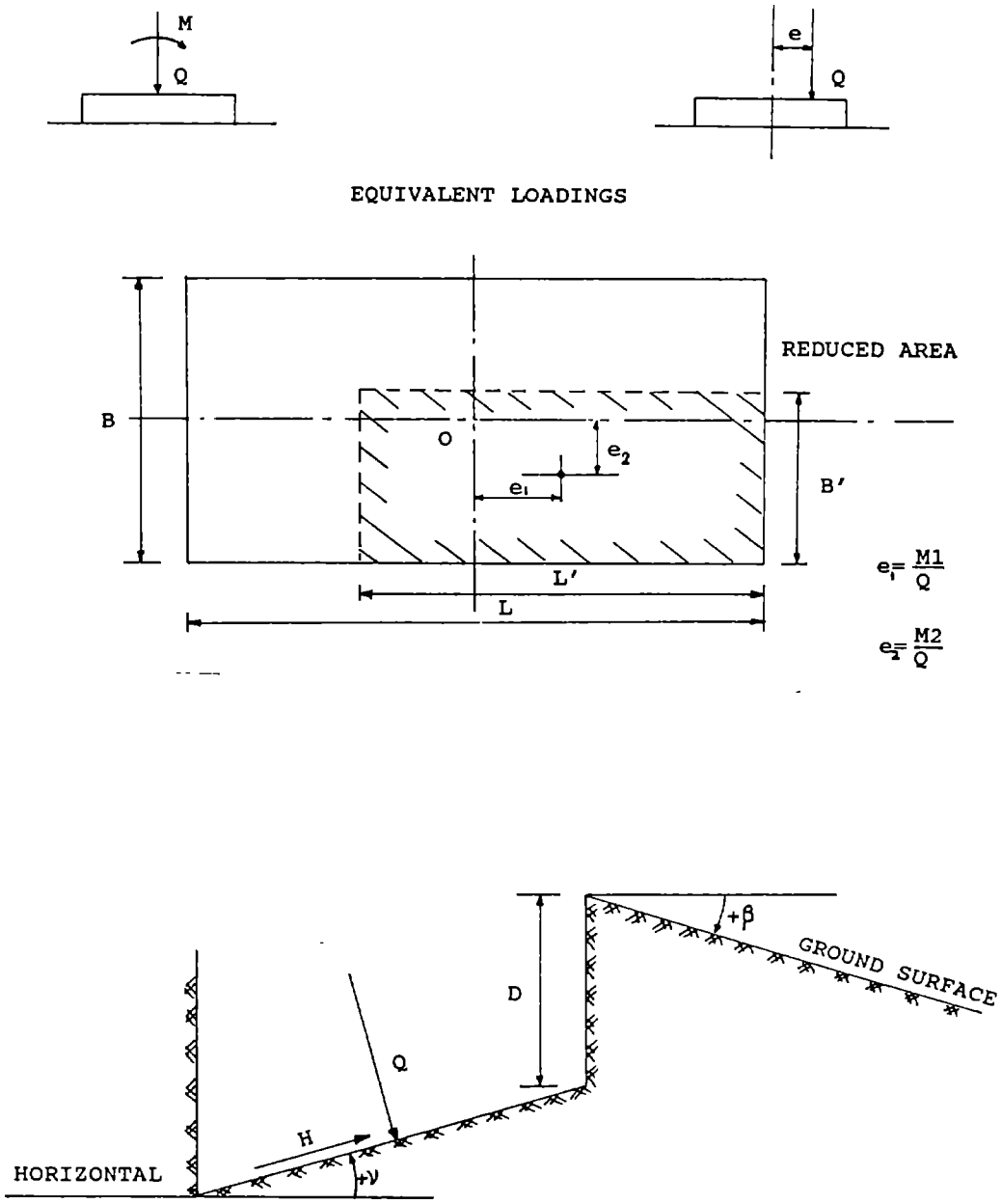

FIG. 7.3. Definition for Load Eccentricity, Inclined Base, and Inclined Ground Surface

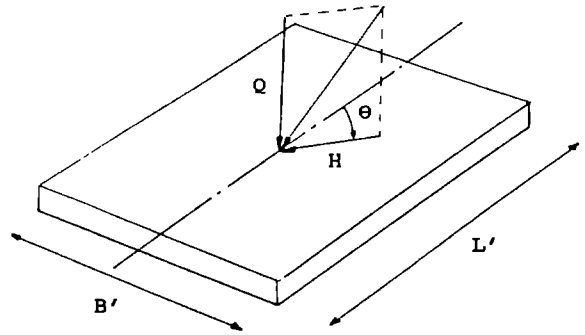

FIG. 7.4. Load Projection

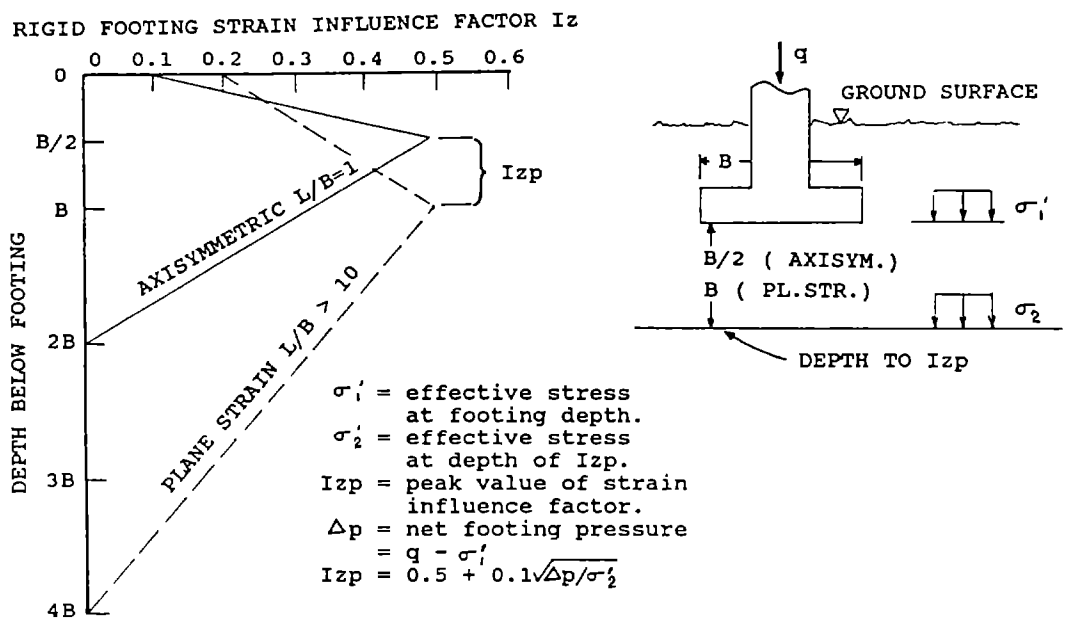

FIG. 7.5. Influence Factor for Footings on Sand (Modified After Schmertmann 1978a)

* Depth factors:

$$d_q = 1 + 2\tan\phi(1-\sin\phi)^2 D/B'$$

where:

ϕ is the friction angle of the sand.

B' is the reduced width of the footing.

D is the depth of embedment.

* Base inclination factors:

$$b_q = (1-\upsilon\tan\phi)^2 = b_\gamma \tag{7.15}$$

where:

ϕ is the friction angle of the sand.

υ is the base inclination angle in radians (Fig. 7.3b).

* Ground inclination factors:

$$g_q = (1-\tan\beta)^2 = g_\gamma \tag{7.16}$$

where:

β is the ground inclination angle in radians (Fig. 7.3b).

Note: For footings on slope, the first step is to ensure that the slope with the footing load is sufficiently safe.

Note: These factors are mostly derived from theory and very little data exists to verify their accuracy.

7.1.1.4 Settlement: Schmertmann's (1970) step-by-step procedure

* Settlement equation:

Computer programs have been written to automate the calculations for this method (SCHMERT (Tucker, Briaud, 1990) and SETSAND (Dumas, 1984)). To estimate the settlement of shallow foundations on sand, Schmertmann (1978) suggests:

$$S = C_1 \cdot C_2 \cdot \Delta p \cdot \sum_1^N \frac{I_{zi} \cdot \Delta z_i}{x \cdot q_{ci}} \tag{7.17}$$

$$C_1 = 1 - 0.5\left(\frac{\sigma'_1}{\Delta p}\right) \tag{7.18}$$

$$C_2 = 1 + 0.2\log_{10}\left(\frac{t_{YR}}{0.1}\right) \tag{7.19}$$

where:

S = settlement in units of Δz.

C_1 = correction factor for depth of embedment.

C_2 = correction factor for creep settlement.

Δp = net foundation pressure increase at the bottom of the footing = $q - \sigma'_1$ (in the same units as q_c).

q = bearing pressure (in the same units as q_c).

σ'_1 = previous vertical effective stress at the elevation of the bottom of the footing.

I_{zi} = strain influence factor at the center of the ith sublayer (Fig. 7.5).

N = number of sublayers.

Δz_i = thickness of the ith sublayer.

t_{yr} = time in years after the application of $\sigma'_1 + \Delta p$ on the soil.

q_{ci} = average value of q_c in the ith layer.

$\times$ = modulus factor = 2.5 for square footing.
= 3.5 for strip footing.
(after Schmertmann, 1978)

$\times \cdot q_{ci}$ = E = equivalent Young's modulus for the sand.

* <u>Procedure:</u>

1. Prepare a table with the following headings:

Layer #	Δz_i	I_{zi}	q_{ci}	$\times$	$\frac{I_{zi}\Delta z_i}{\times \cdot q_{ci}}$

2. Obtain the static cone bearing capacity (q_c) over the depth interval from the proposed footing depth to a depth of 2B (square footing) or 4B (long footing) below the footing depth, or to a boundary layer that can be assumed incompressible, whichever occurs first (B is the footing width).
3. Divide the q_c profile into layers of constant q_{ci} . Each layer shall not be thicker than B.
4. Superimpose the appropriate strain factor diagram (axisymetric or plane strain as required) from Fig. 7.5, and find I_{zi} for each layer i.
5. Estimate $\times$ for each layer.

6. Compute Δp, C_1 and C_2.

7. Compute $S = C_1 \cdot C_2 \cdot \Delta p \sum_{1}^{n} \frac{I_{zi} \cdot \Delta z_i}{x \cdot q_{ci}}$

Note: If 1 < L/B < 10, solve for both the axisymetric and plane strain case, and interpolate between the two results (L is the footing length).

7.1.1.5 Settlement, precision of Schmertmann's method

The method presented by Schmertmann in 1970 and revised in 1978 is considered to be the preferred approach, and has gained considerable popularity over the past ten years. This method is directly applicable only for first load case, and Schmertmann (1978) recommends reducing the predicted settlement by a factor of two if sands are determined to be preloaded (overconsolidation, roller compaction, previous footing . . .). Gifford et al. (1987) evaluated the method using 10 literature case histories gathered in a FHWA project (Fig. 7.6a). The footings were placed on natural granular soil and bearing pressures ranged from 1.52 to 10.60 ksf. The footing width ranged from 8.5 to 23.0 ft. The ratio of calculated/measured settlement had a mean of 1.59 and a standard deviation of 0.74. Briaud et al. (1985) also evaluated the method using the 37 case histories presented in Schemrtmann (1970). The ratio of predicted settlement to measured settlement versus measured settlement is presented in Fig. 7.6b. For these cases, Schmertmann's method, on the average, overpredicted settlement by 30%.

7.1.1.6 Robertson and Campanella revision of Schmertmann's method

Robertson and Campanella (1988) modified the value of $x = E / q_c$ defined in section 7.1.1.4, in order to account for the effect of magnitude of foundation pressure and soil stress history, on the calculated settlement. Robertson and Campanella proposed:

$$x = C_3 \cdot \alpha \qquad (7.20)$$

where:

C_3 = shape correction	=	1.0 for circular footing.
	=	1.75 for strip footing.
	=	1.25 for square footing.
α = empirical factor	=	2.5 to 3.5 (recent N.C. silica sand, age < 100 years).
	=	3.5 to 6.0 (N.C. aged silica sand, age > 3000 years).
	=	6.0 to 10.0 (O.C. silica sand).

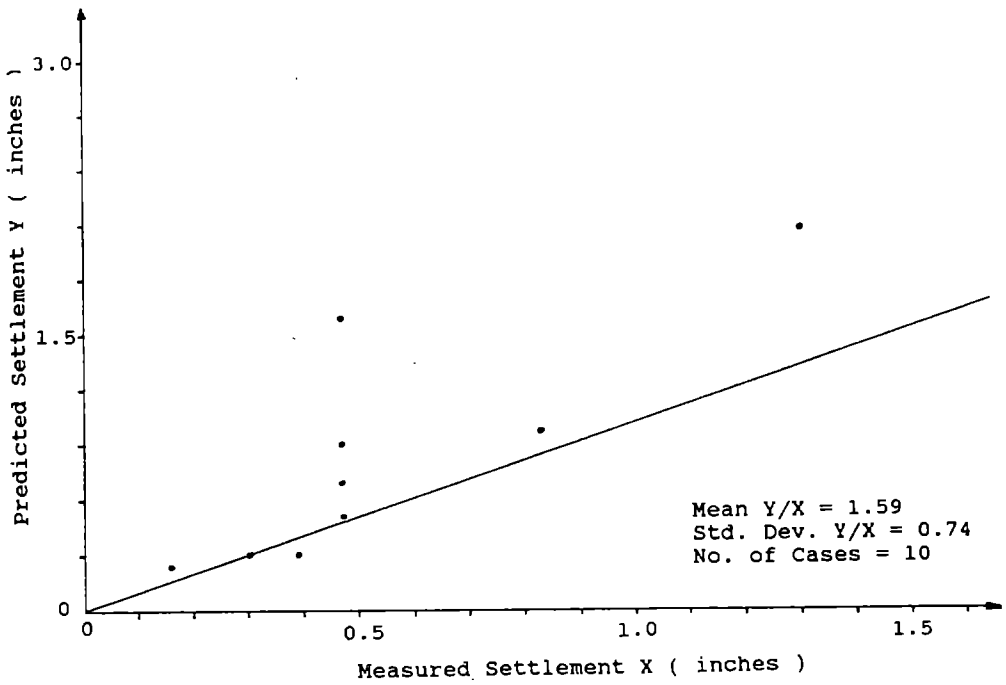

FIG. 7.6a. Comparison of Estimated and Observed Settlement of Shallow Foundation on Sand Using Schmertmann's 1970 Method

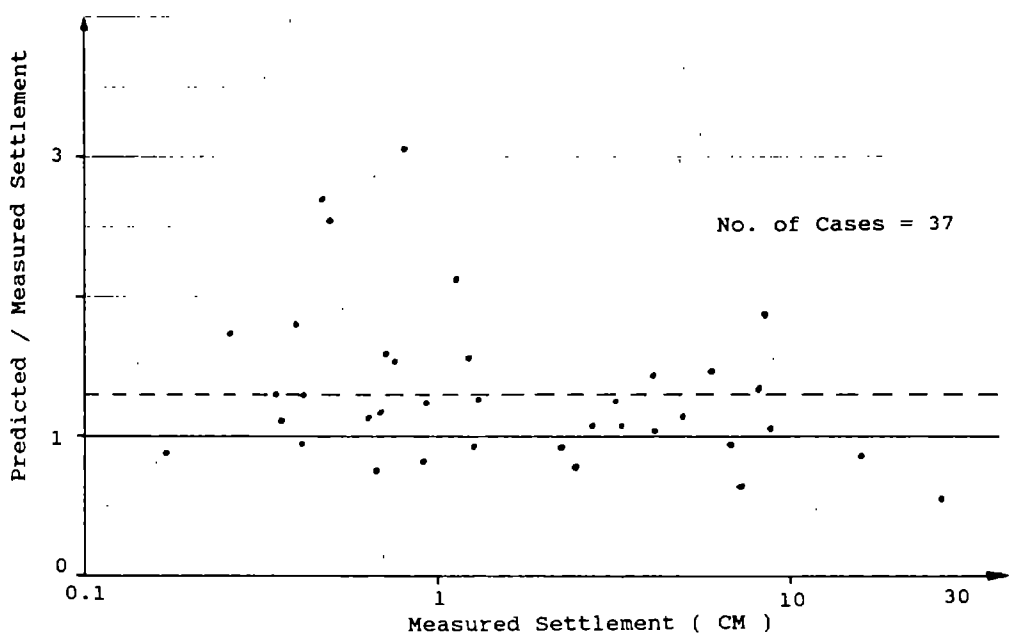

FIG. 7.6b. Ratio of Predicted Settlement to Measured Settlement Versus Measured Settlement for Schmertmann's 1970 Method of Estimating Settlement in Sands

To the authors' knowledge, Schmertmann's (1970) method has not been evaluated with such values of $\times$.

7.1.1.7 Settlement: Meyerhof's (1974) method

Meyerhof (1974) proposed as a simple estimate:

$$S = \frac{P \cdot B}{2\bar{q}_c} \tag{7.21}$$

where:

S = settlement.

P = net foundation pressure.

B = width of the footing.

$\bar{q}_c$ = cone resistance averaged over a depth equal to B below the footing.

7.1.1.8 Settlement: Precision of Meyerhof's method

This method may be used as an alternate to Schmertmann's method, or perhaps as a check. Meyerhof (1974) evaluated his method using 20 case studies which were not used to develop the method (Fig. 7.7). The ratio of calculated/measured settlement had a mean of 1.26 and a standard deviation of 0.44. The sizes of the footings were not given by Meyerhof.

7.1.2 Clay

7.1.2.1 Bearing capacity: Procedure 1

* Bearing capacity equation:

The bearing capacity of clays is generally calculated using the undrained shear strength S_u estimated from cone penetrometer test data.

Skempton (1951) proposed to use the conventional formula:

$$q_u = K_c \cdot N_c \cdot S_u + \gamma \cdot D \tag{7.22}$$

where:

q_u = ultimate bearing capacity.

N_c = Skempton's bearing capacity factor which includes the effect of shape and embedment.

γ = total unit weight of the soil.

D = depth of embedment of the footing.

S_u = undrained shear strength.

K_c = correction factor which accounts for load inclination, inclination of the base, and inclination of the ground surface.

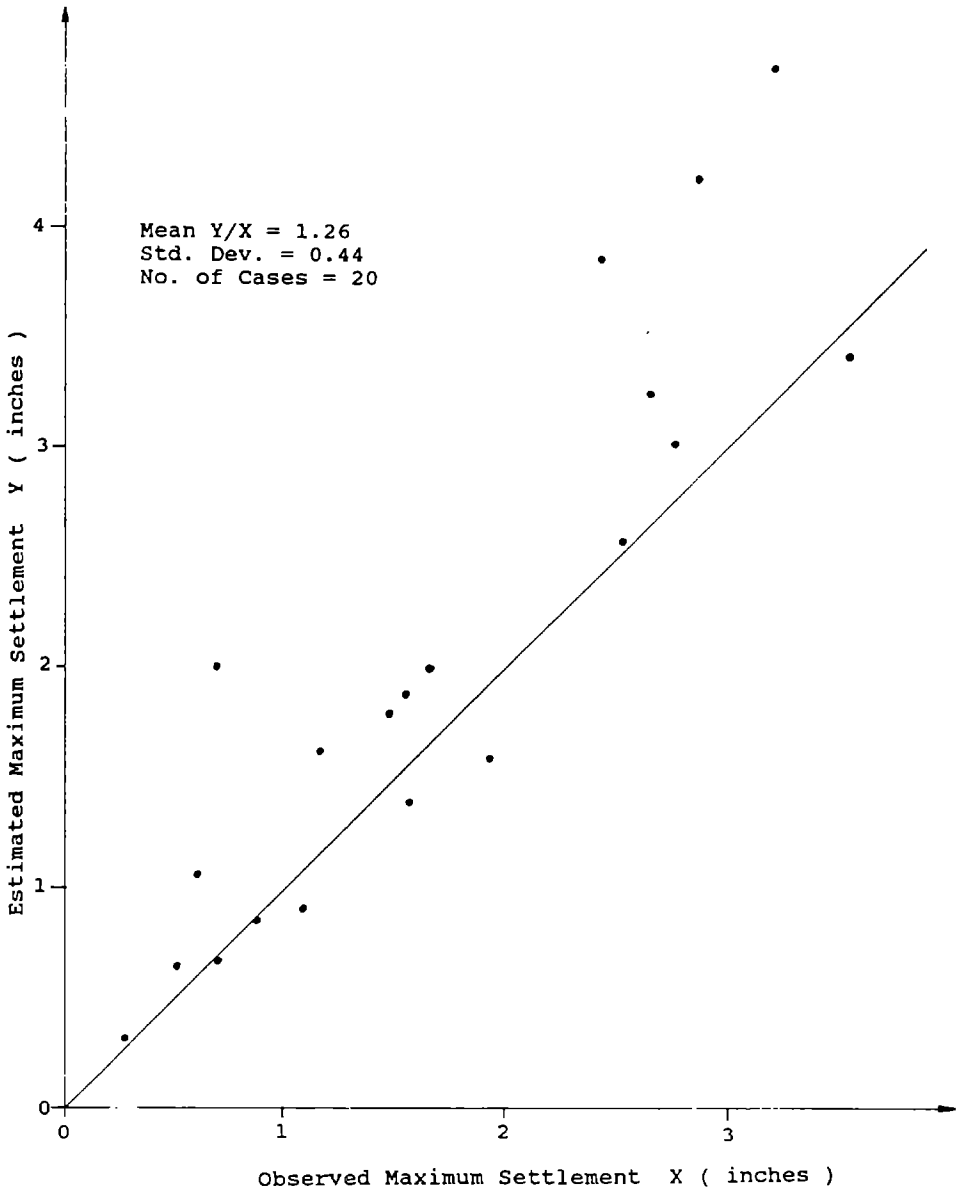

FIG. 7.7. Comparison of Estimated and Observed Settlement of Shallow Foundation in Sand Using Meyerhof's Method (Modified After Meyerhof 1974)

* Procedure:

1. Calculate the geometric average $\bar{q}_c$ from the base of the footing to 1.5 B below the base of the footing:

$$\bar{q}_c = \sqrt{q_{c1} \times q_{c2}}$$

where:

$\bar{q}_c$ = equivalent cone tip bearing.

q_{c1} = average of the cone tip bearing q_c from 0 to 0.5B below the depth of the footing.

q_{c2} = average of the cone tip bearing q_c from 0.5 to 1.5B below the depth of the footing.

B = width of the footing.

2. Estimate S_u from $\bar{q}_c$ using the method discussed in section 6.10.

3. Obtain Skempton's bearing capacity factor N_c using Fig. 7.8. The value of N_c for a footing varies with the ratio of the width B to length L, and with the depth of embedment D. For any given value of D/B, Fig. 7.8 shows that the bearing capacity factor for circular and square footings is approximately 1.2 times the corresponding value for a long continuous footing. A linear interpolation may be used for rectangular footing having intermediate value of B/L:

$$N_{c(B/L)} = N_{c(B/L=0)} + \frac{B}{L}(N_{c(B/L=1)} - N_{c(B/L=0)}) \qquad (7.23)$$

4. Estimate the value of K_c using the method discussed in section 7.1.2.5.

5. Compute q_u from equation 7.22.

7.1.2.2 Bearing capacity: Precision of procedure 1

To date (1991), no extensive data base study has been done to evaluate the precision of this design procedure. This method is the classical method used to calculate the bearing capacity on clay. The added possible error is the one due to getting S_u from q_c.

7.1.2.3 Bearing capacity: Procedure 2

* Bearing capacity equation:

Tand et al. (1986) proposed a procedure for predicting the ultimate bearing capacity of a circular or square footing. This procedure is based on the analysis

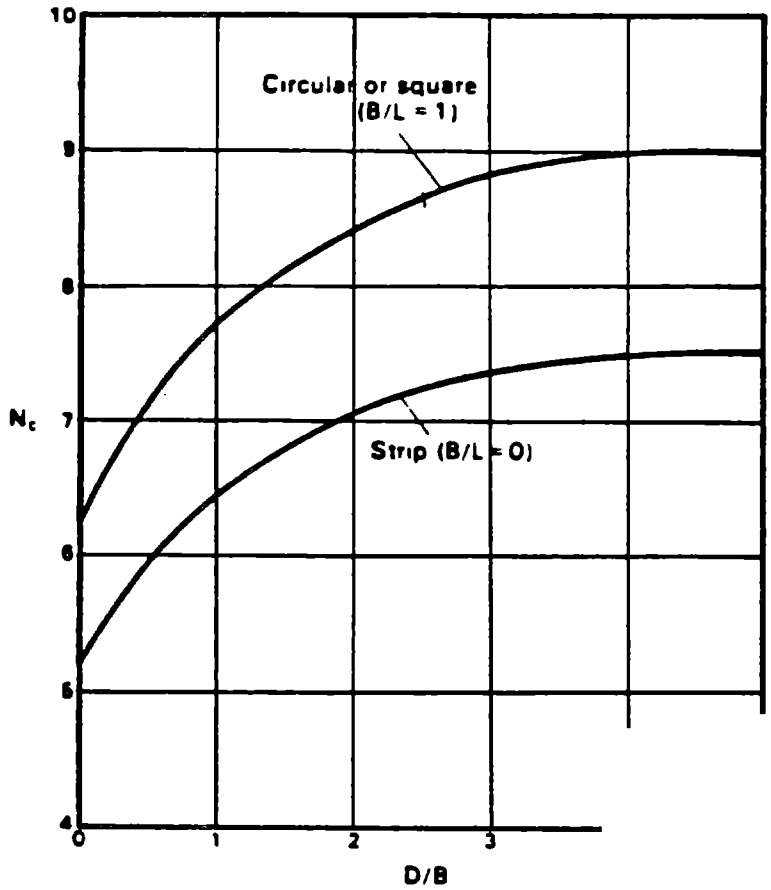

FIG. 7.8. Skempton's Bearing Factor N_c for Undrained Clay Conditions

(From Peck, Hanson, and Thornburn, 1974)

of 16 case histories where cone penetration testing had been performed in conjunction with load testing of plates or full size footings. The clay ranged from lightly to heavily overconsolidated, and from stiff to very stiff. No load tests on normally consolidated clays are present in this data base. Tand et al. (1986) proposed:

$$q_u = K_k \cdot R_k(\bar{q}_c - \gamma D) + \gamma D \tag{7.24}$$

where:

q_u = ultimate bearing capacity.

R_k = bearing capacity factor (Fig. 7.9) for circular or square footings.

$\bar{q}_c$ = equivalent cone tip bearing.

γ = total unit weight of the soil.

D = depth of embedment of the footing.

K_k = correction factor which accounts for load inclination, footing shape, inclination of base, and inclination of the ground surface. This factor is not part of the original recommendations from Tand et al. (1986) and is added here for completion.

* <u>Procedure:</u>

1. Find $\bar{q}_c$ using the method discussed in section 7.1.2.1.

2. Compute the equivalent embedment depth H_e:

$$H_e = \sum_{o}^{D} \Delta z \cdot q_c / \bar{q}_c \tag{7.25}$$

where:

D = unadjusted depth of embedment.

$q_c \cdot \Delta z$ = cone tip bearing in a sublayer within D times the thickness Δz of that sublayer.

$\bar{q}_c$ = equivalent cone tip bearing pressure below the footing.

3. Compute the ratio of equivalent embedment depth to footing size:

$$\frac{H_e}{B}$$

where:

B = width of the footing.

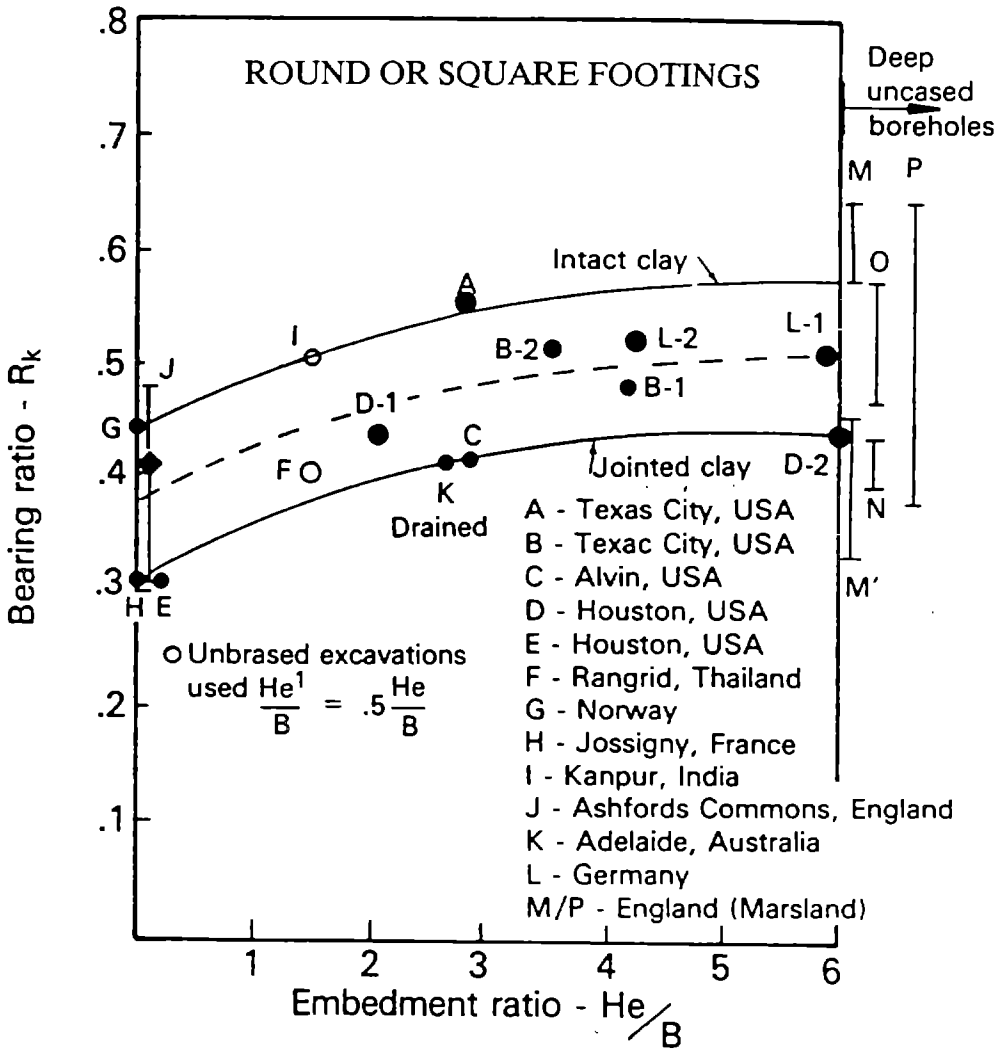

FIG. 7.9. Bearing Ratio R_K vs. Embedment Ratio (Modified After Tand et al. 1986)

4. Scale R_k from Fig. 7.9 using H_e/B. It is recommended that the lower bound curve be used for fissured or slickensided clays and that the average curve be used for all other clays unless load tests verify the use of the upper bound curve for intact clays.
5. Estimate the value of K_k using the method discussed in section 7.1.2.5.
6. Compute q_u from equation 7.24.

7.1.2.4 Bearing capacity: Precision of procedure 2

This method can be evaluated on the data base used to develop it (Tand et al., 1986). The ultimate bearing capacity for the case histories mentioned in Fig. 7.9 is within $\pm$ 20 percent of the average values.

7.1.2.5 Bearing capacity: Eccentric load, inclined load, base and ground inclination, footing shape.

When dealing with eccentric load, inclined load, footing shape, base and ground inclination, one must correct the values of N_c in procedure 1 (section 7.1.2.1) and R_k in procedure 2 (section 7.1.2.3), using the correction factor K_c and K_k respectively such that:

$$K_c = i \cdot b \cdot g \tag{7.26}$$

$$K_k = i \cdot s \cdot b \cdot g \tag{7.27}$$

where i, s, b, g are individual correction factors related to inclined load, footing shape, base and ground inclination respectively. The proposed factors are for a short term analysis characterized by the fact that no dissipation of excess pore pressure occurs.

A long term stability analysis is characterized by the fact that all excess pore pressures have been dissipated. If such an analysis is required for an N.C. clay, one may use the individual correction factors of sand presented in section 7.1.1.3, where ϕ is the friction angle of the clay.

* Eccentric load:

  The effect of load eccentricity on the bearing capacity is discussed in section 7.1.1.3. Once B' and L' have been found, procedure 1 and 2 (see section 7.1.2.1 and 7.1.2.3) can be applied to the $B' \times L'$ footing (instead of the $B \times L$ footing.

* Inclined load:

  Hansen (1961) proposed:

$$i = \left(1 - 1.3\frac{H}{V}\right) \text{with } H \leq 0.4V \tag{7.28}$$

where V is the projection of the load resultant on the axis perpendicular to the footing, and H is the projection of the load resultant on the plan of the footing.

* Footing shape:

Tand (1986) recommends to use Hansen's (1961) shape factor:

$$s = \frac{1}{1.2}\left(1 + 0.2\frac{B'}{L'}\right) \tag{7.29}$$

where B' and L' are defined in Fig. 7.3a.

* Base inclination:

Vesic (1975) proposed:

$$b = 1 - 0.39\upsilon \tag{7.30}$$

where υ is the base inclination angle in radians as defined in Fig. 7.3b.

* Ground inclination:

Vesic (1975) proposed:

$$g = 1 - 0.39\beta \tag{7.31}$$

where β is ground inclination angle in radians as defined in Fig. 7.3b.

* Depth of embedment:

Tand's formula already incorporates the effect of the depth of embedment through the factor R_k (Fig. 7.9).

7.1.2.6 Settlement: Sanglerat's (1972) step-by-step procedure

* Settlement equation:

Sanglerat proposed:

$$S = \sum_{1}^{n} H_o \frac{\Delta\sigma}{\alpha \bar{q}_c} \tag{7.32}$$

where:

S = total settlement, including short term and long term settlement.

H_o = expected change in stress at the middle of a soil layer.

α = soil compressibility coefficient.

$\bar{q}_c$ = average tip resistance for a soil layer.

* Procedure:

1. Prepare a table with the following headings.

Layer #	H_o	$\bar{q}_c$	α	$\Delta\sigma$	$H_o \frac{\Delta\sigma}{\alpha \bar{q}_c}$

2. Divide the soil into layers of approximately constant $\Delta\sigma$. Since $\Delta\sigma$ does not vary linearly with depth, the layer thickness H_o should be small right below the footing, and can increase with depth.
3. Estimate $\bar{q}_c$ for each layer.
4. Estimate α for each layer using Table 7.1.
5. Estimate the expected change in stress $\Delta\sigma$ at the center of each layer, using the following methods; these methods give the increase in stress under the center of the footing.

* <u>Circular</u> <u>footing:</u>

$$\Delta\sigma = \Delta p \left[1 - \left[1 + \left(\frac{R}{z} \right)^2 \right]^{-\frac{3}{2}} \right] \tag{7.33}$$

where:

Δp = net footing pressure = $q - \sigma'_1$.

q = footing bearing pressure.

σ'_1 = effective stress at the footing depth.

R = radius of the footing.

z = distance from the bottom of the footing to the center of the soil layer.

* <u>Rectangular</u> <u>footing:</u>

$$\Delta\sigma = 4\Delta p \cdot I_{(m,n)} \tag{7.34}$$

where:

Δp = net footing pressure defined as before.

$I_{(m,n)}$ = stress influence factor calculated using Fig. 7.10 where $n \times z$ is half the width of the footing, $m \times z$ is half the length of the footing, and z is defined as above.

For the increase in stress $\Delta\sigma$ under the corner of the footing, the equation is:

$$\Delta\sigma = \Delta p \times I_{(m,n)} \tag{7.35}$$

where $I_{(m,n)}$ is obtained as shown on Fig. 7.10.

Table 7.1 - Sanglerat's correlation for M, $M = \alpha \cdot q_c$
(after Costet and Sanglerat, 1975)

q_c (bar)	α	Soil type
$q_c < 7$ $7 < q_c < 20$ $q_c > 20$	$3 < \alpha < 8$ $2 < \alpha < 5$ $1 < \alpha < 2.5$	Clay of low plasticity (CL)
$q_c > 20$ $q_c < 20$	$3 < \alpha < 6$ $1 < \alpha < 3$	Silts of low plasticity (ML)
$q_c < 20$	$2 < \alpha < 6$	Highly plastic silts and clays (MH, CH)
$q_c < 12$	$2 < \alpha < 8$	Organic silts (OL)
$q_c < 7$ $50 < w < 100$ $100 < w < 200$ $w > 200$	 $1.5 < \alpha < 4$ $1 < \alpha < 1.5$ $0.4 < \alpha < 1$	Peat and organic clay (P_t, OH)
$20 < q_c < 30$	$2 < \alpha < 4$	Chalk
$q_c < 50$ $q_c > 100$	$\alpha = 2$ $\alpha = 1.5$	Sand

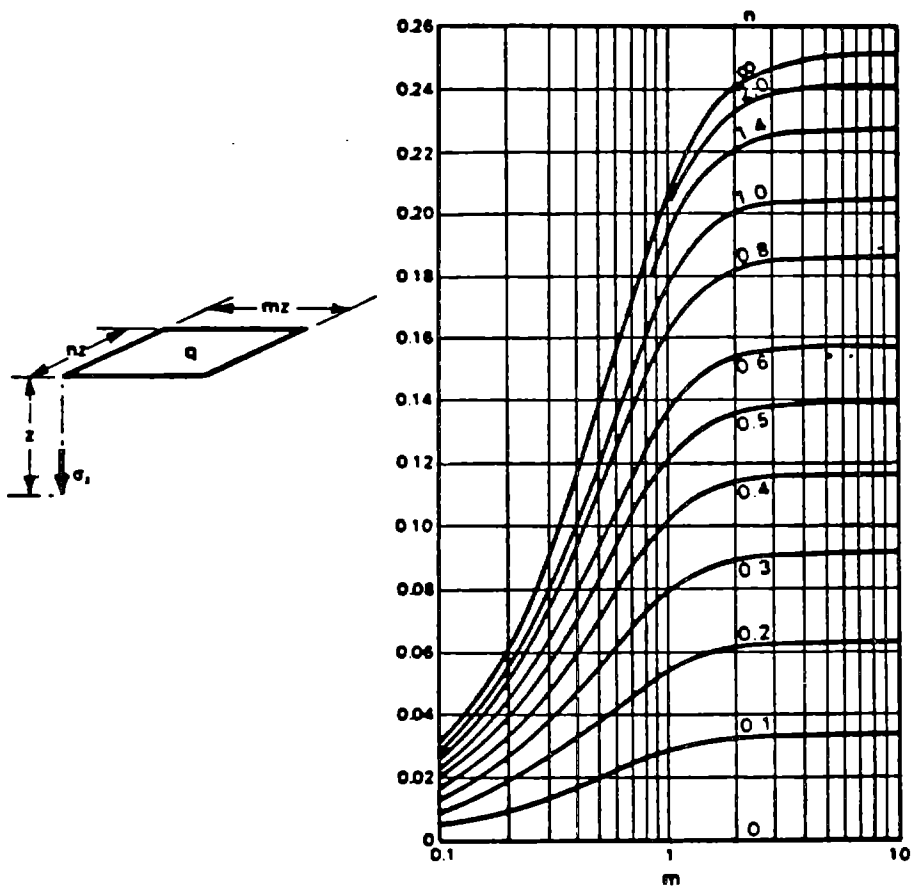

FIG. 7.10. Vertical Stress Under Corner of Uniformly Loaded Rectangular Area (From Fadum 1948)

6. Compute the total settlement using Equation 7.32.

Note: Schmertmann (1978) proposed a method to estimate the settlement on clay which makes use of the compression index C_c. This method is not presented here since it is difficult to assess C_c from a CPT test.

7.1.2.7 Settlement precision of Sanglerat's (1972) method

Sanglerat evaluated his method in 1979, using the data from 17 different sites in France (Fig. 7.11). The ratio of calculated/measured average settlement had a mean of 1.47 and a standard deviation of 0.53. Thus, this method overpredicts the settlement on the average and for this data base. It seems that this inaccuracy is due to the difficulty in assessing α from table 7.1. Therefore, local experience based on field settlement observation will help to adjust the method for any particular clay. Note that Sanglerat's method is not limited to clays and can be applied to other soils as well.

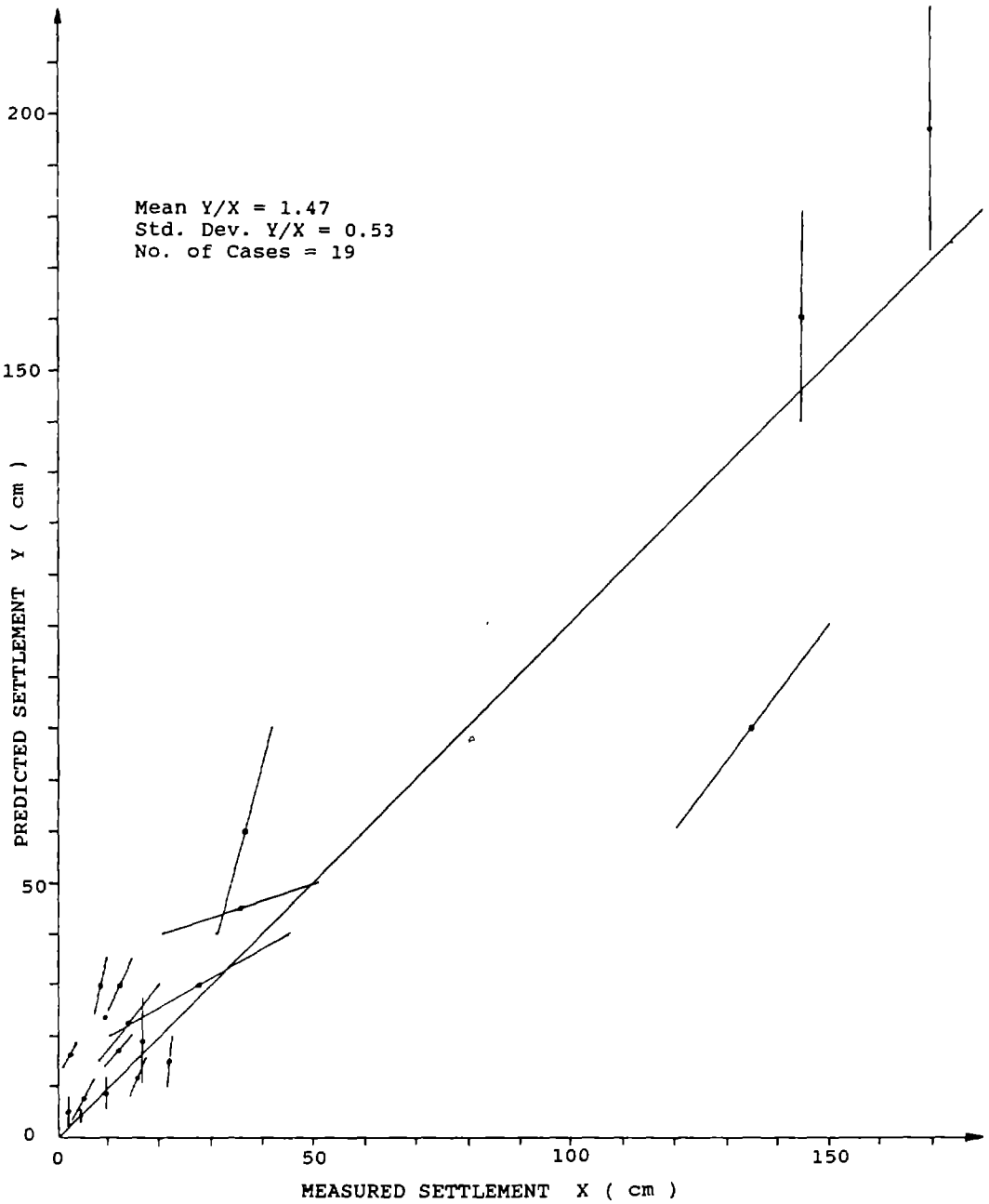

FIG. 7.11. Comparison of Predicted Versus Measured Average Settlement for Sanglerat's Method

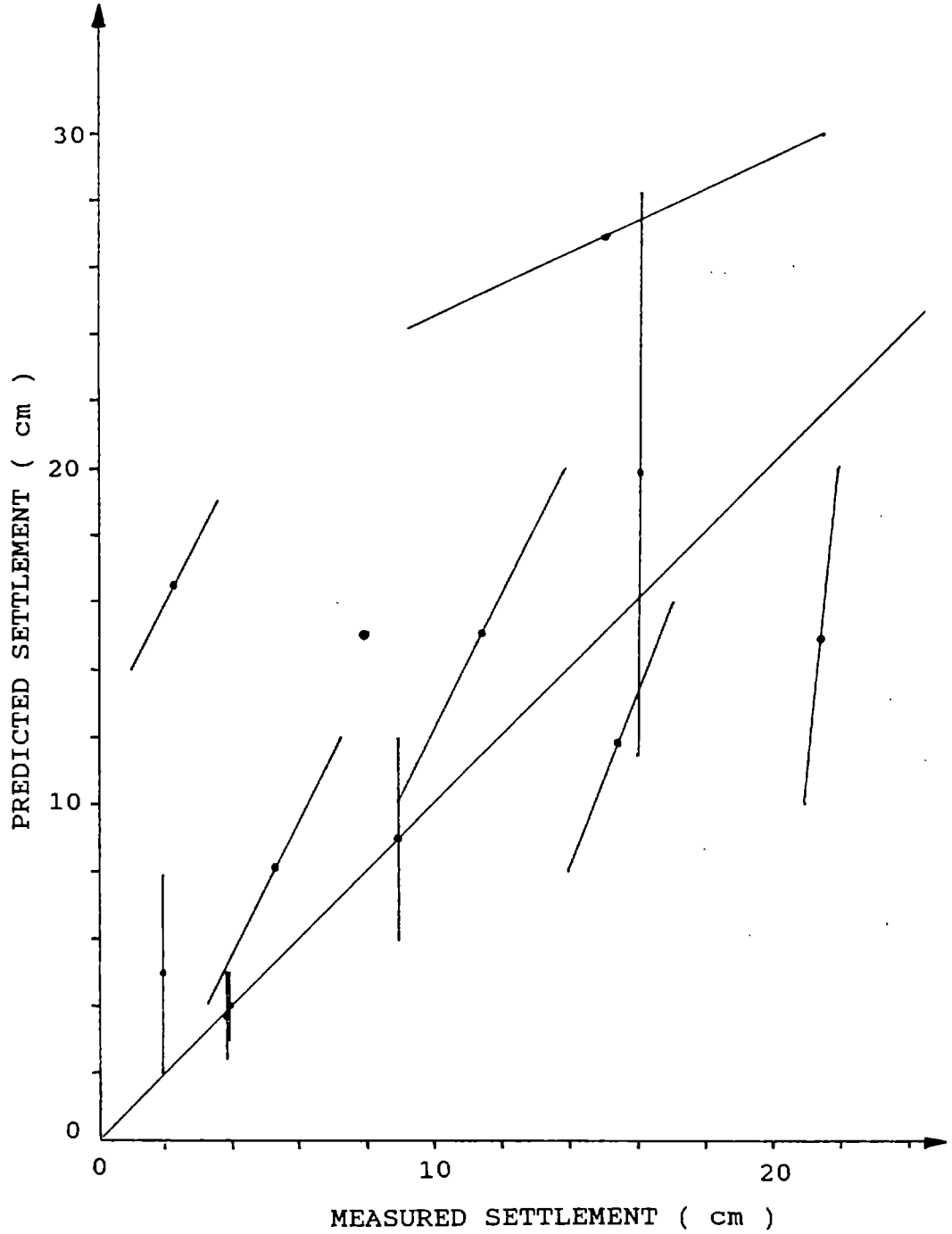

FIG. 7.11. Continued

7.1.3. Design Examples

7.1.3.1 Example problem 1: Rectangular footing on sand

The data from an electric CPT for use in example problem 1, as well as the footing shape, are presented in Fig. 7.12.

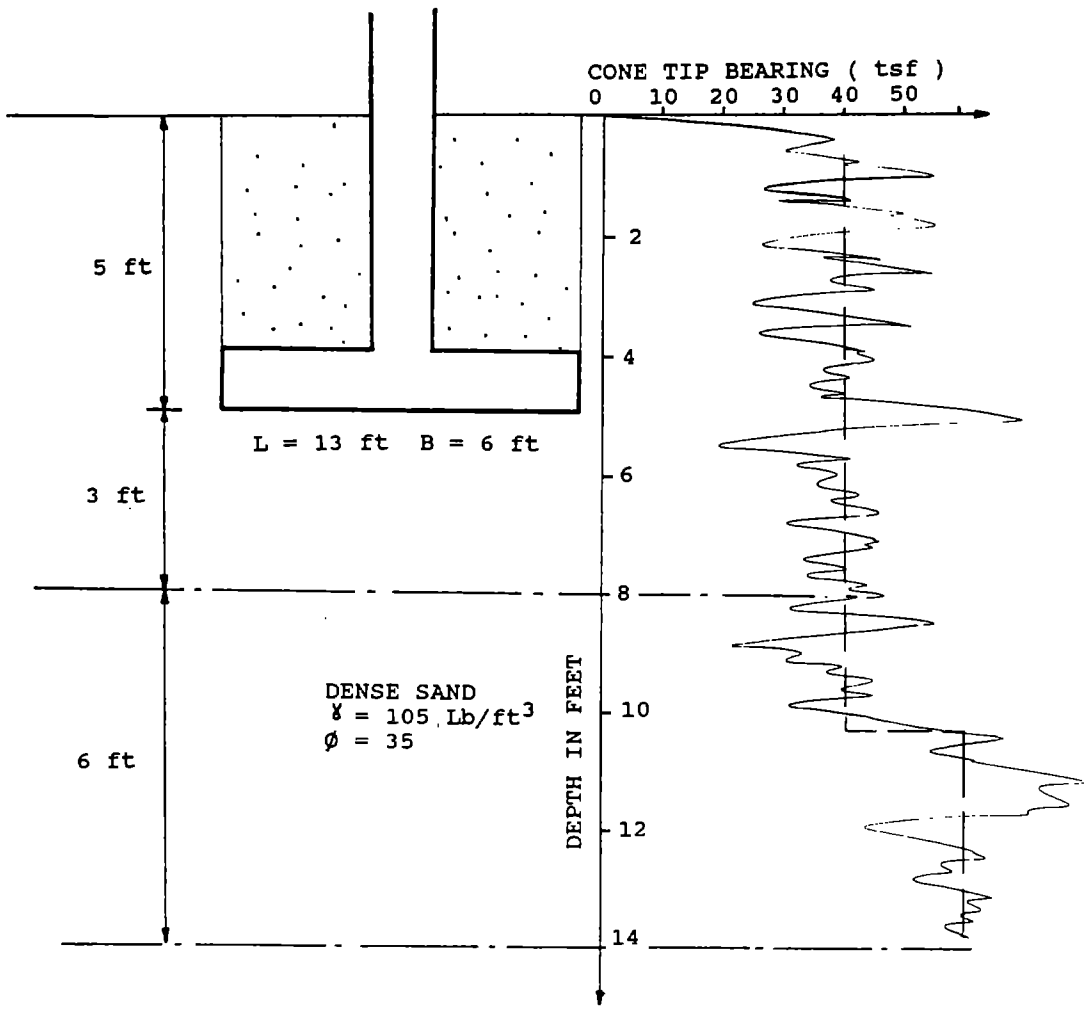

FIG. 7.12. Example Problem 1

EXAMPLE 1 - SHALLOW FOOTING ON SAND (Fig. 7.12)

Bearing Capacity

1. **Schmertmann (see section 7.1.1.1)**

The average of the cone tip bearing q_c from 0 to 0.5B below the footing is:

$$q_{c1} = 40 \quad tsf$$

The average of the cone tip bearing q_c from 0.5 to 1.5B below the footing is:

$$q_{c2} = \frac{(40 \times 2) + (60 \times 4)}{6} = 53.3 \quad tsf$$

Then, the equivalent cone tip bearing is:

$$\bar{q}_c = \sqrt{40 \times 53.3} = 46.2 \quad tsf$$

and

$$N_\gamma = N_q = 1.25 \times 46.2 = 57.7$$

The correction factors K_q and K_γ are:

$$K_q = i_q \cdot s_q \cdot d_q \cdot b_q \cdot g_q$$
$$K_\gamma = i_\gamma \cdot s_\gamma \cdot b_\gamma \cdot g_\gamma$$

where:

$$i_q = i_\gamma = 1$$

$$s_q = 1 + \left(\tfrac{6}{13}\right) \tan 35° = 1.3$$

$$s_\gamma = 1 - 0.4 \tan 35° = 0.8$$

$$b_\gamma = b_q = 1$$

$$g_\gamma = g_q = 1$$

so,

$$K_q = 1.3$$

$$K_\gamma = 0.8$$

Finally, the ultimate bearing capacity q_u is:

$$q_u = 1.3 \times 105 \times 5 \times 57.7 + \tfrac{1}{2} \times 0.8 \times 105 \times 6 \times 57.7$$

$$q_u = 53920.6 \quad lb/ft^2$$

or

$$q_u = 27 \quad tsf$$

The safe bearing capacity is:

$$q_{safe} = 27.0/3 = 9.0 \quad tsf$$

Using the conventional bearing capacity factors: $\phi = 38°$ so that $N_q = 55, N_\gamma = 65$ (Terzaghi and Peck, 1967):

$$q_u = 1.3 \times 105 \times 5 \times 55 + \frac{1}{2} \times 0.8 \times 105 \times 6 \times 65$$

$$= 53918 \quad lb/ft^2$$

$$= 27.0 \quad tsf$$

This is the same capacity as given by Schmertmann's procedure.

2. **Meyerhof (see section 7.1.1.1)**

   The ultimate bearing capacity is:

$$q_u = 40 \times \frac{6}{40}\left(1 + \frac{5}{6}\right) \quad tsf$$

$$q_u = 11 \quad tsf$$

   The safe bearing capacity is then:

$$q_{safe} = \frac{11}{3} \quad tsf$$

$$q_{safe} = 3.7 \quad tsf$$

3. **Awkati (see section 7.1.1.1)**

   From Fig. 7.1, the ultimate bearing capacity is:

$$q_u = 11 \quad tsf$$

   The safe bearing capacity is then:

$$q_{safe} = \frac{11}{3} \quad tsf$$

$$q_{safe} = 3.7 \quad tsf$$

   A q_{safe} value of 3.7 tsf is used as a result of the above calculations.

7.1.3.2 Example problem 2 : Rectangular footing on clay

The data from an electric CPT for use in example problem 2, as well as the footing shape, are presented in Fig. 7.13.

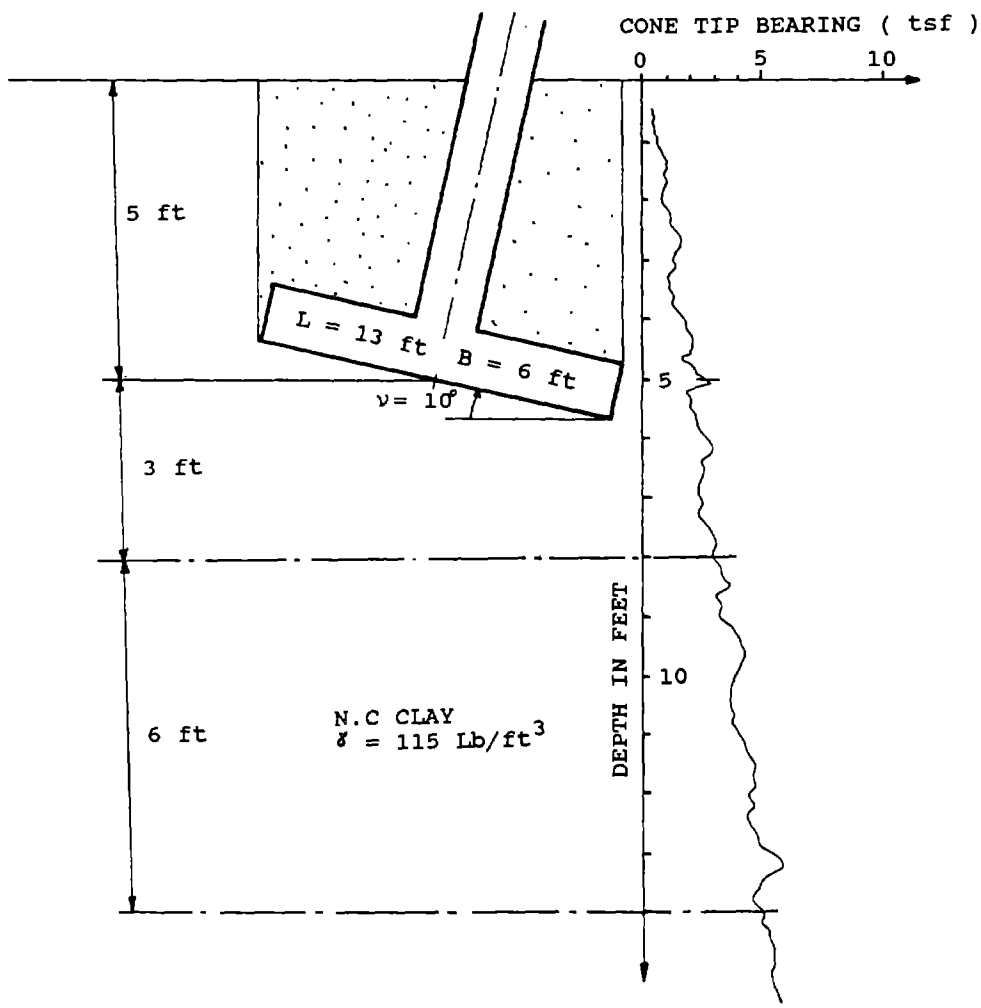

FIG. 7.13. Example Problem 2

EXAMPLE 2 - SHALLOW FOOTING ON CLAY (figure 7.13)

Bearing Capacity

1. **Skempton (see section 7.1.2.1)**

* The average of the cone tip bearing q_c from 0 to 0.5B below the footing is:

$$q_{c1} = \frac{1.7 + 2.9}{2} = 2.3 \quad tsf$$

The average of the cone tip bearing q_c from 0.5 to 1.5B below the footing is:

$$q_{c2} = \frac{2.9 + 4.9}{2} = 3.9 \quad tsf$$

Then, the equivalent cone tip bearing is:

$$\bar{q}_c = \sqrt{2.3 \times 3.9} = 3 \quad tsf$$

* The undrained shear strength S_u is:

$$S_u = \frac{\bar{q}_c - \gamma D}{15}$$

and

$$\gamma D = 115 \times 5 = 575 \quad lb/ft^2$$

or

$$\gamma D = 0.27 \quad tsf$$

so

$$S_u = (3 - 0.27)/15 = 0.18 \quad tsf$$

* N_c from Fig. 7.8 is (D/B = 0.83): N_c = 7.4

* The correction factor K_c is:

$$K_c = i \cdot b \cdot g$$

where:

$$i = 1$$

$$b = 1 - 0.39 \times 0.17 = 0.93$$

$$g = 1$$

so

$$K_c = 0.93$$

* Finally, the ultimate bearing capacity q_u is:

$$q_u = 0.93 \times 7.4 \times 0.18 + 0.27$$

$$q_u = 1.5 \quad tsf$$

2. **Tand (see section 7.1.2.3)**

* The equivalent cone tip bearing is calculated as before:

$$\bar{q}_c = 3 \quad tsf$$

* The equivalent embedment depth H_e is:

$$H_e = \sum_{o}^{D} \Delta z \cdot \frac{q_c}{\bar{q}_c}$$

The q_c profile from the ground level to a depth D is divided in 5 layers of thickness $\Delta z = 1\,ft$.

Layer No.	Δz (ft)	q_c (tsf)	$\Delta z \cdot q_c / \bar{q}_c$ (ft)
1	1	0.4	0.13
2	1	0.7	0.23
3	1	1.0	0.33
4	1	1.4	0.47
5	1	1.7	0.57

$$H_e = 1.73\,ft$$

* The ratio of equivalent embedment depth to footing size is:

$$\frac{H_e}{B} = \frac{1.73}{6} = 0.29$$

* R_k from Fig. 7.9 is: R_k = 0.4 (average curve).

* The correction factor $K_k = i \cdot s \cdot b \cdot g$

where:

i = 1

s = $1/1.2(1+0.2(6/13)) = 0.91$

b = $1 - 0.39x0.17 = 0.93$

g = 1

so

K_k = 0.85

* Finally the ultimate bearing capacity q_u is:

$$q_u = 0.85 \times 0.4 \times (3 - 0.27) + 0.27$$
$$q_u = 1.2 \quad tsf$$

7.1.3.3 Example problem 3 : Rectangular footing on layered soil

The data from an electric CPT for use in this example are presented in Fig. 7.14.

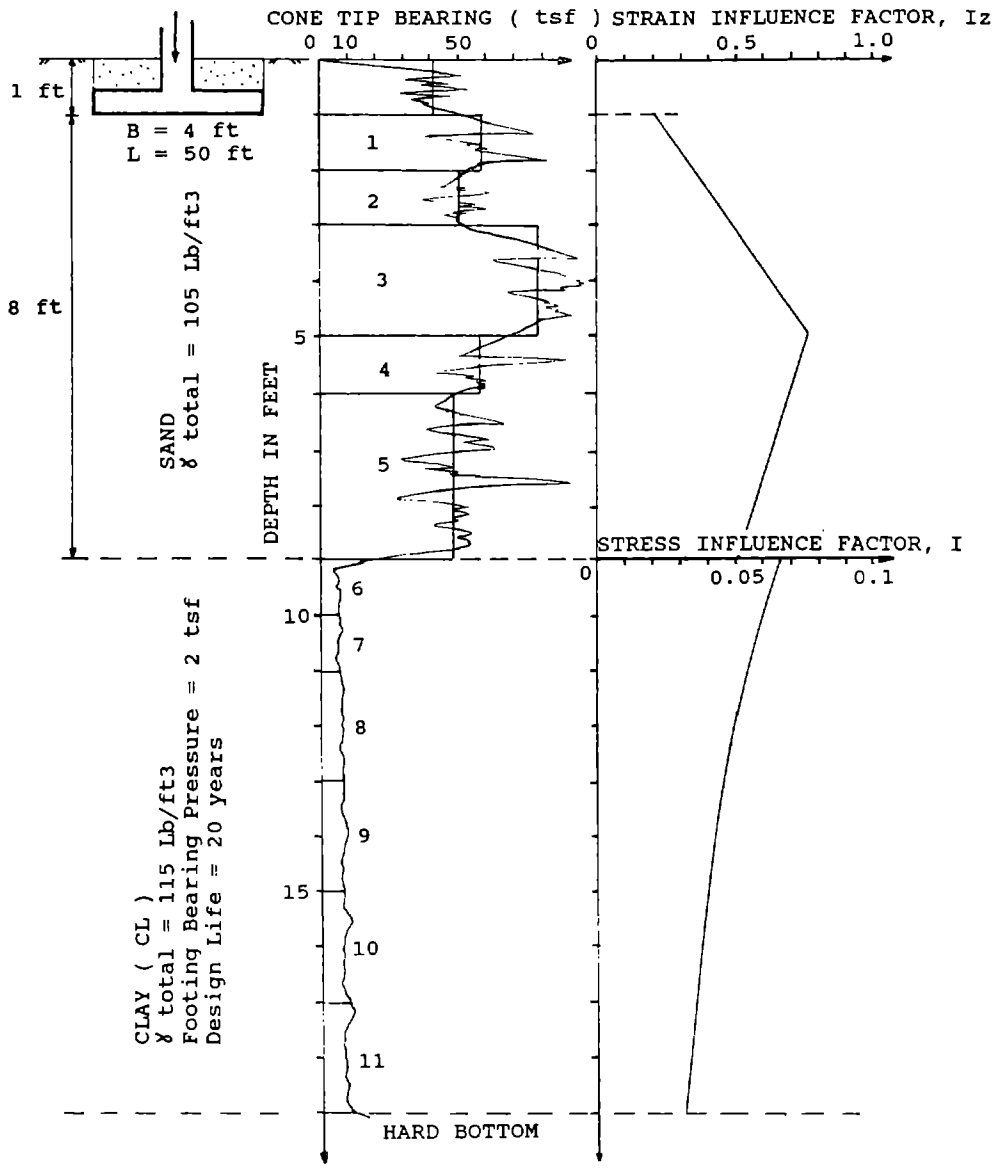

FIG. 7.14. Example Problem 3

EXAMPLE 3 - RECTANGULAR FOOTING ON LAYERED SOIL (Fig. 7.14)

1. Settlement in sand using Schmertmann's 1978 method

* Layer No.	Δz (ft)	I_z	q_c (tsf)	X	$\frac{I_z \Delta z}{x q_c}$
1	1	0.26	58	3.5	0.0013
2	1	0.42	49	3.5	0.0024
3	2	0.62	78	3.5	0.0045
4	1	0.72	59	3.5	0.0035
5	3	0.59	48	3.5	0.0105

$\sum = 0.022 ft^3/t$

* The strain influence factor I_z is calculated as explained on Fig. 7.5. The results are plotted on Fig. 7.14.

$$I_{zp} = 0.5 + 0.1\sqrt{\frac{\Delta p}{\sigma'_2}}$$

where

$$\Delta p = q - \sigma_1$$

and

$$\sigma'_1 = 105 x 1 = 105 lb/ft^2$$

or

$$\sigma'_1 = 0.05 tsf$$

so

$$\Delta p = 2 - 0.05 \quad tsf$$

$$\Delta p = 1.95 \quad tsf$$

also

$$\sigma'_2 = 105 x 5 = 525 lb/ft^2$$

$$\sigma'_2 = 0.25 \quad tsf$$

Finally,

$$I_{zp} = 0.5 + 0.1\sqrt{\frac{1.95}{0.25}} = 0.77$$

* The value of C_1 is:

$$C_1 = 1 - 0.5\,(\sigma'_1/\Delta p)$$

$$C_1 = 1 - 0.5\,(0.05/1.95)$$

$$C_1 = 0.99$$

* The value of C_2 is:

$$C_2 = 1 + 0.2\log_{10}(t_{yr}/0.1)$$

$$C_2 = 1 + 0.2\log_{10}(20/0.1)$$

$$C_2 = 1.46$$

* The settlement of the footing due to the sand layer is:

$$S = C_1 \cdot C_2 \cdot \Delta_p \sum \frac{I_z \cdot \Delta_z}{x \cdot q_c}$$

$$S = 0.99x1.46x1.95x0.022$$

$$S = 0.062ft(1.9cm)$$

2. <u>Settlement in clay using Sanglerat's (1972) method</u>

*

Layer No.	H_o (ft)	$\bar{q}_c$ (tsf)	α	$\Delta\sigma$ (tsf)	$H_o \frac{\Delta\sigma}{\alpha \bar{q}_c}$ (ft)
6	1	6.0	4	0.48	0.020
7	1	6.0	4	0.44	0.018
8	2	7.0	4	0.38	0.027
9	2	7.5	4	0.31	0.021
10	2	7.7	4	0.28	0.018
11	2	8.0	4	0.25	0.016

* From Table 7.1, $\alpha = 4$: low plasticity clay with:

$$q_c < 7 \text{ tsf and } 7 < q_c < 20 \text{ tsf}$$

* The expected change in stress $\Delta\sigma$ is obtained using Equation 7.34, and Fig. 7.10. The stress influence factor $I_{(m,n)}$ is plotted on Fig. 7.14.

The net footing pressure Δp is calculated as before:

$$\Delta p = 1.95 \quad tsf$$

so

$$\Delta\sigma = 4 \times 1.95 \times I_{(m,n)}$$

$$\Delta\sigma = 7.8 \times I_{(m,n)}$$

* The settlement of the footing due to the clay layer is:

$$S = 0.12 \quad ft(3.7cm)$$

3. <u>Total settlement of the footing</u>

The total settlement of the footing is:

$$S = 0.062 + 0.12$$

$$S = 0.182\ ft(5.6cm)$$

7.2 Design of Vertically Loaded Piles

7.2.1 Ultimate bearing capacity: introduction

The ultimate bearing capacity in compression for a pile is:

$$Q_L = Q_p + Q_s \tag{7.36}$$

or

$$Q_L = q_p \cdot A_p + \sum f \cdot A_s \tag{7.37}$$

where

Q_p = total end bearing, lb (kN)

Q_s = skin friction resistance, lb (kN)

f = average unit skin friction, lb/ft^2 (kPa)

A_s = pile shaft area within a chosen layer, ft^2 (m^2)

q_p = ultimate point end bearing, lb/ft^2 (kPa)

A_p = pile gross end bearing area, ft^2 (m^2)

In the special case of an open-ended pipe pile, the ultimate bearing capacity in compression requires the calculation of $Q_{L(unplugged)}$ and $Q_{L(plugged)}$. The value of $Q_{L(plugged)}$ is obtained by equation 7.37. The value of $Q_{L(unplugged)}$ is obtained as follows:

$$Q_{L(unplugged)} = q_p \cdot A'_p + (\sum f \cdot A_s + \sum f \cdot A'_s) \tag{7.38}$$

where

Q_p = total and bearing, lb (kN)

Q_s = skin friction resistance, lb (kN)

f = average unit skin friction, lb/ft^2

A_s = outer pile shaft area within a chosen layer, ft^2 (m^2)

A'_s = inner pile shaft area within a chosen layer, ft^2 (m^2)

q_p = ultimate point bearing, lb/ft^2 (kpa)

A'_p = cross sectional area of pile point = $\pi t(d_o - t)$, ft^2 (m^2)

t = pile wall thickness, ft (m)

d_o = outer pile diameter, ft (m)

The pile capacity is the lower of the two values: $Q_{L(unplugged)}$ and $Q_{L(plugged)}$.

For H piles, the ultimate bearing capacity in compression should be calculated by considering that the pile is half plugged (Tucker and Briaud, 1988). In tension, the enclosing outside perimeter should be used.

7.2.2 Ultimate bearing capacity: step-by-step procedure

Three methods for using the CPT results to predict vertical pile capacity are presented here:

- De Ruiter and Beringen (1979)
- Schmertmann (1978)
- LPC (Bustamante and Gianeselli, 1983)

A microcomputer program exists for the LPC method (Tucker and Briaud, 1986).

For each method, the following procedure should be applied:

1. Obtain the cone bearing resistance q_c and the cone friction resistance f_s over the depth interval from the ground surface to 8 pile diameters below the pile tip.
2. Divide the q_c and f_s profiles in layers. Then, average the values of q_c and f_s for each layer.
3. Assign a soil type to each averaged value (see section 6.3).
4. Estimate the value of f for each layer, and estimate q_p. To do so, enter one of the three methods:
   - De Ruiter and Beringen (section 7.2.3)
   - Schmertmann (section 7.2.4)
   - LPC (section 7.2.5)
5. Compute the ultimate bearing capacity using equations 7.37 and 7.38, and adopt the lowest value of Q_L.

7.2.3 Ultimate bearing capacity: De Ruiter and Beringen method

The method proposed by De Ruiter and Beringen (1979) to estimate q_p and f is the following:

* <u>Sand</u>
  - The unit skin friction f is the minimum of:

$$f_1 = 0.12 \quad MPa \tag{7.39}$$

$$f_2 = CPT \text{ sleeve friction } f_s \tag{7.40}$$

$$f_3 = q_c/300 \text{(compression)} \tag{7.41}$$

$$f_3 = q_c/400 \text{(tension)} \tag{7.42}$$

where

where

$q_c =$
cone resistance

- The unit end bearing capacity q_p is the minimum of:

q_p
from Fig. 7.15

q_p
from Fig. 7.16

* Clay

- The unit skin friction f is:

$$f = \alpha \cdot S_u \tag{7.43}$$

where

α = 1 in. NC clay (see section 6.8)

= 0.5 in. OC clay

S_u = undrained shear strength found as described in section 6.10.

- The unit end bearing capacity q_p is:

$$q_p = 9 \cdot S_u \tag{7.44}$$

7.2.4 Ultimate bearing capacity: Schmertmann's method

The method propsoed by Schmertmann (1978) to estimate q_p and f is the following:

* Sand

- The unit skin friction f is the minimum of:

$$f_1 = K \frac{l}{8D} f_s \quad if \quad l < 8D \tag{7.45}$$

$$f_1 = K \cdot f_s \quad if \quad l > 8D \tag{7.45}$$

$$f_2 = 0.12 MPa \tag{7.46}$$

$$f_3 = c \cdot q_c \tag{7.47}$$

where

K = ratio of f / f_s from Fig. 7.17

l = depth to f_s considered

D = pile width

L = pile length

c = coefficient from Table 7.2

f_s = CPT unit friction

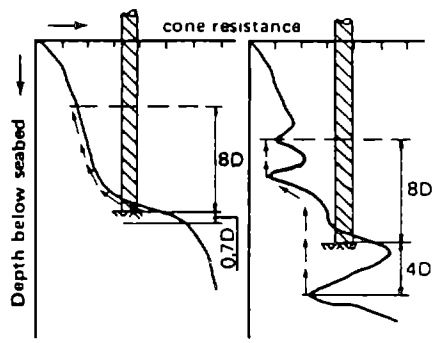

$$q_p = \frac{(I + II)/2 + III}{2}$$

Key

D : Diameter of the pile

I : Average cone resistance below the tip of the pile over a depth which may vary between 0.7D and 4D

II : Minimum cone resistance recorded below the pile tip over the same depth of 0.7D to 4D

III : Average of the envelope of minimum cone resistances recorded above the pile tip over a height which may vary between 6D and 8D. In determining this envelope, values above the minimum value selected under II are to be disregarded

q_p : Ultimate unit point resistance of the pile

FIG. 7.15. Point Bearing of Pile in Sand (From de Ruiter and Beringen 1979)

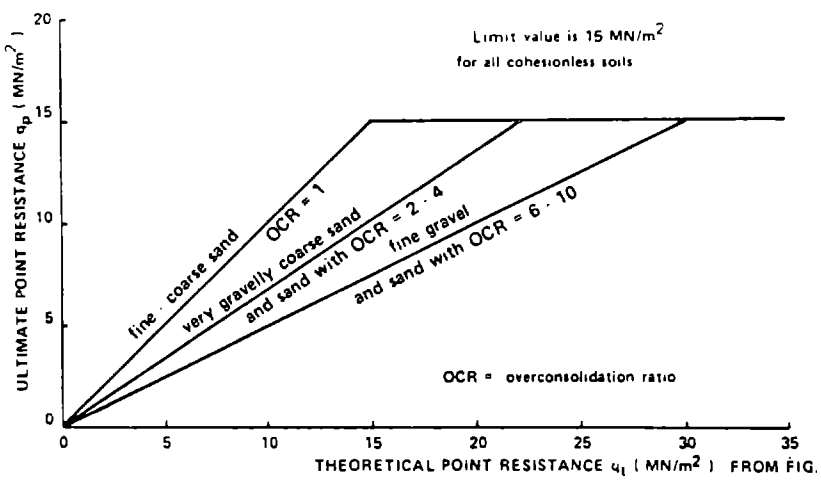

FIG. 7.16. Limit Values for Point Bearing of Piles in Sand (From de Ruiter and Beringen 1979)

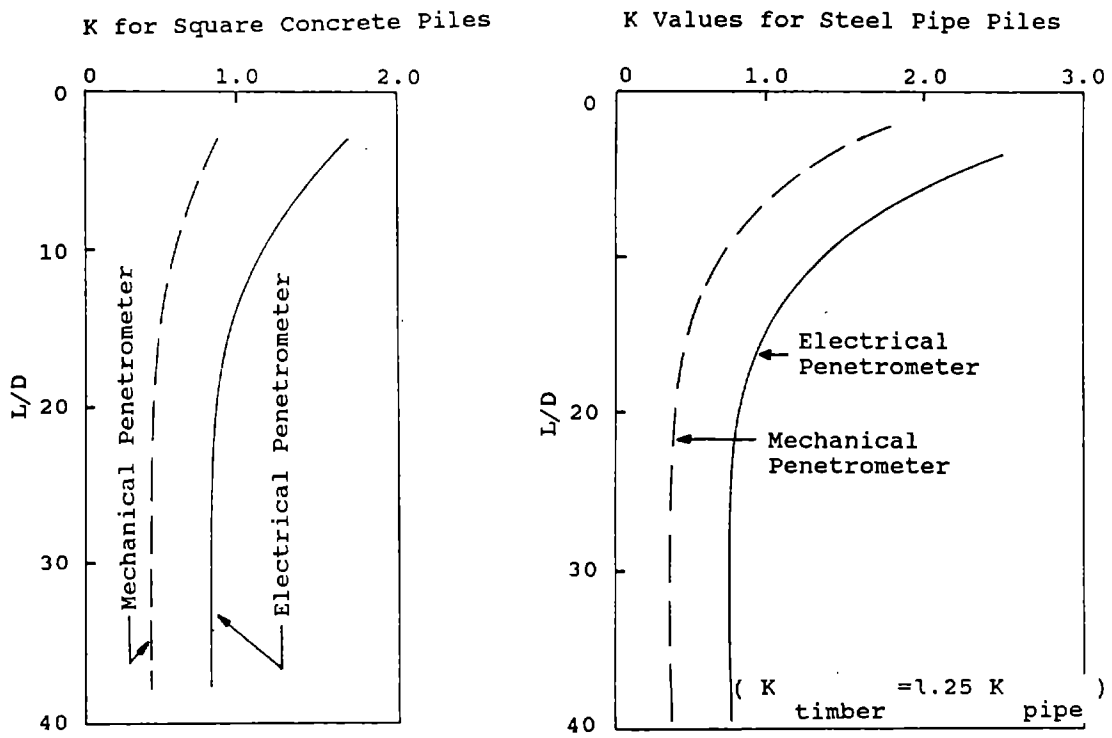

FIG. 7.17. Penetrometer Design Curves for Pile Side Friction in Sand (From Schmertmann 1978a)

Table 7.2 - C values (after Schmertmann 1978)

TYPE OF PILE	C
Precast concrete	0.012
Precast, enlarged base	0.009
Cast in situ displacement	0.018
"Vibro" pile	0.018
Timber	0.018
Steel displacement	0.012
Open-ended steel pile	0.008

q_c = CPT unit resistance

- The unit end bearing capacity q_p is found by using the De Ruiter and Beringen procedure for sand (section 7.2.3).

* Clay

- The unit skin friction of the pile f, is the minimum of:

$$f_1 = \alpha' \cdot S_u \tag{7.48}$$

$$f_2 = \alpha' \frac{l}{8D} f_s \quad if \quad l < 8D \tag{7.49}$$

$$f_2 = \alpha' \cdot f_s \quad if \quad l > 8D \tag{7.49}$$

where

α' = coefficient from Fig. 7.18

S_u = undrained shear strength (found as described in section 6.10) at the depth considered

f_s = CPT unit friction

l = depth to f_s considered

D = pile width

- The unit end bearing capacity of the pile q_p is found by using the De Ruiter and Beringen procedure for sand (section 7.2.3).

7.2.5 Ultimate bearing capacity: LPC method

A computer program (PILECPT) has been developed to automate the calculations for this method.

The Laboratoire des Ponts et Chaussees in France proposed a set of rules for the prediction of vertically loaded piles using CPT results (Bustamante, and Gianeselli, 1983).

First, use Fig. 7.19 to find the pile category based on the pile installation procedure. Then, for each soil layer, enter Fig. 7.20 for the appropriate soil type, pile category and range of cone resistance. This will indicate which curve of Fig. 7.21 to use for determining f. Finally, find the appropriate curve in Fig. 7.21 and obtain the value of f for the given value of q_c at the depth considered.

The unit point resistance q_p is calculated as:

$$q_p = K_c \cdot q_c \tag{7.50}$$

where

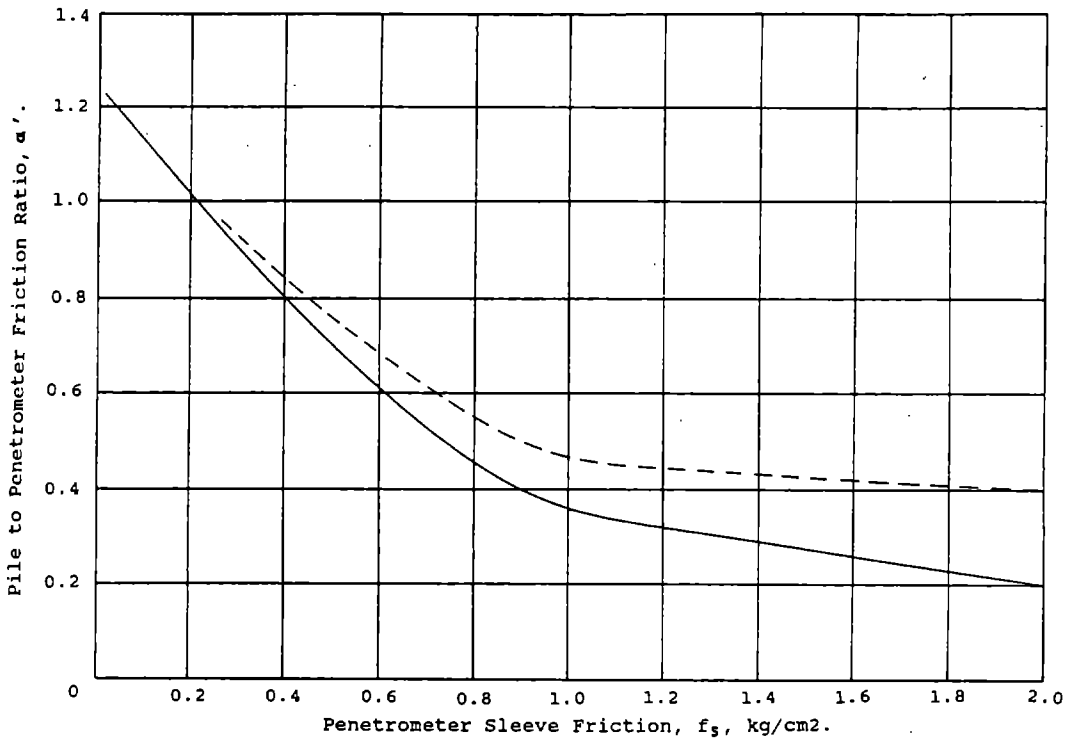

FIG. 7.18. Design Curves for Piles Side Friction in Clay (From Schmertmann 1978a)

GROUP I		
1. FS	Drilled shaft with no drilling mud	Installed without supporting the soil with drilling mud. Applicable only for cohesive soils above the water table.
2. FB	Drilled shaft with drilling mud	Installed using mud to support the sides of the hole. Concrete is poured from the bottom up, displacing the mud.
3. FT (FTU)	Drilled shaft with casing	Drilled within the confinement of a steel casing. As the casing is retrieved, concrete is poured in the hole.
4. FTC	Drilled shaft, hollow auger (auger cast pile)	Installed using a hollow stem continuous auger having a length at least equal to the proposed pile length. The auger is extracted without turning while, simultaneously, concrete is injected through the auger stem.
5. FPU	Pier	Hand excavated foundations. The drilleing method requires the presence of workers at the bottom of the excavation. The sides are supported with restraining elements or casing.
6. FIG (BIG)	Micropile type I	Drilled pile with casing. Diameter less than 250 mm (10 in.). After the casing has bee filled with concrete, the top of the casing is plugged. Pressure is applied inside the casing between the concrete and the plug. The casing is recovered by maintaining the pressure against the concrete.

FIG. 7.19. Description of Pile Categories for the Proposed L.P.C. Method (after Bustamante and Gianeselli, 1983)

GROUP II		
7. VMO	Screwed-in pile	Not applicable for cohesionless of soils below water table. A screw type tool is placed in fromt of a corrugated pipe which is pushed and screwed in place. The rotation is reversed for pulling out the casing while concrete is poured.
8. BE	Driven pile, concrete coated	- pipe pile 150 mm (6 in.) to 500 mm (20 in.) external diameter - steel-H pile - caissons made of 2, 3, or 4 sheet pile sections The pile is driven with an oversized protecting shoe. As driving proceeds, concrete is injected through a hose near the oversized shoe producing a coating around the pile.
9. BBA	Driven prefabricated pile	Reinforced or prestressed concrete pile installed by driving or vibro-driving.
10. BM	Steel driven pile	Pile made of steel only and driven in place. - H pile, pipe pile or any shape obtained by welding sheet-pile sections
11. BPR	Prestressed tube pile	Made of hollow cylinder elements of lightly reinforced concrete assembled together by prestressing before driving. Each element is generally 1.5 to 3 m (4-9 ft) long and 0.7 to 0.9 m (2-3 ft) in diameter; the thickness is approximately 0.15 m (6 in.). The piles are driven open-ended.
12. BFR	Driven pile, bottom concrete plug	Driving is achieved through the bottom concrete plug. The casing is pulled out while low slump concrete is compacted in it.
13. BMO	Driven pile, molded	A plugged tube is driven until the final position is reached. The tube is filled with medium slump concrete to the top and the tube is extracted.
14. VBA	Concrete pile, pushed-in	Pile is made of cylindrical concrete elements prefabricated or cast-in-place, 0.5 to 2.5 m (1.5 to 8 ft) long and 30 to 60 cm (1 to 2 ft) in diameter. The elements are pushed in by a hydraulic jack.
15. VME	Steel pile, pushed-in	Pile made of steel only is pushed in by a hydraulic jack.
16. FIP	Micropile type II	Drilled pile <250 mm (10 in.) in diameter. The reinforcing cage is placed in the hole and concrete placed from bottom up.
17. BIP	High pressure injected pile, large diameter	Diameter >250 mm (10 in.). The injection system should be able to produce high pressures.

FIG. 7.19. Continued

CLAY AND SILT

CURVE #	q_c (ksf)	PILE TYPE (see Fig. 1)	COMMENTS ON INSERTION PROCEDURE
1	<14.6	1-17	
	>14.6	1,2	Very probable values when using tools without teeth or with oversized blades and where a remolded layer of material can be deposited along the sides of the drilled hole. Use these values also for deep holes below the water table where the hole must be cleaned several times. Use these values also for cases when the relaxation of the sides of the hole is allowed due to incidents slowing or stopping the pouring of the concrete. For all the previous conditions, experience shows, however, that f_{max} can be between curves 1 and 2; use an intermediate values of f_{max} is such values is warranted by a load test.
2	>25.1	4, 5, 8, 9, 10, 11, 13, 14, 15	For all steel piles, experience shows that, in plastic soils, f_{max} is often as low as curve 1; therefore, use curve 1 when no previous load test is available. For all driven concrete piles use curve 3 in low plasticity soils with sand or sand and gravel layers or containing boulders and when q_c>52.2 ksf.
	>25.1	7	Use these values for soils where q_c<52.2 ksf and the rate of penetration is slow; otherwise use curve 1. Also for slow penetration, when q_c>93.9 ksf, use curve 3.
	>25.1	6	Use curve 3 based on previous load test.
	>25.1	1,2	Use these values when careful method of drilling with an auger equipped with teeth and immediate concrete pouring is used. In the case of constant supervision with cleaning and grooving of the borehole walls followed by immediate concrete pouring, for soils of q_c>93.9 ksf, curve 3 can be used.
	>25.1	3	For dry holes. It is recommended to vibrate the concrete after taking out the casing. In the case of work below the water table, where pumping is required and frequent movement of the casing is necessary, use curve 1 unless load test results are available.
3	>25.1 <41.8	12	Usual conditions of execution as described in DTU 13.2
5	>41.8	16,17	In the case of injection done selectively and repetitively at low flow reate it will be possible to use curve 5, if it is justified by previous load test.

FIG 7.20. Pile Type and Insertion Procedures for the Proposed L.P.C. Method (after Bustamante and Gianeselli, 1983)

SAND AND GRAVEL

CURVE #	q_c (ksf)	PILE TYPE (see Fig. 1)	COMMENTS ON INSERTION PROCEDURE
1	<73.1	2, 3, 4, 6, 7, 8, 9, 10, 11, 12, 13, 14, 15	
2	>73.1	6, 7, 9, 10, 11, 12, 13, 14, 15	For fine sands. Since steel piles can lead to very small values of f_{max} in such soils, use curve 1 unless higher values can be based on load test results. For concrete piles, use curve 2 for fine sands of q_c > 156.6 ksf.
	>104.4	2, 3	Only for fine sands and bored piles which are less than 30 m (100 ft) long. For piles longer than 30 m (100 ft) in fine sand, f_{max} may vary between curves 1 and 2. Where no load test data is available, use curve 1.
	>104.4	4	Reserved for sands exhibiting some cohesion.
3	>156.6	6, 7, 9, 10, 13, 14, 15, 17	For coarse gravelly sand or gravel only. For concrete piles, use curve 4 if it can be justified by a load test.
	>156.6	2, 3	For coarse gravelly sand or gravel and bored piles less than 30 m (100 ft) long.
			(For gravel where q_c > 83.5 ksf, use curve 4.)
4	>156.6	8, 12	For coarse gravelly sand and gravel only.
5	>104.4	16, 17	In the case of injection done selectively and repetitively at low flow rate it will be possible to use curve 5, if it is justified by previous load test.

CHALK

CURVE #	q_c (ksf)	PILE TYPE (see Fig. 1)	COMMENTS ON INSERTION PROCEDURE
1	<62.6	1, 2, 3, 4, 6, 7, 8, 9, 10, 11, 12, 13, 14, 15	
3	>62.6	7, 8, 9, 10, 11, 13, 14, 15	Experience shows that in some chalks where q_c < 146.1 ksf, below water table, steel or smooth concrete piles may exhibit f_{max} values as low as those of curve 2. When no load test is available use curve 2 for q_c < 146.1 ksf. For chalk of q_c > 250.5 ksf use curve 4 based on a load test.
	>93.9	6, 8	
	>93.9	1, 2, 3, 5, 7	For bored piles above the water table and concrete poured immediately after boring. For type 7 piles, use a slow penetration thus creating corrugations alon the hole walls. Also for chalk above the water table and for q_c > 250.5 ksf use curve 4 if based on a load test.
			Below the water table and with tools producing a smooth wall or when a deposit of remolded chalk is left on the walls of the hole, experience shows that f_{max} can drop to values given by curve 2. Use higher values only on the basis of load tests.
4	>93.9	12	
	>93.9	16, 17	In the case of injection done selectively and repetitively at low flow rate it will be possible to use curve 4, if it is justified by previous load test.

FIG. 7.20. Continued

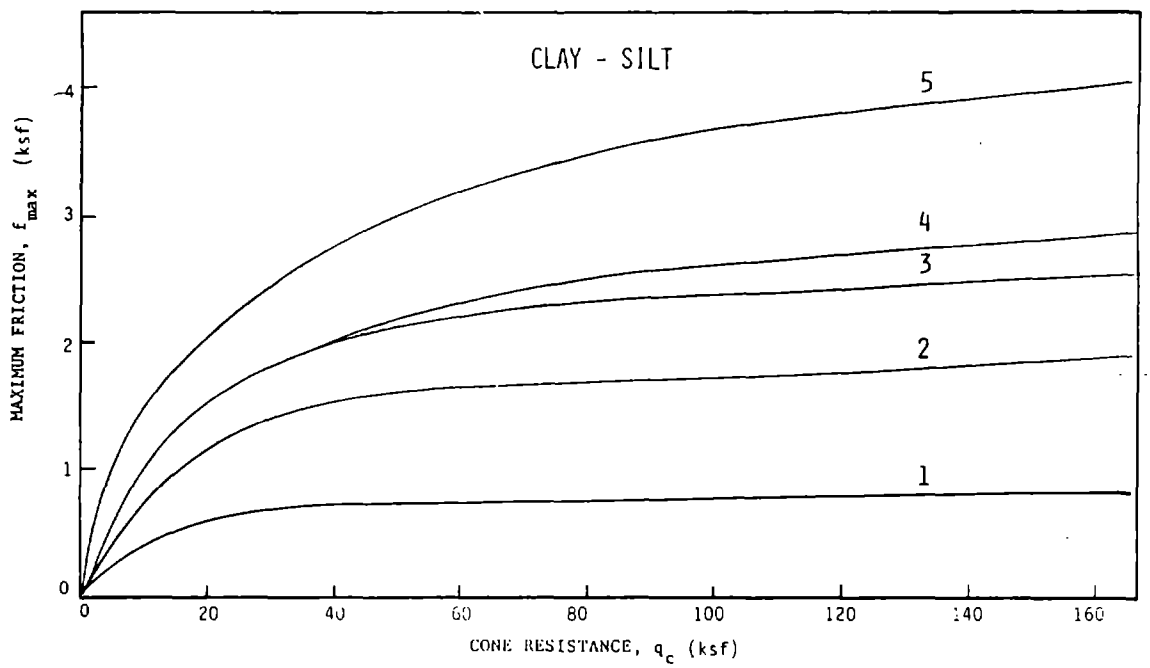

FIG. 7.21. Maximum Friction Curves for L.P.C. Method

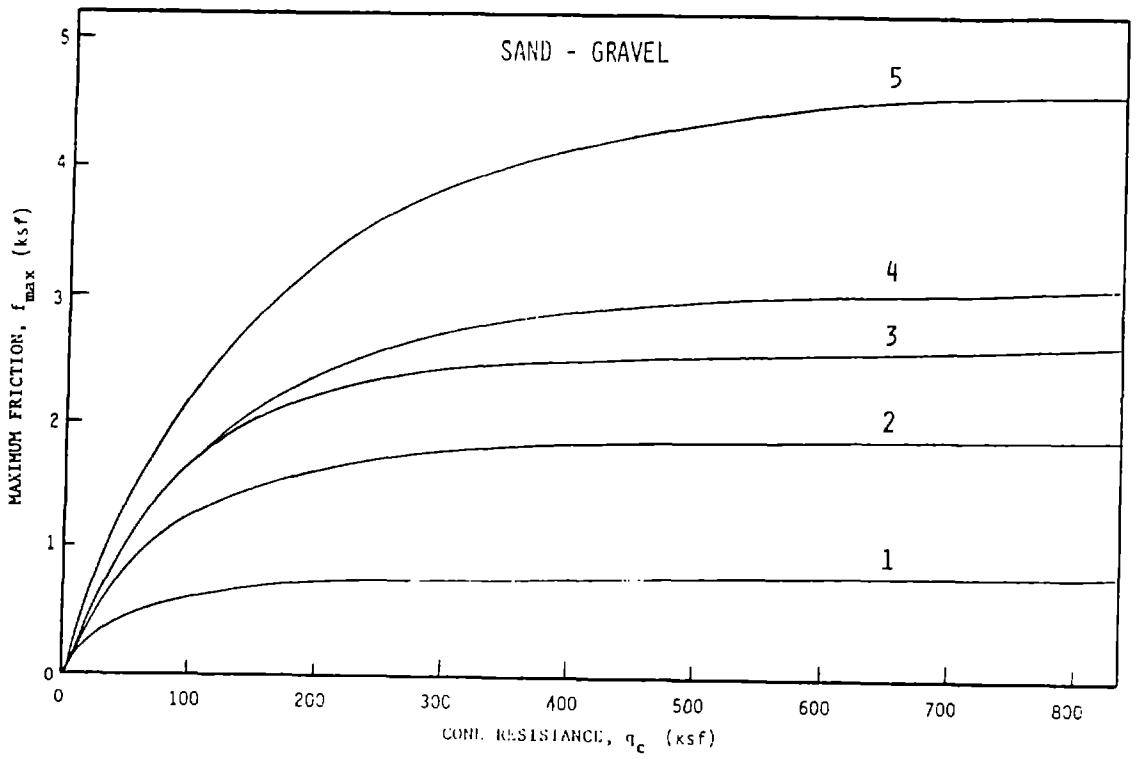

FIG. 7.21. Continued

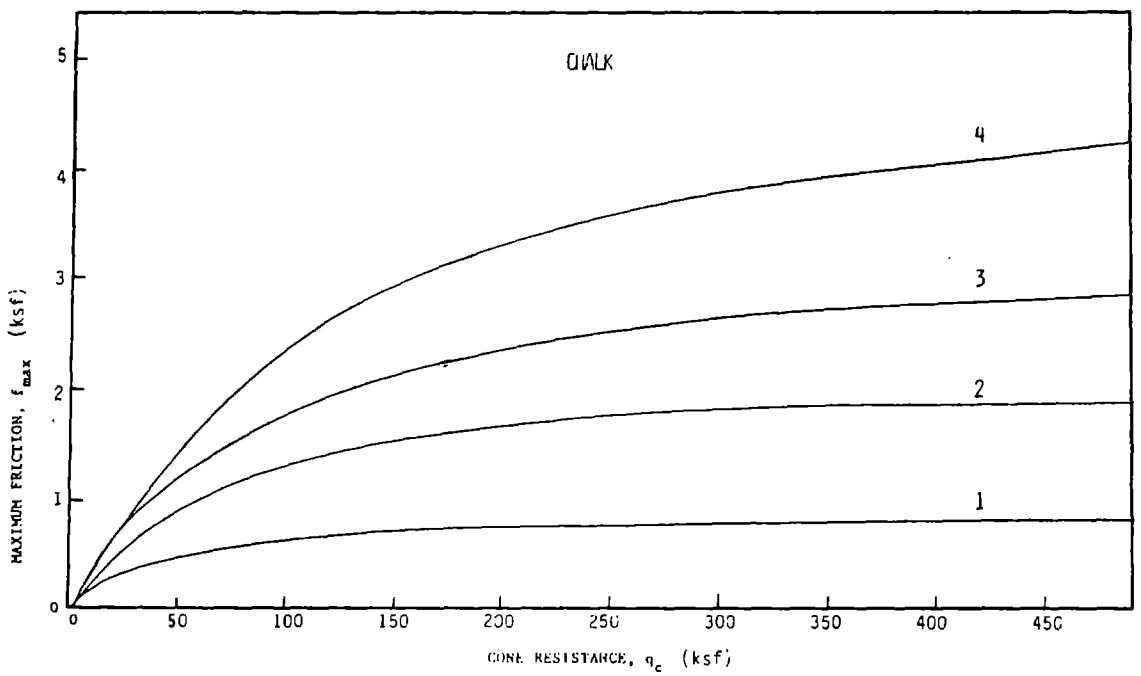

FIG. 7.21. Continued

K_c = cone bearing capacity factor from Fig. 7.22 based on installation procedure and soil type.

q_c = average cone tip resistance below the tip of the pile (1 pile diameter).

	POINT BEARING FACTOR, K_c	
TYPE OF SOIL	BORED PILE	DRIVEN PILE
CLAY-SILT	0.375	0.600
SAND-GRAVEL	0.150	0.375
CHALK	O.200	0.400

FIG. 7.22 - Cone Bearing Capacity Factors for Proposed L.P.C. Method

7.2.6 Ultimate bearing capacity: precision of the methods

The previous methods have been checked by Briaud and Tucker (1988) against a data base of 68 pile load tests which were not used in the development of the methods. The cone penetrometer used was a mechanical cone. The pile data base was formed of square concrete piles, ranging from 14-18 in. in width, H-piles, and drilled shafts ranging from 12-16 in. in diameter. The length of the piles varied from 10-82 ft. The piles were either entirely in sand, entirely in clay, or in layered soils. 62 piles were driven and 6 were bored. The predicted loads were compared to loads measured at a settlement equal to one-tenth of the pile diameter plus the elastic compression of the pile. The results are shown on Figs. 7.23, 7.24, and 7.25. A statistical analysis of the ratio of predicted to measured loads yielded the results presented in Table 7.3.

Overall, the methods overpredict the ultimate load as defined here. However, this may be due to the fact that the data base is somewhat biased towards the weaker piles. Indeed, the higher capacity piles, those that carried more than four times the design load Q_d could not be included since the load test stopped at 4 Q_d.

Robertson and Campanella (1988a) checked the methods by De Ruiter and Beringen (1982), Schmertmann (1978) as well as an earlier version of the L.P.C. method (Bustamante, Gianeselli, 1982) against a smaller data base of 7 pile load tests on five different pipe piles. The cone penetrometer used was an electrical cone. Two of the piles were open-ended and four were close-ended. The length to diameter ratio (L/D) for the piles

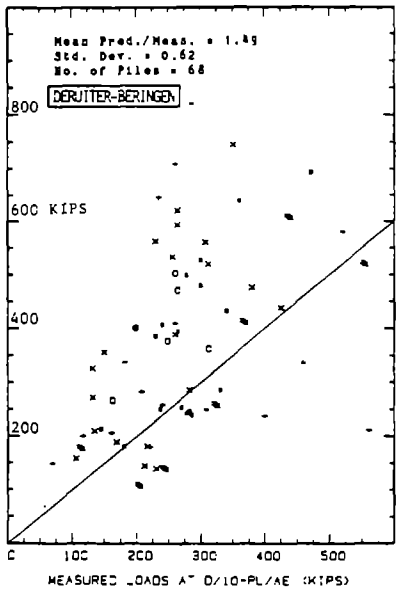

FIG. 7.23. de Ruiter and Beringen Method. Predicted vs. Measured Loads at D/10 + PL/AE (Modified After Briaud and Tucker 1988)

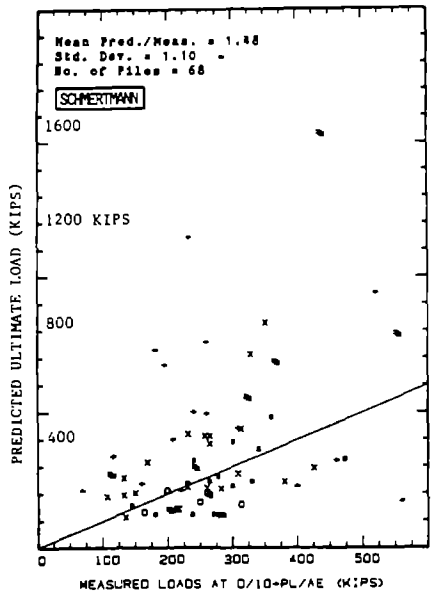

FIG. 7.24. Schmertmann's Method. Predicted vs. Measured Loads at D/10 + PL/AE (Modified After Briaud and Tucker 1988)

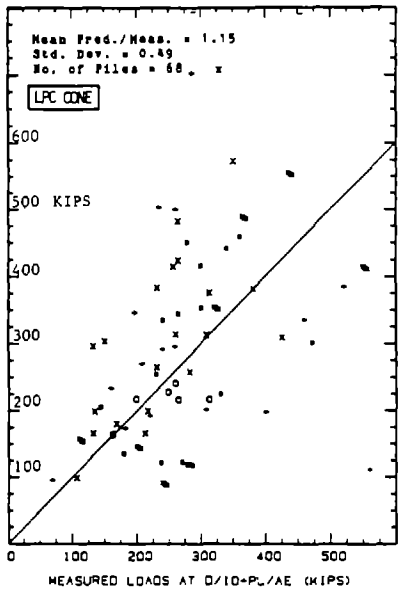

FIG. 7.25. L.P.C. Cone Method. Predicted vs. Measured Loads at D/10 + PL/AE (Modified After Briaud and Tucker 1988)

Table 7.3 - Statistical analysis for ultimate loads (Briaud, Tucker, 1988).

	Method	Number of tests	Mean	Std deviation	Cov
Piles driven in sand	A	7	0.97	0.38	0.39
	B	7	1.51	0.63	0.40
	C	7	0.98	0.38	0.38
Piles driven in clay	A	17	1.32	0.37	0.28
	B	17	0.83	0.33	0.40
	C	17	0.95	0.43	0.45
Piles driven in layered soils tip in sand	A	17	1.43	1.69	0.48
	B	17	2.04	1.21	0.59
	C	17	1.20	0.57	0.47
Piles driven in layered soils tip in clay	A	21	1.70	0.68	0.40
	B	21	1.31	0.53	0.40
	C	21	1.34	0.43	0.32
Piles bored in clay	A	6	1.68	0.31	0.18
	B	6	0.76	0.18	0.24
	C	6	0.91	0.14	0.15
Overall analysis	A	68	1.49	0.62	0.42
	B	68	1.48	1.10	0.74
	C	68	1.15	0.49	0.43

METHODS: A = de Ruiter and Beringen, B = Schmertmann, C = L.P.C.

Table 7.4 - Statistical analysis for ultimate loads (Robertson and Campanella, 1988)

	De Ruiter and Beringen	Schmertmann	L.P.C. (9182)
Mean	1.09	0.94	1.00
Standard deviation	0.14	0.25	0.15

ranged from 40 to 100. One pile was entirely in clay, two piles were in clay with tip in sand, and two piles were in layered soils with tip in clay. A statistical analysis of the ratio of predicted to measured loads yielded the results presented in Table 7.4.

Sharp et al. (1987) compared the L.P.C. method (Bustamante and Gianeselli, 1983) to a data base of 11 pile load tests on 10 prestressed concrete piles and one round pipe pile. The cone penetrometer used was an electrical cone for three sites and a mechanical cone for eight sites. The length to width ratio varied from 13 to 82. Five piles were entirely in sand, five piles were in sand and silty sand, and one pile was in clay over sand. A statistical analysis of the ratio of predicted to measured loads (using the Fuller-Hoy failure criteria) yielded the following results:

Mean	1.23
Standard Deviation	0.45
Coefficient of Variation	0.36

The safe bearing capacity Q_{safe} is defined as:

$$Q_{safe} = \frac{Q_p + Q_s}{F} - W_p \tag{7.51}$$

where

W_p = weight of the pile

F = factor of safety

Briaud and Tucker (1988) showed that the following factors of safety would ensure that the measured ultimate load for any of the piles in the data base would be smaller or equal to the predicted ultimate load devided by the factor of safety:

De Ruiter and Beringen: F = 3.2

Schmertmann: F = 4.0

L.P.C.: F = 2.3

Robertson and Campanella (1988a) recommend to use F = 2.25 for standard electric CPT and for the three methods.

Overall, it seems that the L.P.C. method should be favored as it led to predictions with less scatter. A computer program (PILECPT) has been developed to automate the calculations of this method. Zuidberg (1991) points out that the method by De Ruiter and Beringen (1982) is no longer used by Fugro McClelland Engineers in Holland because

it may overpredict pile capacity. Zuidberg (1991) also has reservations about Schmertmann's method as it relies on f_s measurements for which precision and accuracy may be poor.

7.2.7 Settlement: Introduction

In order to predict the entire load-settlement behavior of a vertically loaded pile, the load transfer characteristics of the soil must be known. This consists of the unit skin friction versus pile movement ($f - w$) curves and the unit point resistance versus pile movement ($q - w$) curve. Knowing these curves and the pile dimensions, the entire top load-top settlement curve may be obtained by using an axially loaded pile computer program. Briaud and Tucker (1986) developed such a program, which combines the LPC method for ultimate load with a method by Verbrugge (1981) for predicting the load transfer characteristics of the soil.

7.2.8 Settlement: Verbrugge (1981) step-by-step procedure

Verbrugge proposed an elastic-plastic model for the $f - w$ and $q - w$ curves based upon CPT results (Fig. 7.26). The slope of the elastic portion of the curves are given by:

$$\frac{q}{w} = \frac{3.125E}{D} \tag{7.52}$$

$$\frac{f}{w} = \frac{0.22E}{D} \tag{7.53}$$

where

D = diameter of a circular pile or 1.2 times the width of a square pile.

E = $10340 + 6.6\,q_c$ (kN/m^2) for bored pile. (7.54)

The relationship for E is recommended for $q_c > 400$ kN/m^2. Verbrugge recommended a lower value of E for bored piles than for driven piles. However, based on the data base described in section 7.2.8, it is recommended that equation 7.54 be used for both driven and bored piles.

1. Obtain the cone bearing resistance q_c and the friction resistance f_s over the depth interval from the ground surface to 4 pile diameters below the pile tip.
2. Divide the q_c profile in "n" layers of constant thickness, no longer than 3 m (10 ft). Number each layer starting from the deepest one. Average the value of q_c for each layer, and assign a soil type to each layer as explained in section 6.2 (Fig. 7.30).
3. Divide the pile in segments of thickness equal to the thickness of the layers of the q_c profile. Number each segment starting from the deepest one (Fig. 7.30).

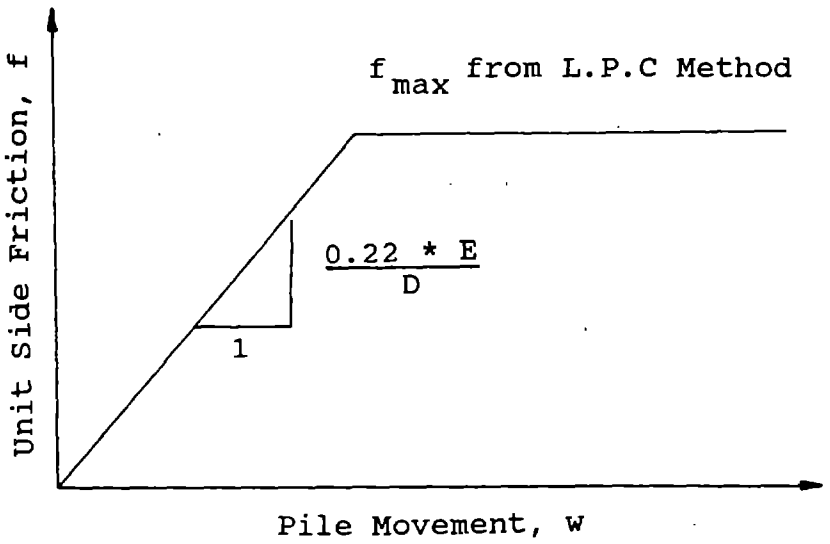

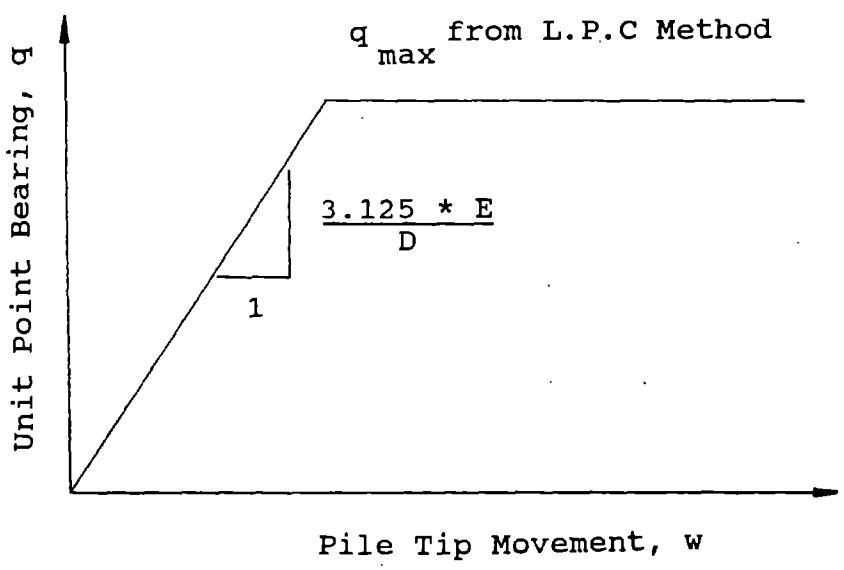

FIG. 7.26. Modified Verbrugge Load Transfer Curves (From Briaud and Tucker 1986)

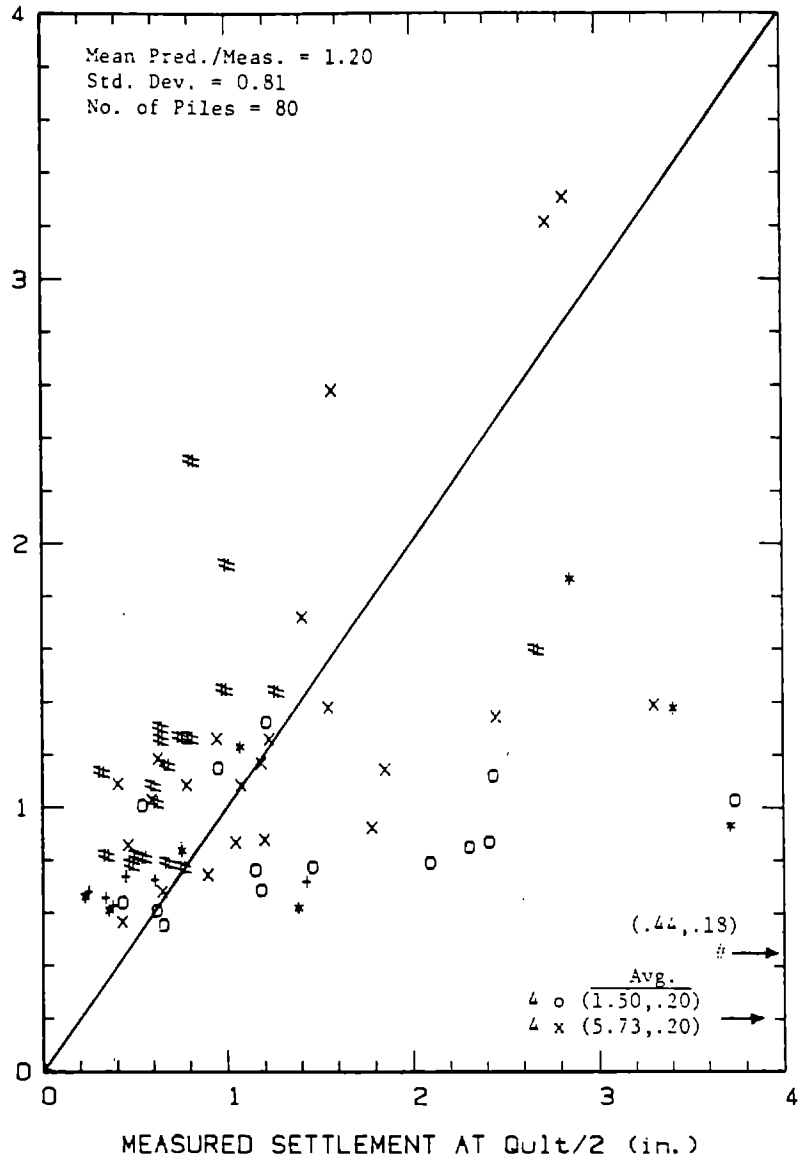

FIG. 7.27. L.P.C. Cone Method. Predicted vs. Measured Settlement at Qult/2 (From Briaud and Tucker 1986)

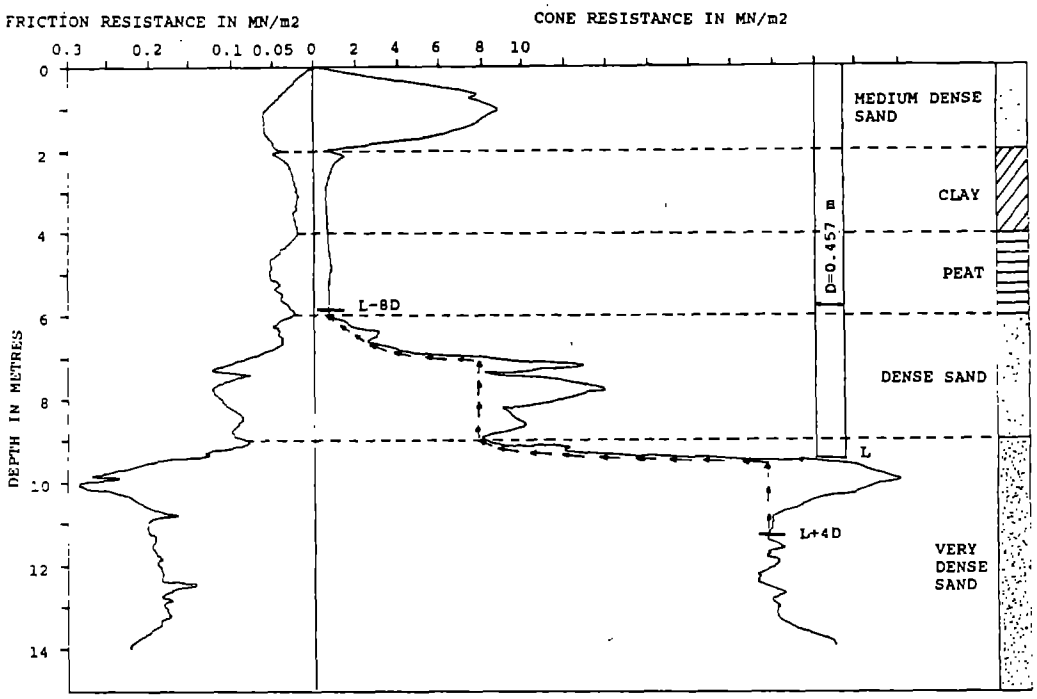

FIG. 7.28. Cone Penetration Test

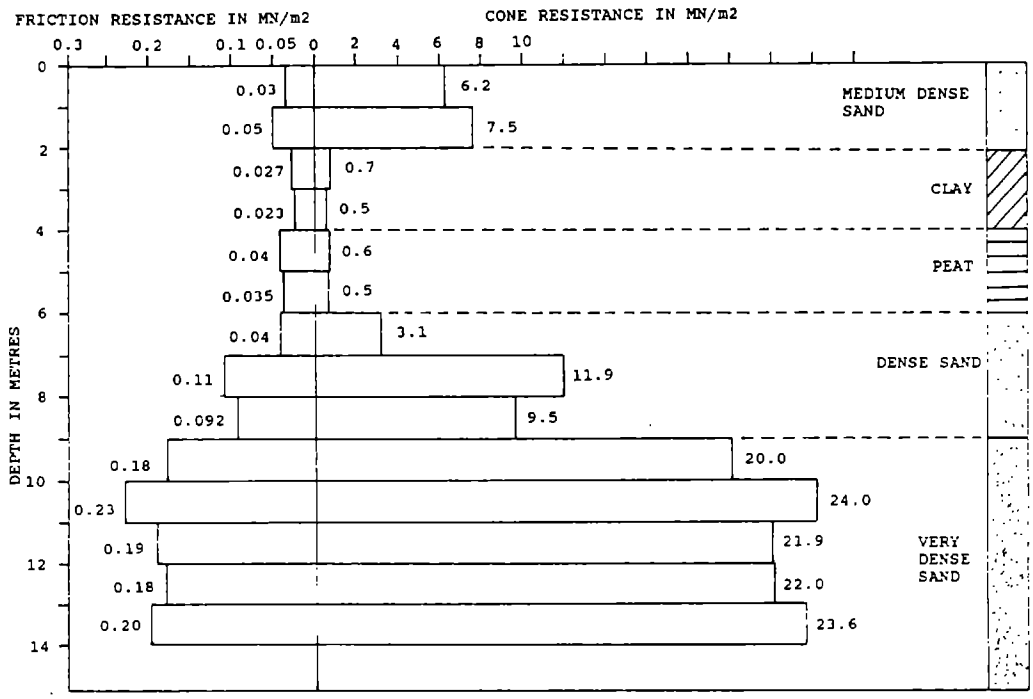

Figure 7.29. Interpreted qc and fs Profiles.

FIG. 7.29. Interpreted q_c and f_s Profiles

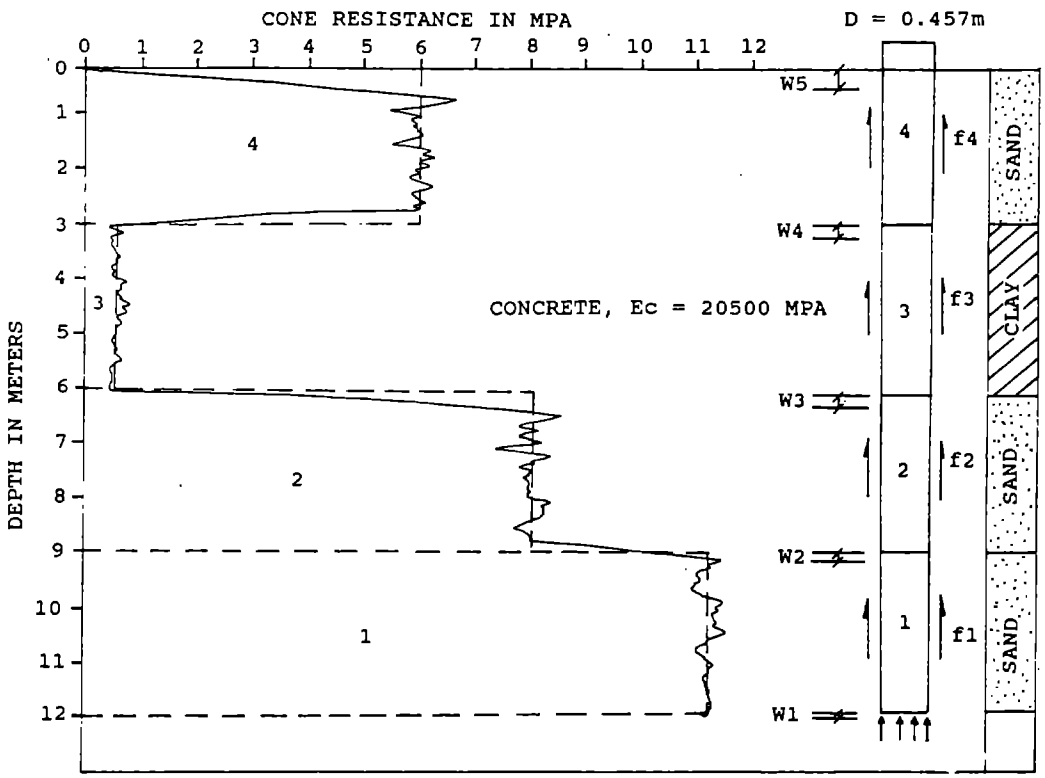

FIG. 7.30. Example Pile for Load - Settlement Calculations

4. For each soil layer, calculate E_i from equation 7.54, and calculate the maximum value of the skin friction $f_{i\,max}$ by using the L.P.C. method (section 7.2.5, where $f_{i\,max} = f$). Also, calculate the maximum value of the unit point resistance for the pile $q_{1\,max}$ at the bottom of the pile using the LPC method (section 7.2.5, where $q_{1\,max} = q_p$).
5. Assume a value of $q_1 < q_{1\,max}$. Then calculate w_i, f_i, and q_i for each layer (for i varying from 1 to n + 1) using each of the following formulas successively:

$$w_1 = \frac{q_1 D}{3.125 E_1} \tag{7.55}$$

$$w_{i+1} = w_i + \frac{q_i \times \Delta L}{E_{pile}} ; 1 < i < n \tag{7.56}$$

$$f_i = \text{minimum} \quad of \left[w_i \times \frac{0.22 E_i}{D} \quad \text{and} \, f_{i\,max} \right] \tag{7.57}$$

$$q_{i+1} = q_i + \frac{\Delta L \times f_i \times p}{A} \tag{7.58}$$

The settlement at the top of the pile is w_{n+1}. This settlement corresponds to a load P applied at the top of the pile:

$$P = q_{n+1} \times A \tag{7.59}$$

where

n = number of pile segments or soil layers

i = number of the ith pile segment

E_i = Young's modulus of the ith soil layer

D = Diameter of circular pile or 1.2 times the width of a square pile

w_i = settlement at the bottom of segment i

f_i = skin friction on segment i

E_{pile} = Young's modulus of the pile

ΔL = length of each segment

A = area of the pile top

p = perimeter of the pile

This procedure yields one point on the load-settlement curve for the pile. In some cases, it is not necessary to obtain the whole curve. Indeed, the engineer may only be interested in estimating the settlement corresponding to a load P at the top of the pile. In order to estimate the value of the unit point resistance q_1 which corresponds to P, it is possible to use Cassan's (1968) formulas:

$$q_1 = \frac{P}{A} \cdot \frac{1}{1 + 0.5\frac{L}{D}} \quad \text{bored pile} \tag{7.60}$$

$$q_1 = \frac{P}{A} \cdot \frac{1}{1 + 0.2\frac{L}{D}} \quad \text{driven pile} \tag{7.61}$$

where

L = length of the pile

Verbrugge's method can then be used with such values of q_1. However, it will yield a value P' different from P. A new iteration will be run with $q_1 = (P/P') \cdot q_1$, and so on until an acceptable value of P' is obtained.

Note: A microcomputer program (PILECPT) exists which automates this process.

McVay et al. (1988) proposed a method for calculation of settlement of pile groups based on CPT data.

7.2.9 Settlement: Precision of Verbrugge method

The method has been checked against a data base of 80 pile load tests which were not used in the development of the method. The piles were square prestressed concrete piles driven in place, round concrete piles cast-in-place, and steel H-piles driven in place. The piles ranged from 12 in. to 16 in. in diameter and from 9.6 ft to 82.0 ft in length. The piles were entirely in sand, entirely in clay, or in layered soils.

The predicted settlements were compared to the measured settlements at one-half of the predicted ultimate load. The results are shown on Fig. 7.27. A statical analysis of the ratio of predicted to measured settlement yielded the following results:

Mean: = 1.20
Standard deviation: = 0.81
Coefficient of variation: = 0.67

Note that these settlements are settlements measured in hours long load tests and are not long term settlements.

7.2.10 Design examples

In order to illustrate the use of the various methods presented, some design examples are given and solved. The examples are as follows:

Example 1: Ultimate bearing capacity (De Ruiter and Beringen method)

Example 2: Ultimate bearing capacity (Schmertmann method)

Example 3: Ultimate bearing capacity (LPC method)

Example 4: Settlement (Verbrugge method)

The data from an electrical CPT for use in Examples 1 through 3 are presented in Fig. 7.28. The interpreted q_c and f_s profiles are presented in Fig. 7.29. The pile studied in those examples is a circular close-ended steel pile, 9.5 m long and 0.457 m in diameter.

The data from an electrical CPT for use in Example 4 are presented in Fig. 7.30. The pile studied is a circular concrete pile, 12 m long and 0.457 m in diameter.

EXAMPLE 1 - De Ruiter and Beringen Method

Point

As explained in section 7.2.3, Figs. 7.15 and 7.16 are used to find the end bearing capacity q_p of the pile. From examination of the q_c profile in Fig. 7.28, it can be seen that the minimum value of I will be at 4D below the pile tip.

At 4D: $I = \frac{(0.5)(23.2+28)(0.5)+(0.5)(28+22)(1.3)}{1.8} = 25.17\,MN/m^2$. The minimum II is the minimum value over this same depth, which is 22 MN/m^2 at 4D below the pile tip.

The value of III is:

$$III = \frac{(0.5)(22+8)(0.5)+(2)(8)+(0.5)(8+0.6)(1.1)}{3.6} = 7.84\,MN/m^2$$

so,

$$q_p = \frac{(25.17+22)(0.5)+7.84}{2} = 15.7\,MN/m^2$$

From Fig. 7.16, for sand with OCR = 1, the maximum value of q_p is 15 MN/m^2

So,

$$q_p = 15\,MN/m^2.$$

Finally,

$$Q_p = (15)\left(\frac{\pi}{4}\right)(0.457)^2 = 2.46\,MN$$

$$Q_p = 2.46\,MN$$

Side

The method presented in section 7.2.3 is used to estimate the unit skin friction f every one meter. The results are presented in Table 7.5.

Finally,

$$Q_s = \sum f \cdot A_s \quad \text{(closed-ended pile)}$$

$$Q_s = 0.42\,MN$$

Total Capacity

$$Q_L = 2.46 + 0.42 = 2.88\,MN$$

The total recommended load at the ground surface is:

$$Q = \frac{Q_p + Q_s}{F} - w_p = \frac{2.46+0.42}{2.25} - 0.03$$

$$Q = 1.25\,MN$$

EXAMPLE 2 - Schmertmann method

Point

Schmertmann uses the De Ruiter and Beringen procedure for sand, for end bearing calculation:

$$Q_p = 2.46 MN$$

Side

The method presented in section 7.2.4 is used to estimate the unit skin friction f every one meter. From Fig. 7.17, for $L/D = (9.5)/(0.457)$, and an electric cone, $K = 0.78$. Table 7.2 gives $C = 0.012$. The results are presented in Table 7.6.

Finally,

$$Q_s = \sum f \cdot A_s \quad \text{(closed-ended pile)}$$

$$Q_s = 0.51 MN$$

Total Capacity

$$Q_L = 2.46 + 0.51 = 2.97 MN$$

The total recommended load at the ground surface is:

$$Q = \frac{Q_p + Q_s}{F} - w_p = \frac{2.46 + 0.51}{2.25} - 0.03$$

$$Q = 1.29 MN$$

EXAMPLE 3 - LPC method

Point

The end bearing capacity q_p of the pile is:

$$q_p = k_c \cdot q_c$$

From Fig. 7.22 we get: $k_c = 0.375$

From Fig. 7.28 we get: $q_c = 23.4 MN/m^2$

So,

$$q_p = 23.4 \times 0.375$$

$$q_p = 8.8 MN/m^2$$

Finally,

$$Q_p = (8.8 MN/m^2)\left(\frac{\pi}{4}\right)(0.4572)^2 = 1.44 MN$$

$$Q_p = 1.44 MN$$

Side

The method presented in section 7.2.5 is used to estimate the unit skin friction f every one meter. From Fig. 7.19, the pile type is selected: $10 \cdot BM$ (Group 11). From Fig. 7.20 and Fig. 7.21:

Curve 2 is selected for the medium dense sand

Curve 3 is selected for the other sands

Curve 1 is selected for the clay

Then the values of f can be calculated using these curves. The results are given in Table 7.7.

Finally,

$$Q_s = \sum f \cdot A_s \quad \text{(closed-ended pile)}$$

$$Q_s = 0.79 MN$$

Total capacity

$$Q_L = 1.44 + 0.79 = 2.23 MN$$

The total recommended load at the ground surface is:

$$Q = \frac{Q_p + Q_s}{f} - w_p = \frac{1.44 + 0.79}{2.25} - 0.03$$

$$Q = 0.96 MN$$

Table 7.5 - De Ruiter and Beringen method

Depth (m)	Material	q_c MPA	f1 MPA	f2 MPA	f3 MPA	f4 MPA	S_u MPA	α	f Clay MPA	f MPA	f * A_s MN
0.5	SAND	6.2	0.12	0.03	0.021	-	-	-	-	0.021	0.030
1.5	SAND	7.5	0.12	0.05	0.025	-	-	-	-	0.025	0.036
2.5	CLAY	0.7	-	-	-	-	0.043	1	0.043	0.043	0.062
3.5	CLAY	0.5	-	-	-	-	0.029	1	0.029	0.029	0.042
4.5	PEAT	0.6	-	-	-	-	0.034	1	0.034	0.034	0.049
5.5	PEAT	0.5	-	-	-	-	0.026	1	0.026	0.026	0.037
6.5	SAND	3.1	0.12	0.04	0.010	-	-	-	-	0.010	0.014
7.5	SAND	11.9	0.12	0.11	0.040	-	-	-	-	0.040	0.058
8.5	SAND	9.5	0.12	0.09	0.030	-	-	-	-	0.032	0.046
9.5	SAND	20.0	0.12	0.18	0.070	-	-	-	-	0.066	0.047

Table 7.6 - Schmertmann method

Depth (m)	Material	q_c MPA	f_s MPA	K	C	f1 MPA	f2 MPA	f3 MPA	f MPA	f * A_s MN
0.5	SAND	6.2	0.030	0.78	0.012	0.003	0.12	0.074	0.003	0.004
1.5	SAND	7.5	0.050	0.78	0.012	0.016	0.12	0.090	0.016	0.023

Depth (m)	Material	q_c MPA	f_s MPA	α′	S_u MPA	f1 MPA	f2 MPA	f MPA	f * A_s MN
2.5	CLAY	0.7	0.027	0.92	0.043	0.039	0.017	0.017	0.024
3.5	CLAY	0.5	0.023	0.91	0.029	0.026	0.020	0.020	0.029
4.5	PEAT	0.6	0.040	0.80	0.034	0.027	0.032	0.027	0.039
5.5	PEAT	0.5	0.035	0.85	0.026	0.032	0.030	0.022	0.032

Depth (m)	Material	q_c MPA	f_s MPA	K	C	f1 MPA	f2 MPA	f3 MPA	f MPA	f * A_s MN
6.5	SAND	3.1	0.040	0.78	0.012	0.031	0.12	0.040	0.031	0.045
7.5	SAND	11.9	0.110	0.78	0.012	0.086	0.12	0.140	0.086	0.124
8.5	SAND	9.5	0.092	0.78	0.012	0.072	0.12	0.114	0.072	0.104
9.5	SAND	20.0	0.180	0.78	0.012	0.140	0.12	0.240	0.120	0.086

Table 7.7 - L.P.C. method

Depth (m)	Material	q_c MPA	f MPA	f * A_s MN
0.5	SAND	6.2	0.065	0.094
1.5	SAND	7.5	0.069	0.099
2.5	CLAY	0.7	0.024	0.035
3.5	CLAY	0.5	0.019	0.027
4.5	PEAT	0.6	0.021	0.030
5.5	PEAT	0.5	0.019	0.027
6.5	SAND	3.1	0.057	0.082
7.5	SAND	11.9	0.112	0.161
8.5	SAND	9.5	0.105	0.151
9.5	SAND	20.0	0.120	0.086

EXAMPLE 4 - Verbrugge Method

The cone data and the interpreted q_c profile used inthis example are presented in Fig. 7.30.

1. Calculating E_i, $f_{i\,max}$ and $q_{1\,max}$

*E_1

Layer 1: $E_1 = 10.34 + 6.6 \times 11.2 = 84.3 MPa$

Layer 2: $E_2 = 10.34 + 6.6 \times 8 = 63.1 MPa$

Layer 3: $E_3 = 10.34 + 6.6 \times 0.6 = 14.3 MPa$

Layer 4: $E_4 = 10.34 + 6.6 \times 6 = 49.9 MPa$

*$f_{i\,max}$

Using the LPC method presented in section 7.2.5 the following information is obtained:

- The pile category is 9BBA from Fig. 7.19.
- Using Figs. 7.20 and 7.21, and the previous information, the values of $f_{i\,max}$ are:

Layer 1: $f = f_{1\,max} = 0.110 MPa$

Layer 2: $f = f_{2\,max} = 0.098 MPa$

Layer 3: $f = f_{3\,max} = 0.019 MPa$

Layer 4: $f = f_{4\,max} = 0.062 MPa$

*$q_{1\,max}$

From Fig. 7.22, $k_c = 0.375$.

so,

$$q_p = q_{1\,max} = k_c \cdot q_c = 0.375 \times 11.2$$
$$q_p = q_{1\,max} = 4.2 MPa$$

2. Calculating the settlement

The first step is to calculate the value of the load applied at the top of the pile. The LPC method presented in section 7.2.5 gives the following results:

Total end bearing: $Q_p = (0.457)^2 \times \left(\frac{\pi}{4}\right) \times 4.2 = 0.69 MN$

Skin friction resistance:

$$Q_s = (\pi \times 0.457 \times 3)[0.110 + 0.098 + 0.019 + 0.062]$$
$$Q_s = 1.24 MN$$

The total recommended load P is:

$$P = \frac{Q_p + Q_s}{F} - w_p$$

$$P = \frac{0.69 + 1.24}{2.25} - 0.03$$

$$P = 0.83 MN$$

Using Cassan's formula (equation 7.61), q_1, is approximately:

$$q_1 = \frac{P}{A} \cdot \frac{1}{1 + 0.2\frac{L}{D}}$$

$$q_1 = \frac{0.83}{\frac{\pi \times (0.457)^2}{4}} \cdot \frac{1}{1 + 0.2 \times \frac{12}{0.457}} = 0.81 MPa$$

Assuming that $q_1 = 0.81 MPa, w_i, f_i$ and q_i can be estimated for i varying from 1 to 5.

$$w_1 = \frac{q_1 D}{3.125 E_1} = \frac{0.81 \times 0.457}{3.125 \times 84.3} = 0.0014 m$$

$$f_1 = \text{minimum of} \left[0.0014 \times \frac{0.22 \times 84.3}{0.457}; \text{ and } 0.110 \right]$$

$$f_1 = 0.057 MPa$$

Then,

$$q_2 = q_1 + \frac{\Delta L \times f_1 \times p}{A} = 0.81 + \frac{3 \times 0.057 \times 1.43}{0.164}$$

$$q_2 = 2.30 MPa$$

$$w_2 = 0.0014 + \frac{0.83 \times 3}{20500} = 0.0015 m$$

$$f_2 = \text{minimum of} \left[0.0015 \times \frac{0.22 \times 63.1}{0.457}; \text{ and } 0.098 \right]$$

$$f_2 = 0.045 MPa$$

Then,

$$q_3 = 2.30 = \frac{3 \times 0.045 \times 1.43}{0.164}$$

$$q_3 = 3.48 MPa$$

$$w_3 = 0.0015 + \frac{2.3 \times 3}{20500} = 0.0018 m$$

$$f_3 = \text{minimum of} \left[0.0018 \times \frac{0.22 \times 14.3}{0.457}; \quad \text{and} \quad 0.019 \right]$$

$$f_3 = 0.012 MPa$$

Then,

$$q_4 = 3.48 + \frac{3 \times 0.012 \times 1.43}{0.164}$$

$$q_4 = 3.79 MPa$$

$$w_4 = 0.0018 + \frac{3.48 \times 3}{20500} = 0.0023 m$$

$$f_4 = \text{minimum of} \left[0.0023 \times \frac{0.22 \times 49.9}{0.457}; \quad \text{and} \quad 0.062 \right]$$

$$f_4 = 0.055 MPa$$

Then,

$$q_5 = 3.79 + \frac{3 \times 0.055 \times 1.43}{0.164}$$

$$q_5 = 5.23$$

$$w_5 = 0.0023 + \frac{3.79 \times 3}{20500} = 0.0028 m$$

The settlement at the top of the pile is 2.8 mm. This settlement corresponds to a load P applied at the top of the pile:

$$P = q_5 \times A = 0.86 MN$$

This value of P is different from the initial P value (0.83 MN). A new iteration is started with a new value of q_1:

$$q_1 = \frac{0.83}{0.86} \times 0.81 = 0.78 MPa$$

This iterative process is followed until the initial value of P is obtained.

8. ADVANTAGES, DISADVANTAGES AND COSTS

The following list of advantages and disadvantages provides a guide to the strengths and weaknesses of the CPT and CPTU.

8.1 Advantages

The advantages of using the CPT or CPTU are:

1. The CPT and CPTU give a rapid and continuous strength profile of a soil deposit. This technique is considered to be the best technique for delineation of stratigraphy.
2. The CPT and CPTU are much less operator dependant than other in situ tests and the test sequence is simple. As a result, the data from a CPT or a CPTU are reproducible. (Possible exception to this is pore pressure measurements. (See section 8.2, Item 6.)
3. The parameters are measured in place under the actual in situ stress conditions.
4. The cost of a CPT or a CPTU is definitely lower than the cost of other kinds of soil tests, considering the amount of data which is obtained.
5. The CPT is very well suited to the design of vertically loaded piles because of the close analogy of loading.
6. The CPT has been used for a long time and a number of design rules are well documented.
7. The dimensions of the penetrometer tip have been standardized (ASTM).

In addition the CPTU has the following advantages:

8. The use of a CPTU provides finer soil profiling and soil identification than a CPT.
9. When performing a CPTU, correction of the cone resistance and the sleeve friction for the effect of unbalanced water pressures can be done.
10. Running a CPTU gives the possibility of evaluating the consolidation characteristics of a soil, and the groundwater conditions (i.e. u_o).
11. A CPTU enables to know whether the penetration is drained or not.

8.2 Disadvantages

The drawbacks of the CPT and CPTU are:

1. The penetration depth is limited in the stronger soils. The CPT and CPTU cannot be used reliably in cobbles, boulders and rocks.

2. The CPT and CPTU methods cannot provide some of the material characteristics which can only be obtained by use of other in situ tests or careful borings, sampling and laboratory testing. This is due to the fact that the penetration of the CPT is a continuous failure mechanism, therefore the small strain properties of the soil cannot be obtained directly.
3. Special equipment is necessary. Cone trucks with 20-ton push capability represent expensive initial investments. Drill rigs provide only limited vertical reaction (< 7 tons), unless anchors are placed to increase this value.
4. Performing a CPT or a CPTU requires skilled operators with a knowledge of electronics.
5. The location of the porous filter influences the CPTU test results and has not yet been standardized.
6. The complete saturation of the pore pressure measuring system (CPTU) is difficult, but necessary in order to obtain accurate pore pressure readings.
7. The methods used to obtain the soil parameters (chapter 6) are mainly based on correlations instead of theory. A few methods have a theoretical framework.

8.3 Cost and Time Required

The costs of modern equipments are the following. An electric penetrometer tip costs about $4,000-$6,000. A data acquisition system (section 2.3) costs about $15,000-$25,000. A heavy duty truck with a 20 tons push capability (truck, cabin, hydraulic jack, penetrometer, data acquisition system) costs about $200,000. The charge for a cone penetrometer test ranges from $6.00-$8.50 per foot of penetration plus the mobilization and demobilization. About 500 feet of penetration testing can be expected in one day for a 20-ton truck and for a standard geotechnical investigation. For a drill rig this footage is somewhat reduced. The price per foot increases and productivity decreases if site access is difficult or if the soundings are shallow (<50 ft).

On the average a CPT sounding is one-third of the cost of a SPT/sample boring to the same depth with associated laboratory tests and report. However, the CPT and laboratory tests should not be viewed as competitive but more as complementing each other.

9. REFERENCES

Awkati, Z. 1970, unpublished, prepared for office use while employed by Soil Exploration Company, St. Paul, Minn.

ASTM, 1986, "Standard Test Method for Deep Quasi-static, Cone and Friction Cone Penetration Tests of Soil, D3441-86," ASTM Committee D-18 on Soil and Rock.

Baldi, G., Bellotti, R., Ghionna, V., Jamiolkowski, M. and Pasqualini, E., 1981, "Cone Resistance of a Dry Medium Sand," 10th International Conference on Soil Mechanics and Foundation Engineering, Stockholm, Vol. 2, pp. 427-432.

Baldi, G., Bellotti, R., Ghionna, V., Jamiolkowski, M. and Pasqualini, E., 1982, "Design Parameters for Sands from CPT," Proceedings of the Second European Symposium on Penetration Testing, ESOPT II, Amsterdam, Vol. 2, pp. 425-438, May 1982.

Baldi, G., Bellotti, R., Ghionna, V., Jamiolkowski, M. and Pasqualini, E., 1986, "Interpretation of CPT's and CPTU's, 2nd Part: Drained Penetration on Sands," 4th Int. Geotechnical Seminar, Nenying Technological Institute, Singapore, Field Inst. & In Situ Measurements, pp. 143-162.

Baldi, G. et al. 1988, "Seismic Cone in Po River Sand," Proc. ISOPT-1 Orlando, Flo.

Baligh, M.M. and Levadoux, J.N., 1980, "Pore Pressure Dissipation After Cone Penetration," Massachusetts Institute of Technology, Department of Civil Engineering, Construction Facilities Division, Cambridge, Massachusetts 02139.

Baligh, M.M. et al. 1985, "The Piezo-Lateral Stress Cell," Proc. XI ICSMFE, San Francisco.

Barentsen, P., 1936, "Short Description of a Field Testing Method with Cone-shaped Sounding Apparatus," Proc. Int. Conf. Soil Mech. Found. Eng., 1st, Cambridge, 1936, 1 (B/3): 7-10.

Battaglio, M., Jamiolkowski, M., Lancellotta, R., Maniscalco, R., 1981, "Piezometer Probe Test in Cohesive Deposits," ASCE, Geotechnical Division, Symposium on Cone Penetration Testing and Experience, pp. 264-302.

Berardi, R., Jamiolkowski, M., and Lancellotta, R., 1991, "Settlement of Shallow Foundations in Sands: Selection of Stiffness on the Basis of Penetration Resistance," ASCE Geotechnical Engineering Congress, Special Publication No. 27, Vol. I.

Briaud, J.L., 1992, *The Pressuremeter*, A. A. Balkema, Rotterdam.

Briaud, J.L., Tucker, L.M. and Douglas, B., 1985, "Cone Penetrometer and Foundation Design," Short Course Notes, Texas A & M University, Aug. 1985, Vol. 2, Ch.III.

Briaud, J.L. and Tucker, L., 1986, "User's Manual for PILECPT," Civil Engineering Department, Texas A&M University, March 1986.

Briaud, J.L. and Tucker, L., 1988, "Evaluation of Cone Penetration Test Methods Using 98 Load Tests," Proceedings of the First International Symposium on Penetration Testing, ISOPT-I, Orlando, 20-24 March 1988, pp. 687-697.

Bruzzi, D. 1987, Personal Communication to M. Jamiolkowski.

Bustamante, M. and Gianeselli, L. 1982, "Pile Bearing Capacity Prediction by Means of Static Penetrometer CPT," European Symposium on Penetration Testing, 2. ESOPT 2, Amsterdam, Proc. Vol. 2, pp. 493-500.

Bustamante, M. and Gianeselli, L. 1983, "Prevision de la Capacite Portante des Pieux par la Method Penetrometrique," Compte Rendu de Recherche FAER 1.05.022, Laboratoire Central des Ponts et Chaussees, in private communication.

Campanella, R.G. and Robertson, P.K., 1981, "Applied Cone Research," Symposium on Cone Penetration Testing and Experience, Geotechnical Engineering Division, ASCE, Oct. 1981, pp. 343-362.

Campanella, R.G. & Robertson, P.K., 1984. "A Seismic Cone Penetrometer to Measure Engineering Properties of Soil," LIV Annual International Meeting and Exposition of the Society of Exploration Geophysicists, Atlanta, Georgia.

Campanella, R.G., Robertson, P.K., Gillespie, D.G. and Greig, J. 1985, "Recent Developments in In situ Testing of Soils," Proceedings of XI ICSMFG, San Francisco, Vol. 2, pp. 849-854.

Campanella, R.G., Robertson, P.K., and Gillespie, D.G., 1986, "Seismic Cone Penetration Test," In situ '86. Proc. Spec. Conf. GED, ASCE, Virginia Tech., Blacksburg.

Cassan, M., 1968, "Le Tassement des Pieux," Sols-Soils, No. 18, 19 and 20.

Chapman, G.A. and Donald, I.B., 1981, "Interpretation of Static Penetration Tests in Sand," 10th International Conference on Soil Mechanics and Foundation Engineering, Stockholm, Vol. 2, pp. 455-458.

Costet, J. and Sanglerat, G., 1975, "Cours Pratique de Mechanique des Sols. Tome 1: Plasticite et Calcul des Tassements," Dunod.

De Ruiter, J. and Beringen, F.L., 1979, "Pile Foundations for Large North See Strictures," Marine Geotechnology, Vol. 3, No. 3, pp. 267-314.

De Ruiter, J., 1981, "Current Penetrometer Practice," Proceedings of the Symposium on Cone Penetration Testing and Experience, Geotechnical Engineering Division ASCE, St.Louis.

De Ruiter, J., 1982, "The Static Cone Penetration Test State-of-the-Art Report," Proceedings of the Second European Symposium on Penetration Testing, ESOPT II, Amsterdam.

Douglas, B.J., and Olsen, R.S., 1981, "Soil Classification Using Cone Penetrometer," Symposium on Cone Penetration Testing and Experience, Geotechnical Engineering Division, ASCE, Oct. 1981, St. Louis, pp. 209-227.

Douglas, B.J., 1984, "The Electric Cone Penetrometer Test: A User's Guide to Contracting for Services, Quality Assurance, Data Analysis," The Earch Technology Corporation, Long Beach, California.

Dumas, C.E., (1984), SETSAND Manual and Program, available through McTrans, University of Florida, 512 Weil Hall, Gainesville, Florida, 32611-2083.

Durgunoglu, H.T. and Mitchell, J.K., 1975, "Static Penetration Resistance of Soils: I-Analysis," Proceedings, ASCE, Specialty Conference on In-Situ Measurements of Soil Parameters, Raleigh, Vol. I.

Eid, W.K., 1987, "Sealing Effect in Cone Penetration Testing in Sands," Ph.D. thesis in Civil Engineering, Virginia Polytechnic Institute and State University.

Fadum, R.E., 1948, "Influence Values for Estimating Stresses in Elastic Foundations," Proc. Second Int. Conf. on SM&FE, Vol. 2.

Gifford, D.G., Kraemer, S.R., Wheeler, J.R. and Mc Kown, A.F., 1987, "Spread Footing for Highway Bridges," FHWA/RD-86/185, October.

Hansen, J. Brinch, 1961, "A General Formula for Bearing Capacity," Danish Geotechnical Institute, Bulletin No.11.

Heijnen, W.J., 1973, "The Dutch Cone Test: Study of the Shape of the Electric Cone," Proceeding of the 8th International Conference on Soil Mechanics and Foundation Engineering, Vol. 1.1, Moscow.

Hekma, L., 1991, Personal written communication, Feb. 18.

Hughes, J.M.O and Robertson, P.K. 1985, " Full Displacement Pressuremeters Testing in Sands ",Canadian Geotechnical Journal, No. 3.

Hunstman, S.R., 1985, " Determination of In situ Lateral Pressure of Cohesionless Soils by Static Cone Penetrometer ", Ph.D. Thesis, University of California, Berkeley.

Hunstman, S.R., Mitchell, J.K., Klejbuk, L.W., Shinde, S.B., 1986, " Lateral Stress Measurement During Cone Penetration ", In situ ' 86, Proc. Spec. Conf. GED ASCE, Virginia Tech., Blacksburg.

Imai, T. and Tonouchi, K., 1982, "Correlation of N Value With S Wave Velocity and Shear Modulus," Proceeding of the Second Symposium on Penetration Testing, ESOPT II, Amsterdam, Vol. 1, pp. 67-72.

International Society for Soil Mechanics and Foundation Engineering, ISSMFE Technical Committee on Penetration Testing (1988)," International Reference Test Procedure". Proposal to ISSMFE, Orlando, USA.

International Society for Soil Mechanics and Foundation Engineering, ISSMFE Technical Committee on Pressuremeter and Dilatometer Testing 1991, "Summary Report on Push-In Pressuremeter."

Jamiolkowski, M., Ladd, C.C., Germaine, J.T. and Lancellotta, R., 1985, "New Developments in Field and Laboratory Testing of Soils". State of the Art Report. 9th International Conference on Soil Mechanics and Foundation Engineering, San Francisco, USA. Proc. Vol. 1, pp. 57-153.

Jamiolkowski, M., Ghionna, V.N., Lancellota, R. and Pasqualini, 1988, "New Correlations of Penetration Test for Design Practice," Invited lecture, ISOPT-I, Disney World, March, Balkema Publ., pp. 263-296.

Janbu, N. and Senneset, K., 1974, "Effective Stress Interpretation of In situ Static Penetration Tests," Proceedings of the European Symposium on Penetration Testing, ESOPT I, Stockholm, Sweden, Vol. 2.2, pp. 181-193.

Jezequel, J., Pinel, M. and Ravilly, G., 1969, "Penetrometre electrique a mesure continue". Bull. Liaison Lab. Routier ponts et Chaussees, 36: 17-19.

Jezequel, J.F., Lamy, J.L. and Perrier, M., 1982, "The LPC-TLM Pressio-Penetrometer," Proc. of Symposium on the Pressuremeter and its Marine Applications, Paris.

Joustra, K., 1974, "Comparative Measurements of the Influence of the Cone Shape on Results of Soundings," Proceeding of the European Symposium on Penetration Testing, ESOPT I, Vol. 2.2, Stockholm.

Kroezen, M., 1981, "Measurement of In situ Density in Sandy/Silty Soil," Canadian Geotechnical Society Newsletter, Sept. Vol. 18, No. 4.

Ladd, C.C. and Foott, R., 1974, "New Design Procedure for Stability of Soft Clays," Journal of the Geotechnical Engineering Division, ASCE, Vol. 100, No. GT7, pp. 763-786.

Ladd, C.C. and Foott, R., Ishihara, K., Schlosser, F., and Poulos, H.G., 1977, "Stress-Deformation and Strength Characteristics," Proceedings, 9th International Conference on Soil Mechanics and Foundation Engineering, Tokyo, Japan, Vol. 11, pp. 421-494.

Ledoux, J.L., Menard, J. and Soulard, P., 1982, "The Penetro-gammadensimeterc," Proceedings of the Second European Symposium on Penetration Testing, Amsterdam, May, Vol. 2.

Levadoux, J.N. and Baligh, M.M., 1986, "Consolidation After Undrained Piezocone Penetration. I: Prediction," Journal of Geotechnical Division, ASCE, Vol. 112, No. 7, pp. 707-726.

Lunne, T., 1991, Personal written communication, February.

Lunne, T. and Christoffersen, H. P., 1983, "Interpretation of Cone Penetrometer Data for Offshore Sands," 15th Annual Offshore Technology Conference, pp. 181-192.

Lunne, T., Lacasse, S., Rad, N.S. and Decourt, L. 1989, "SPT, CPT, Pressuremeter Testing and Recent Developments on In situ Testing," NGI Report, No. 591390-1, 26 May 1989.

Masood, T. 1988, "Comparison of In situ Methods to Determine Lateral Earth Pressure at Rest in Soils," Ph. D. thesis in preparation, University of California, Dept. of Civil Engineering, Berkeley, USA.

Masood, T., Mitchell, J.K., Lunne, T. and Hauge, E.A., 1988, "Joint U.C. Berkeley and Norwegian Geotechnical Institute in-situ testing at Hamilton Air Force Base and Bay Farm Island, California," Dept. of Civil Engineering, Berkeley, USA.

Marr, L.S., 1981, " Offshore Application of the Cone Penetrometer ", ASCE, Symposium on Cone Penetration Testing and Experience, Oct., pp. 456-476.

McVay, M.C., Townsend, F.C., Bloomquist, D., O'Brien, M.P., and Casper, R.D., 1988, "Development of Design Procedures for Estimating Capacity and Deformation of Pile Groups," Report to Florida Dept. of Transportation, Report No. FL/DOT/BMR/88/326.

Meyerhof, G.G., 1956, "Penetration Tests and Bearing Capacity of Cohesionless Soils," Journal of the Soil Mechanics and Foundations Division, ASCE, Vol. 82, No. SM1, Proc. Paper 866.

Meyerhof, G.G., 1957, Closure to "Penetration Tests and Bearing Capacity of Cohesionless Soils," Journal of the Soil Mechanics and Foundations Division, ASCE, Vol. 83, No. SM1, Proc. Paper 1155.

Meyerhof, G.G., "Penetration Testing Outside Europe," General Report, European Symposium on Penetration Testing. Stockholm, 1974, Proceedings, Vol. 2.1, pp. 40-48.

Mitchell, J.K., 1988, "New Developments in Penetration Tests and Equipment," ISOPT-1, pp. 245-261, Balkema.

Mitchell, J.K. and Gardner, W.S., 1975, "In situ Measurement of Volume Change Characteristics", State-of-the-art-report, Proceedings of the Conference on In situ Measurement of Soil Properties, Specialty Conference of the Geotechnical Division, North Carolina State University, Raleigh, Vol. II.

Morrison, M.J., 1984, "In situ Measurement on a Model Pile in Clay". Ph.D. Thesis, MIT, Cambridge, Mass.

Muromachi, T., 1981, "Cone Penetration Testing in Japan", Symposium on Cone Penetration Testing and Experience, Geotechnical Engineering Division, ASCE, October, St.Louis, pp. 76-107.

Nieuwenhuis, J.K. and Smits, F.P., 1982, "The Development of a Nuclear Density Probe in a Cone Penetrometer," Proceedings of the Second European Symposium on Penetration Testing, Amsterdam, May, Vol. 2.

Parez, L., 1963, "Les penetrometres et leur utilisation," Lab. Centr. Ponts et Chaussees Journees Fond. (6-11 mai 1963), 32 pp.

Parkin, A.K., Holden, J., Aamot, N. and Lunne, T., 1980, "Laboratory Investigation of CPT's in Sand," Norwegian Geotechnical Institute, Report 52108-9, Oslo.

Peck, R.B., Hanson, W.E., and Thornburn, T.H. 1974, *Foundation Engineering*, 2nd Ed., John Wiley & Sons, New York, N.Y.

Robertson, P.K., 1990, Personal written communication, August.

Robertson, P.K., 1990, "Soil Classification Using the Cone Penetration Test," Canadian Geotechnical Journal, Vol. 27, No. 1, February, pp. 151-158.

Robertson, P.K. and Campanella, R.G. 1983, "Interpretation of Cone Penetration Tests - Part I (Sand)," Canadian Geotechnical Journal, Vol. 20, No. 4, pp. 734-745.

Robertson, P.K. and Campanella, R.G., 1985, "Evaluation of Liquefaction Potential of Sands Using the CPT", Journal of Geotechnical Division, ASCE, Vol III, No. 3, March, pp.384-407.

Robertson, P.K. and Campanella, R.G., 1988a, "Axial Capacity of Driven Piles in Deltaic Soils Using CPT," Proceedings, ISOPT-I, Vol. 2, pp. 919-928.

Robertson, P.K. and Campanella, R.G., 1988b, "Guidelines for Using the CPT, CPTU and Marchetti DMT for Geotechnical Design," U.S. Department of Transportation, Federal Highway Administration, Office of Research and Special Studies, Report No. FHWA-PA-87-023 + 84-24.

Robertson, P.K., Woeller, D.J. and Finn, W.D., "Seismic CPT for Evaluating Liquefaction Potential," accepted for publication in the Canadian Geotechnical Journal, Vol. 29, 1992.

Sanglerat, G. 1972, "The Penetrometer and Soil Exploration," Elsevier, Publishing Co., Amsterdam.

Sanglerat, G. et al., 1979, "Controle In situ Des Previsions de Tassements Basees sur les Essais de Penetration Statique pour 79 Ouvrages sur 17 Sites Differnts," Annales de l'institut technique du batiment et des travaux publics, Feb. 1979, pp. 29-50.

Sasaki, Y. et al. 1984, US-JAPAN Cooperative Research on In situ Testing Procedures for Assessing Soil Liquefaction (No. 1). XVI Joint Meeting. Washington, D.C.

Schaap, L.H.J. and Zuidberg, H.M., 1982, "Mechanical and Electrical Aspects of the Electric Cone Penetrometer Tip," Proceedings of the Second European Symposium on Penetration Testing, ESOPT II, Amsterdam, Vol. 2, pp. 841-851, A.A. Balkema.

Schaap, L.H.J. and Hoogedoorn, H.G., 1984, "A Versatile Measuring System for Electric Cone Penetration Testing," in Kovari, K. (ed.) Field Measurements in Geomechanics, Int. Symp. Proc. 1:313-324, Balkema.

Schmertmann, J.H., 1970, "Static Cone to Compute Static Settlement Over Sand," ASCE, J-SM & FD, Vol. 96, SM3, May, pp. 1011-1043.

Schmertmann, J.H., 1978, "Guidelines for Cone Penetration Test Performance and Design," US Departement of Transportation, Federal Highway Administration, Offices of Research and Development, Report No. FHWA-TS-78-209.

Schmertmann, J.H., 1978, "Study of Feasibility of Using Wissa-Type Piezometer Probe to Identify Liquefaction Potential of Saturated Sands," U.S Army Engineering Waterways Experiment Station, Report S-78-2.

Senneset, K., Sandven, R. and Janbu, N., 1989, "The Evaluation of Soil Parameters from Piezocone Tests," Symposium on Insitu Testing of Soil Properties for Transportation Facilities, Washington, D.C. USA. January 22-26.

Sharp, M.R., McVay, M.C., and Townsend, F.C., 1987, "Development of Design Procedures in Estimating Capacity and Deformation of Pile Groups. Volume 1: An Evaluation of Axial Pile Capacity from In Situ Tests," Florida Dept. of Transportation, Report FL/DOT/BMR/88-326.

Shibata, T. and Teparaksa, W., 1988, "Evaluation of Liquefaction Potentials of Soils Using Cone Penetration Tests," Soil and Foundations, Vol. 28, No. 2, pp. 49-60.

Skempton, A.W., 1951, "The Bearing Capacity of Clays," Proceedings Building Research Congress, Vol. 1.

Skempton, A.W., 1957, "Discussion: The Planning and Design of the New Hong Kong Airport," Proceedings, Institution of Civil Engineering, London, 7, pp. 305-307.

Sweeney, and Clough, W., 1990, "Design of Large Calibration Chamber," ASTM Journal of Geotechnical Testing, March, pp. 36-44.

Tand, K.E., Funegard, E.G. and Briaud J.L. 1986, "Bearing Capacity of Footing on Clay CPT Method," ASCE Spec. Conf. In situ '86, Use of In situ Tests in Geotechnical Engineering, Blacksburg, Virginia, USA, pp. 1017-1033.

Teparaksa, W., 1991, "Utilization of Cone Penetration Test to Evaluate Liquefaction Potential of Soils," 2nd Int. Conf. on Recent Advances in Geotech. Earthquake Engrg. and Soil Dynamics, St. Louis.

Terzaghi, K. and Peck, R.B., 1967, *Soil Mechanics and Engineering Practice*, John Wiley and Sons, New York.

The Earth Technology Corporation, 1991, "The Cone Penetration Test: A Guide to Equipment, Methodology and Data Interpretation," Long Beach, California.

Tjelta, T.I., Tieges, A.W.W., Smits, F.P., Geise, J.M., and Lunne, T., 1985, "In Situ Density Measurements by Nuclear Backscatter for an Offshore Soil Investigation," 17th Offshore Technology Conference, Vol. 2, pp. 201-206.

Tokimatsu, K. and Yoshimi, Y., 1983, "Empirical Correlation of Soil Liquefaction Based on SPT N-value and Fines Content," Soils and Foundations, Vol. 23, No. 4, pp. 56-74.

Torstensson, B.A., 1984. "A New System for Groundwater Monitoring," Groundwater Monitoring Review, Vol. 4, No. 4, pp. 131-138.

Tringale, P.T. and Mitchell, J.K., 1982, " An Acoustic Cone Penetrometer for Site Investigations ", Proceedings of the Second European Symposium on Penetration Testing, Amsterdam, May, Vol. 2.

Tucker, L.M. and Briaud, J.L., 1988, "Analysis of the Pile Load Test Program of the Lock and Dam 26 Replacement Project," U.S. Army Engineer Waterways Experiment Station, Mics. paper GL-88-11.

Tucker, L.M. and Briaud, J.L., 1990, "SCHMERT: A Microcomputer Program for Settlement on Sand by Schmertmann Method", Civil Engineering, Texas A&M University.

Veismanis, A., 1974, "Laboratory Investigation of Electrical Friction-Cone Penetrometers in Sand," Proceedings of the European Symposium on Penetration Testing, ESOPT I, Stockholm, Vol. 2.2.

Verbrugge, J.C., 1981, "Evaluation du Tassement des Pieux a Partir de l'Essais de Penetration Statique," Revue Francaise de Geotechnique, No. 15, May, pp. 75-82.

Vesic, A.S., 1975, "Bearing Capacity of Shallow Foundations", Foundation Engineering Handbook, edited by H.F. Winterkorn and H.Y. Fang, Van Nostrand Publishing Company. pp. 121-147.

Villet, W.C.B and Mitchell, J.K., 1981, "Cone Resistance, Relative Density and Friction Angle," Symposium on Cone Penetration Testing and Experience, Geotechnical Engineering Division, ASCE, Oct. 1981, pp. 178-208.

Witters, N.J., Schaap, L.H.J., Kolk, K.J. and Dalton, J.C.P., 1986, "The Development of the Full Displacement Pressuremeter," The Pressuremeter and its Marine Applications, II Int. Symp., ASTM STP 950, Texas A&M University.

Yilmaz, R., 1991, Personal written communication, February 28.

Zuidberg, H.M., 1991, Personal written communication, March 1.

★U.S. GOVERNMENT PRINTING OFFICE: 1992-621-231/41679